A thesis entitled

STRESS PULSES IN CURVED MECHANICAL WAVEGUIDES

submitted to the

UNIVERSITY OF LONDON

by

GORDON OWEN LANGLEY, B.Sc.(LOND.)

in candidature for the degree

of

DOCTOR OF PHILOSOPHY

JUNE, 1968.

A thesis entitled

STRESS PULSES IN CURVED MECHANICAL WAVEGUIDES

submitted to the

UNIVERSITY OF LONDON

by

GORDON OWEN LANGLEY, B.Sc.(Lond.)

in candidature for the degree

of

DOCTOR OF PHILOSOPHY

June, 1968.

ACKNOWLEDGEMENTS

The work described in this thesis was carried out at the Chelsea College of Science and Technology, London. I would like to thank Dr. W.G.B. Britton for the continued encouragement that he has given me during the course of this work.

I am indebted to the Science Research Council for a Research Studentship during the three academic years 1964 to 1967.

ABSTRACT

A wide-band, short-duration, pulse technique has been used to investigate the nature of stress wave propagation in straight rods and helical springs. The stress pulses were initiated by means of electromechanical transducers and the distortion of the pulses, due to dispersion, was investigated by recording the surface strain at various points along the waveguides using small ceramic strain gauges. Two types of generating transducer were used, one employing the electrostrictive properties of PZT-5 ceramic, supplied by Brush Clevite Company, and the other employing the magnetostrictive properties of nickel wire. The latter was used for all the quantitative experimental results obtained. The surface strain gauges were made from the PZT-5 ceramic. The signal from the strain gauge was amplified and displayed on an oscilloscope screen from which direct measurements were taken. The oscilloscope traces were also photographed.

Some of the mathematical theories used to describe the propagation of flexural waves along a straight rod have been outlined; these include the exact and three approximate theories, namely an elementary theory, an improved theory due to Rayleigh and the more accurate Timoshenko theory. Approximate theories for helical springs and plane rings, which are comparable with the Timoshenko theory for a straight rod,

are now available and these theories were investigated in this work.

The accuracy of the approximate theories has been assessed by obtaining the corresponding dispersion curves and then comparing the theoretical predictions, according to Kelvin's method of stationary phase, with the experimental results. The comparison indicates that the approximate theories investigated give a good indication of the dispersion characteristics for the lowest longitudinal, torsional and flexural modes in a helical spring over the frequency range considered.

CONTENTS

CHAPTER ONE

INTRODUCTION

If a stress wave propagates in a MEDIUM and the lateral dimensions of the MEDIUM are small compared to the distance travelled by the wave then the MEDIUM forms a mechanical waveguide for the stress wave. Common examples of mechanical waveguides are straight rods, curved rods, circular rings and helical springs. The behaviour of these waveguides when they are subject to rapidly varying stresses is of considerable practical importance, for example, a spring manufactured to withstand a certain maximum static load may fail when smaller transient loads are applied. In some cases failure may be due to causes which are characteristic of the material itself, for example, metal fatigue. In other cases, the cause may be an increase in stress, over and above that associated with static loading, due to stress waves which are set up in the spring. In addition to springs many straight and curved metal components are used in machines and supporting structures and failure of these components can be very undesirable.

Another important use of mechanical waveguides is to produce a guided wave delay line. To do this an electrical signal is converted into a mechanical pulse which is then

introduced into the waveguide. The mechanical pulse then propagates along the guide to the other end where it is converted back into an electrical signal. The electrical pulse is, therefore, delayed by a time which depends on the length of the guide and the velocity of propagation of the pulse. For very large delays a very long waveguide, or a very slow pulse velocity, is required and therefore many delay lines of this type are coiled to save space. The effect of curvature of the waveguide on the pulse profile is therefore of considerable interest.

In general the propagation of a stress wave in a mechanical waveguide is a dispersive phenomena, i.e., the phase velocity of an infinite train of monochromatic sinusoidal waves is a function of wavelength of the waves; under these circumstances a transient pulse, which can be regarded from the standpoint of a Fourier integral as possessing a spectrum of sinusoidal waves, will change in form as it travels along the guide.

The aim of the work described in this thesis is to extend the knowledge of the dynamical behaviour of plane rings and helical springs by computing theoretical dispersion curves for the relevant geometries of the waveguides used and by performing experiments to assess the accuracy of these theories.

The problem of stress wave dispersion in mechanical waveguides has been studied in some detail. One aim of the

theory is to derive the characteristic, or dispersion, equations of the wave motion; these equations represent the relation between the phase velocity of the wave, the wavelength, the lateral dimensions of the solid and the mechanical properties of the material. In the exact theory approach the characteristic equations are derived from the general theory of elasticity by applying the boundary conditions appropriate to the geometry of the waveguide. The method is so complex that only in a few cases have the exact characteristic equations been obtained. The solution for a straight cylindrical guide has been achieved by Pochhammer [1876] and Chree [1889] and a characteristic equation has been presented by Hudson [1943] . The solution of this equation results in an infinity of longitudinal modes all of which are dispersive, a double infinity of flexural modes [May 1964] all of which are dispersive and an infinity of torsional modes all of which are dispersive with the exception of the lowest (Zeroth) mode.

For helical springs the exact theory approach is so complex that we are forced to resort to less accurate and more empirical approaches which usually have their basis in the theory of the strength of materials. For flexural waves in a straight rod the more empirical approach leads to three degrees of approximation which result in an elementary theory, an improved theory due to Rayleigh [1894] and a more accurate theory developed by Timoshenko [1921] . In the elementary theory, the motion of the element of the rod is considered

to be purely translational; in Rayleigh's approximation the theory is extended to include the effect of rigid-body rotation of the elements (the rotary inertia correction) and finally, in Timoshenko's theory, the effect of the shearing of the elements is also taken into account. The lower flexural mode obtained from the Timoshenko theory is in very good agreement with the lowest flexural mode predicted by the exact theory but the higher mode of the Timoshenko theory does not agree well with a higher mode of the exact theory. It is apparent from the above theories that a shear correction must be included if an accurate approximate theory is to be obtained.

Approximate theories have also been put forward for longitudinal waves in a straight cylindrical rod. Again it is found that when a shear correction is made the lowest mode of an approximate theory is in good agreement with the lowest mode of the exact theory [Abramson, Plass and Ripperger 1958] but the higher mode of the approximate theory does not agree well with a higher mode of the exact theory [Mindlin and Herrmann 1951, Herrmann 1954] . The elementary theory for longitudinal waves in a straight rod predicts one dispersionless mode which travels at the bar velocity Co.

The elementary approach for torsional waves in straight cylinders gives a result which is in agreement with the lowest mode of the exact theory.

For the case of a helical spring even the approximate

theories are complex and it is instructive to first consider the case of a plane circular ring which can be regarded as a helical spring of zero pitch angle . In this case two types of flexural waves may be propagated. In the first type the elements of the ring suffer displacements which are in the plane of the ring and in the second type the displacements are normal to this plane. Elementary theories relating to these two cases have been derived by Lamb [1931] and Michel [1889] . Both of these theories are based on assumptions which are identical with those used in deriving the elementary theory in the case of a straight rod. A correction to both these theories allowing for rotary inertia of the elements has been discussed by Britton [1957] but, as mentioned above, it is necessary to include a shear correction if the lowest flexural mode dispersion curves are to be a good approximation to an exact theory. Theories, which include shear corrections, have been put forward by Morley [1961] , for vibrations in the plane of a ring, and by Wittrick [1966] for vibrations both in and perpendicular to the plane of a ring of slight curvature. Both these theories are discussed in chapter 5.

In this work the Morley and Wittrick equations were solved for the particular geometry of the guides used and the corresponding dispersion curves were computed.

In the case of a helical spring, the elementary theory, due originally to Kirchoff and Clebsch, led to the equations

of motion of an elastic bar whose central elastic line is in the form of a tortuous curve; this theory has been extended by Love [1900] to the case of the propagation of flexural waves in a thin helical spring. A correction to this theory, allowing for rotary inertia of the elements has been discussed by Britton [1957] but again it is evident that a shear correction is necessary if the lowest flexural mode dispersion curves are to be a good approximation to an exact theory. A theory for a helical spring, of slight curvature, which includes a shear correction has been put forward by Wittrick [1966] . This theory is discussed in chapter 5.

In this work the Wittrick theory, for a helical spring, was solved and the corresponding dispersion curves were plotted.

Experimental investigations have been carried out to assess the accuracy of the various theories mentioned above. There are three main methods which can be used to investigate the variation of velocity with wavelength of a stress wave, these being a resonance method, a narrow-band pulse method and a wide-band pulse method. The narrow-band method involves measurements of travel time of a pulse having a given carrier frequency. This method has an advantage in that only a single frequency is propagated in the guide and therefore different modes will propagate at different velocities unless their dispersion curves happen to cross at the frequency considered.

The method has a disadvantage in that to obtain a short pulse, with a sufficiently narrow bandwidth, high carrier frequencies must be used and the envelope of the pulse must be shaped to have a narrow frequency spectrum. Gaussian shaped pulses have been used by previous workers [Meitzler 1961, May 1960] . It is seen in chapter 5 that the effect of guide curvature is expected to be greatest in the low frequency (long wavelength) section of the dispersion characteristic but a low carrier frequency would increase the bandwidth of the pulse. Instead of reducing the carrier frequency of the pulse a thinner waveguide could be used. However, to investigate the dispersion curves over the required low frequency region a very thin guide would be ncessary. Due to the difficulties described above, the narrow-band method was not used in this work.

The wide-band method involves the introduction of a short duration pulse of simple shape into the waveguide and, because of its broad frequency spectrum, the pulse will change shape as it propagates along the guide. The method involves the measurement of travel time of a given predominant period at some point along the guide. A disadvantage of this method is that several modes of propagation can arrive simultaneously at a point along the guide, however, a more direct indication of how stress pulses disperse as they propagate along waveguides is obtained.

The wide-bandwidth pulse method was used in this thesis and

the experimental results were interpreted according to Kelvin's method of stationary phase. The stress pulses were introduced into the various waveguides by electrostrictive and magnetostrictive transducer techniques as described in chapter 2. The dispersion effects were studied by the use of highly sensitive PZT-5 ceramic strain gauges as described in chapter 3. The high sensitivity of the receiving apparatus enabled stresses in the waveguide material to be kept well below the elastic limit.

Experimental investigations were carried out into the lowest flexural, longitudinal and torsional mode dispersion characteristics in a helical spring and in particular the effect of change of mean radius and pitch angle of the spring on these characteristics was investigated. The experimental techniques enabled results to be taken over a wide range of predominant period.

CHAPTER TWO

THE WAVEGUIDES AND GENERATION OF STRESS PULSES

2.1 GENERAL

The experimental investigations involved the introduction of short-duration mechanical pulses of simple shape into straight rods and helical springs, together with the detection of the resulting stress patterns at various positions along the rods.

Two techniques have been used to introduce the required pulse into the rods. The first makes use of an electrostrictive ceramic transducer [Oliver 1957]. Small cylindrical transducer elements of various dimensions were specially manufactured by the Brush Clevite Company using their PZT-5 ceramic. The second method, which was used in most of the experiments described here, makes use of the magnetostrictive properties of nickel wire. In order to obtain the required pulses a generating system with a low mechanical Q is required. This ensures short pulses with little ringing of the transducer [Redwood 1963]. Two steps can be taken to reduce the mechanical Q to a minimum, one being to choose a transducer

material with a high intrinsic mechanical damping (e.g.PZT-5) and the other being to provide a well matched backing for the transducer.

We will first consider the electrostrictive transducer method of generation. It has been found that, as far as mechanical matching is concerned, a newly developed high damping Cu/Mn alloy, M.C.3., supplied by Langley Alloys Ltd., provides a good backing for PZT-5 elements. Typical values of characteristic mechanical impedance $Zo = \rho Co$, where ρ is the density of the material and Co is the velocity of infinitely long wavelength longitudinal waves in the material, are given below

Z_o (PZT-5) = 21×10^5 gm sec^{-1} cm^{-2}

Z_o (Lead) = 14×10^5 gm sec^{-1} cm^{-2}

Z_o (M.C.3.Alloy) = 23×10^5 gm sec^{-1} cm^{-2}

Z_o (Silver steel) = 41×10^5 gm sec^{-1} cm^{-2}

The M.C.3. alloy has a relatively low mechanical impedance, due to a low Young's modulus E, compared with other materials of similar mechanical strength (e.g. steel). The alloy has the advantage of being easier to handle, than lead for example, when machining to provide sufficiently flat surfaces for the attachment of the transducer elements and when aligning the transducer elements with the rod under investigation.

PZT-5 transducer elements of various dimensions were tried in an attempt to produce the required pulse. The end faces of these elements were coated, to our requirements, with electrolus copper which enabled various solders to be tried as coupling agents; these included an Indium/Tin alloy which has a melting point of about 117°C and consists of 52% Indium and 48% Tin and Roses alloy which has a melting point of about 95°C and consists of 52% Bismuth, 32% Lead and 16% Tin. The elements were coupled to the M.C.3. alloy by a thin layer of solder or phenyl salicylate (salol). The latter was found easier to use and provided a firm coupling which was easily removed by heating to 60°C which is well below the Curie temperature of the PZT-5 ceramic. Dow resin, silicone oil and vaseline were all tried as agents for coupling the transducer to the mechanical waveguide. Vaseline was found to be the most satisfactory coupling agent for this purpose.

Satisfactory pulses were introduced into a $\frac{1}{2}$ inch diameter straight rod by applying a 200 volt electrical square pulse across a PZT-5 ceramic transducer of dimensions $\frac{3}{4}$ inch long and $\frac{1}{8}$ inch diameter. The transducer was coupled to one end of a long M.C.3 alloy backing rod of $\frac{3}{8}$ inch diameter which was tapered down to the diameter of the transducer at this end. The transducer was positioned with its axis along the axis of the waveguide (see Figure 2.1) thus encouraging the longitudinal

Longitudinal mode excitation in a ½ inch diameter straight rod by the electrostrictive transducer method.

FIGURE 2.1

modes to be excited in the rod. The reason for using a long thin transducer is that a simple particle displacement configuration is then encouraged over the cross-section of the transducer [Shaw 1956].

It was not found possible to record the initial stress pulse in the waveguide due to the high electrical voltage applied across the transducer: the direct electrical pick-up signal far exceeded the signal resulting from the mechanical disturbance of the rod. Another disadvantage of using the above technique is that stress waves reflected from the end of the backing rod arrive simultaneously with slower-velocity components of the initial pulse and therefore, if the stress pattern is detected at some distance x along the waveguide, the length of the backing rod limits the portion of the dispersion pattern that can be studied. This interference is particularly troublesome when flexural wave dispersion is being investigated.

Another technique, used in most of the experiments described here, avoided most of the difficulties outlined above. This involved the use of a very long length of nickel wire $^1/_{16}$ inch in diameter and about 100 foot long (see Figure 2.2). Three different lengths of coil 3·5 cm, 1·2 cm and 0·7 cm were wound from 40 s.w.g. enamelled copper wire onto formers which could slide on the nickel wire. Each coil contained five

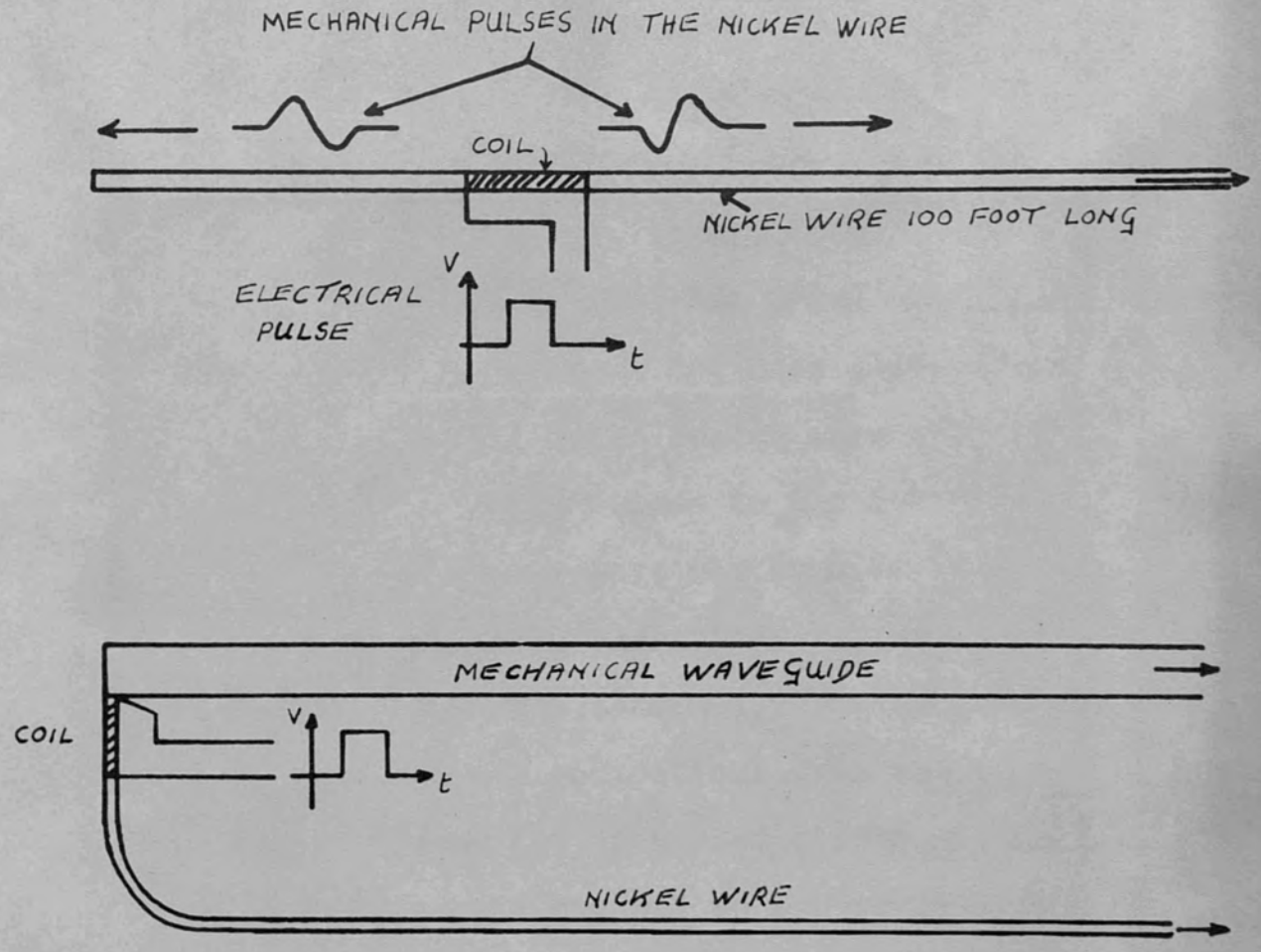

The generation of flexural pulses in a straight mechanical waveguide by a magnetostrictive method.

FIGURE 2.2

layers of windings each containing about 40 turns/cm. When the coil is positioned at one end of the nickel wire we have a transducer with a very long perfectly matched backing. The type of mechanical pulse obtained in the nickel wire by this method is shown in Figure 2.3. The top trace was obtained by applying a 60 volt square pulse of 6·4 μsec duration to the 3·5 cm coil; the second and third traces were obtained by applying 4·2 μsec and 2·7 μsec pulses to the 1·2 cm and 0·7 cm coils respectively. The sweep rate was 20 μsec/graticule division. It can be seen that mechanical pulses of approximately 20, 12 and 8 μsecs were obtained. The long length of nickel wire ensures that any reflections from the end of the wire do not interfere with the dispersed stress pattern being studied. The transducer was coupled to the waveguide with Dow resin.

Using the above techniques it is an easy matter to ensure that the coupling layers are less than $\lambda/_{100}$ thick, where λ is the wavelength of the stress wave component. The wavelengths that we are concerned with are always greater than $\frac{1}{4}$ inch.

The mechanical disturbance introduced into the waveguide is received at some point along the guide by small surface strain gauges (see Figure 2.4). The use of these gauges is discussed in chapter 3. The three orientations of the

The mechanical pulse obtained in the nickel wire

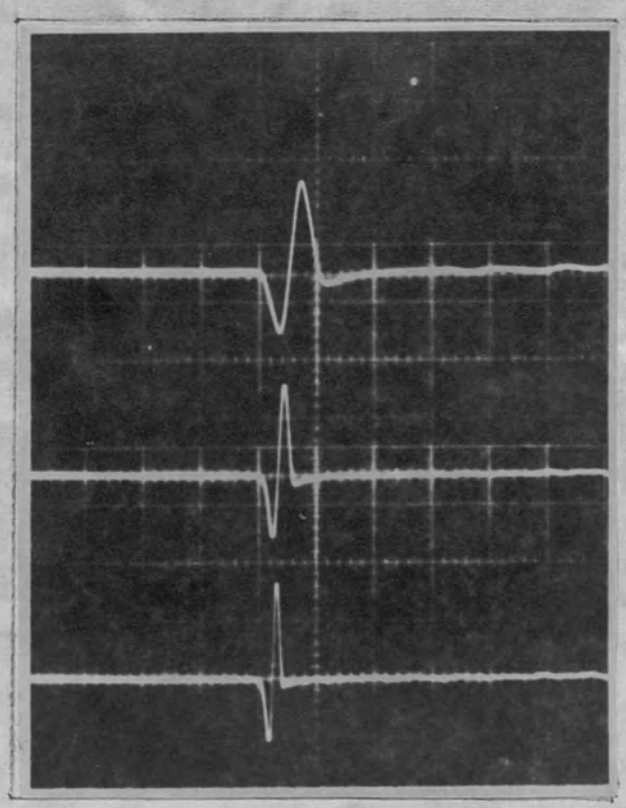

Sweep rate - 20 μsecs. per graticule division

Upper trace - By applying a 6·4 μsec. pulse to a 3·5 cm. coil

Second trace - By applying a 4·2 μsec. pulse to a 1·2 cm. coil

Third trace - By applying a 2·7 μsec. pulse to a 0.7 cm. coil

FIGURE 2.3

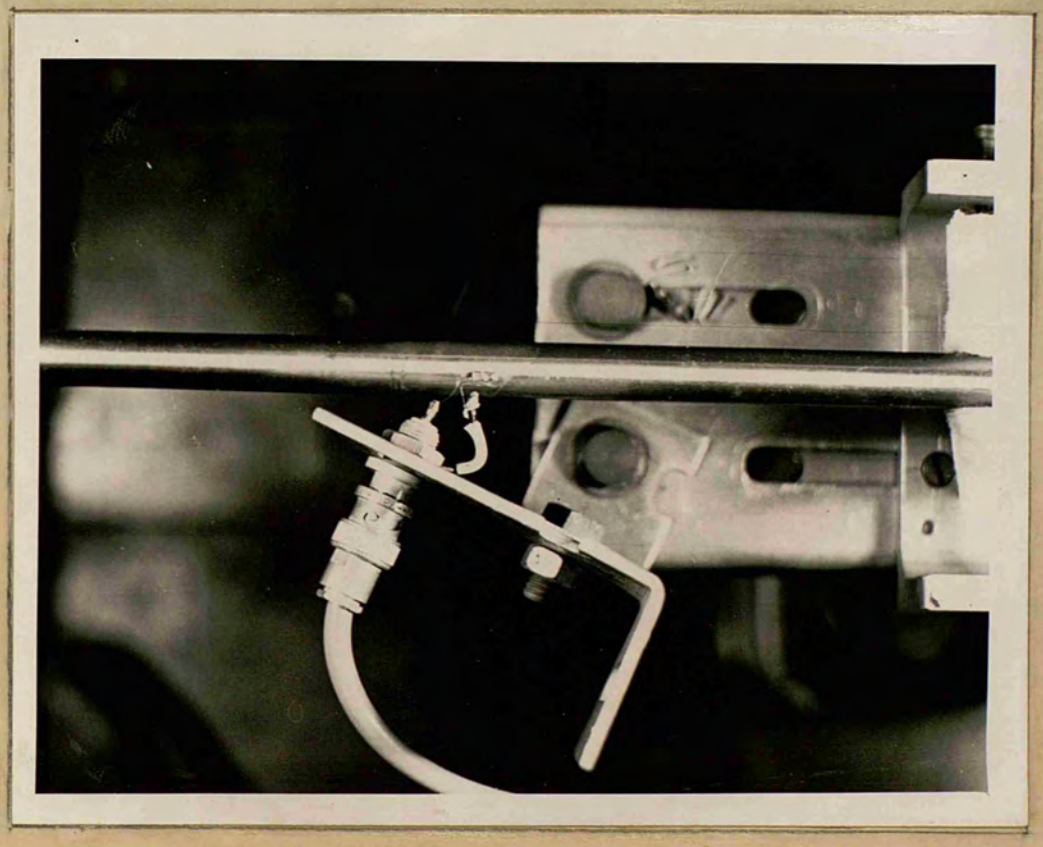

A small surface strain gauge attached to a $\frac{1}{2}$ inch diameter straight rod.

FIGURE 2.4

generating transducer and the corresponding positions of the receiving strain gauge used in the experiments reported here are shown in Figure 2.5. For the straight rod direction 1 encourages the longitudinal (extensional) modes to be excited and directions 2 and 3 encourage the excitation of the flexural modes. For the helical spring directions 2 and 3 must be distinguished from each other. Direction 2 encourages the excitation of the faster flexural wave and corresponds to vibrations in the plane of a circular ring and direction 3 encourages the excitation of the slower flexural wave and corresponds to vibrations perpendicular to the plane of a circular ring. The reason for associating faster and slower flexural waves with directions 2 and 3 respectively will become clear from the theory section (chapter 5). Direction 1 again encourages the excitation of the longitudinal modes.

Figure 2.6 is a block diagram of the apparatus used in this work and Figure 2.7 is a photograph of the components used. The time-mark generator provides, in addition to the time-mark pulses, synchronised pulses which can be used to trigger the pulse generator. The pulse generator provides square pulses of variable duration and amplitude which are applied to the electromechanical transducer. The resulting mechanical pulses are introduced into the waveguide and the resulting strain at some point x along the guide is detected

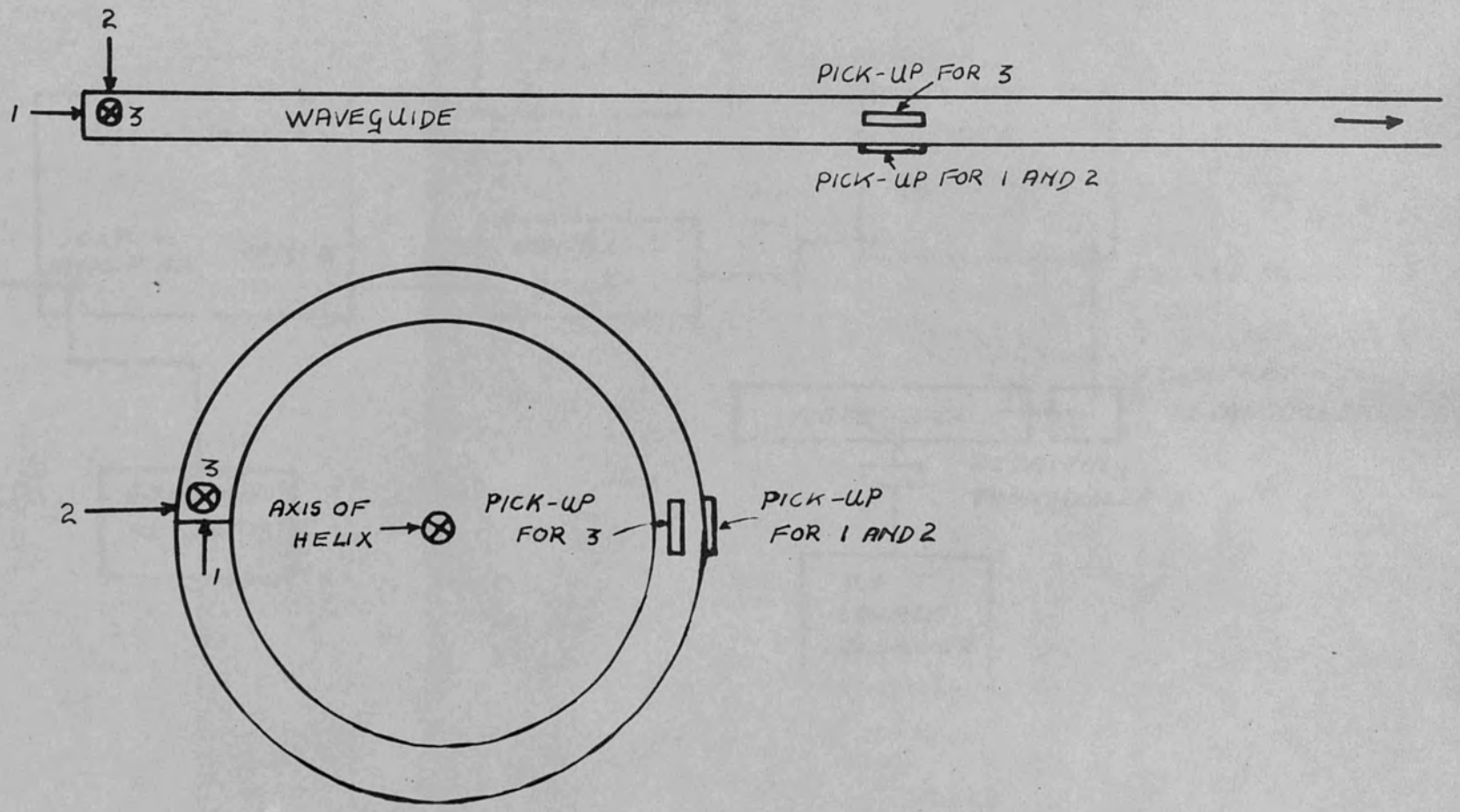

The orientation of the generating transducer and the corresponding positions of the receiving strain gauge.

FIGURE 2.5.

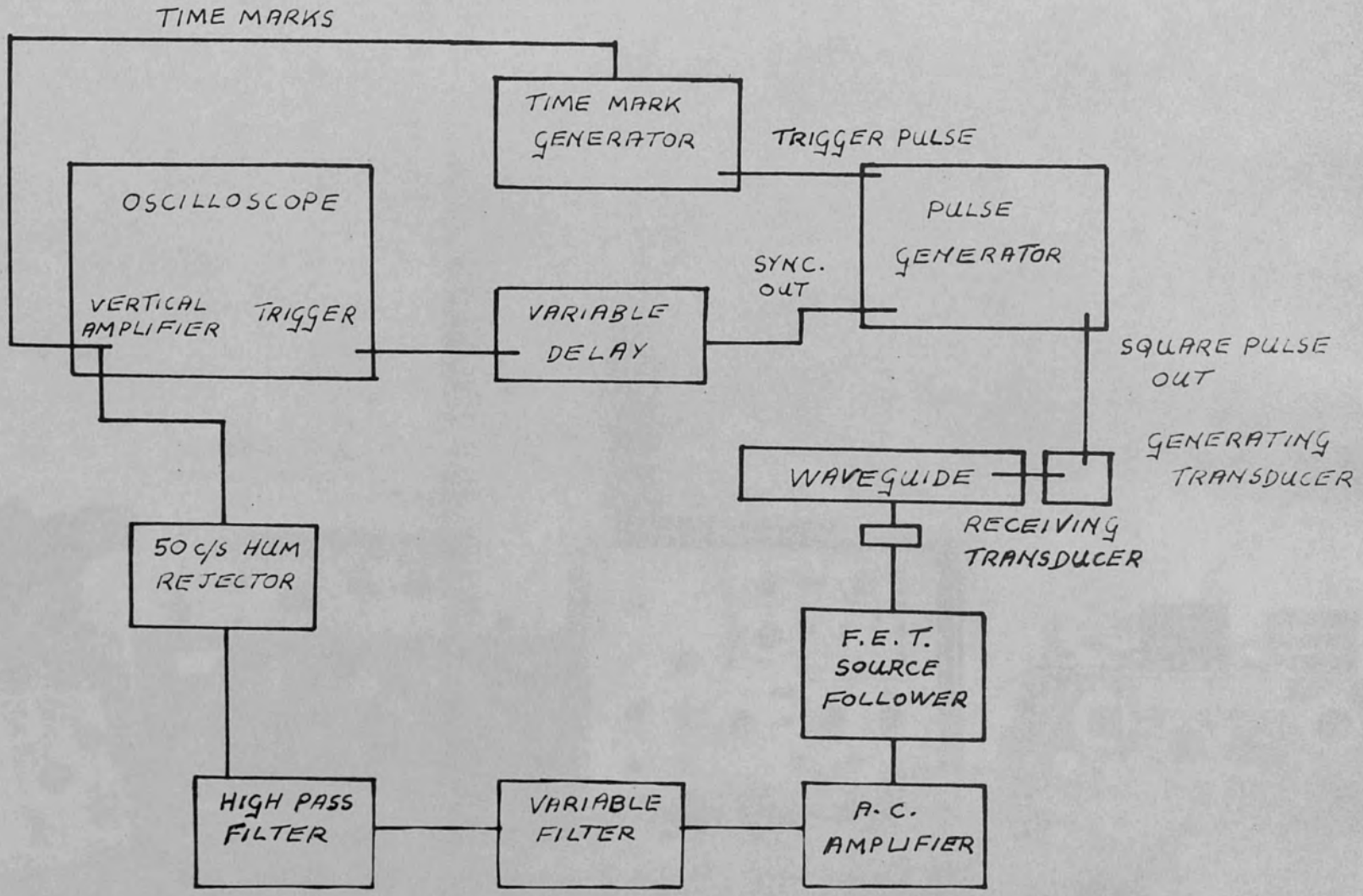

A block diagram of the apparatus

FIGURE 2.6

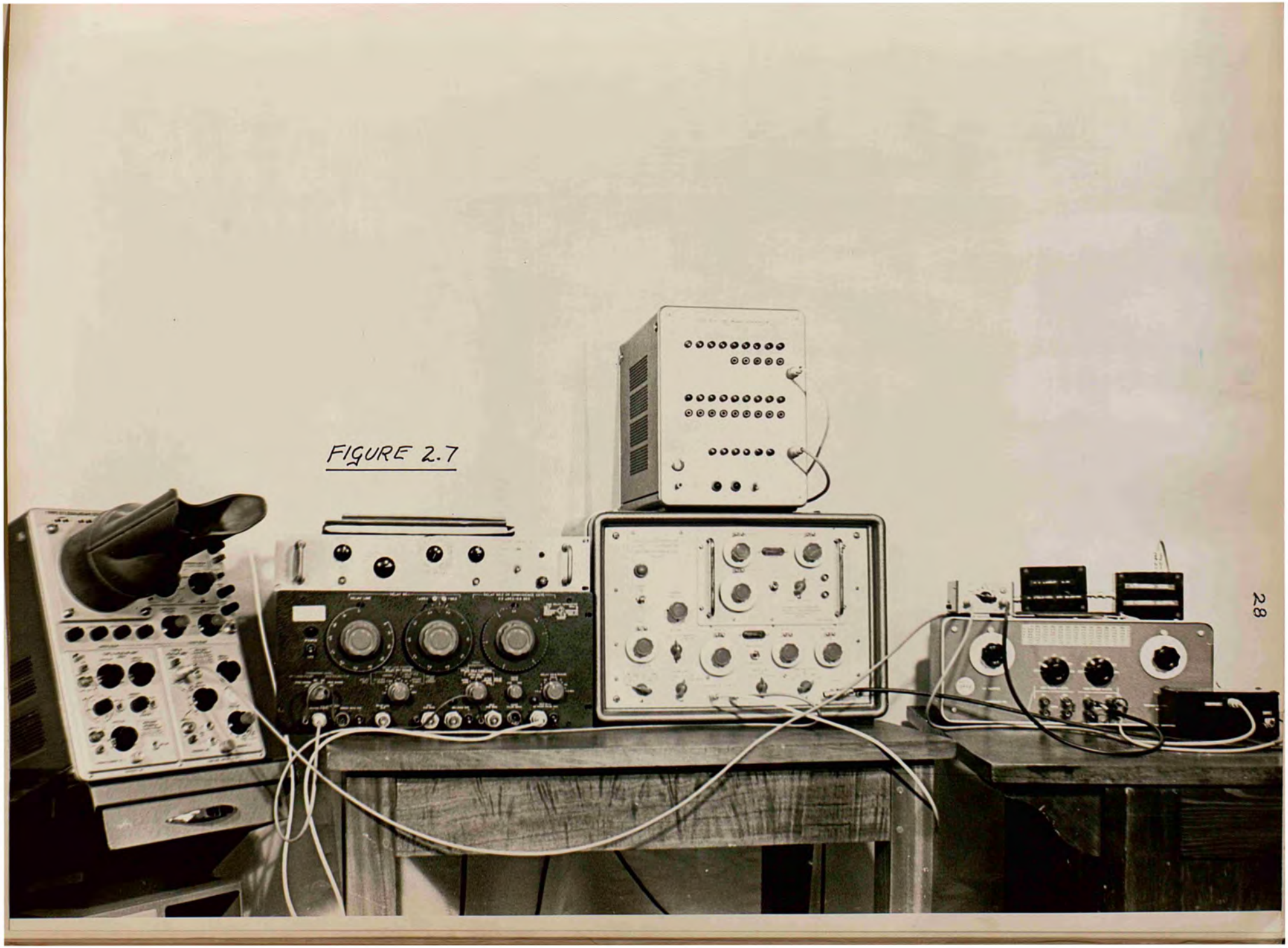

FIGURE 2.7

by the strain gauge elements. These gauges convert the strain into an electrical signal which then passes through a high input impedance, low output impedance source-follower which enables the signals to be amplified with little introduction of noise before they pass through a variable filter which can be used as a high-pass, low-pass or band-pass system. The signal then passes through two fixed filter systems, a high-pass system which attenuates signals below 4 Kc/s and a 50 c/s hum rejector. The former cuts out signals due to resonance effects caused by repeated reflections of mechanical disturbances from end to end of the waveguide and the latter eliminates the effects of electromagnetic pick-up at mains frequency. These filters ensure little spurious movement of the oscilloscope trace. The signal is then fed to the oscilloscope where it is further amplified before being applied to the Y plates of the cathode ray tube. The X-sweep of the oscilloscope beam is initiated by trigger pulses from the pulse generator (sync-out) which are synchronised with the pulses used to excite the generating transducer. In this way a stationary strain, time pattern is obtained on the oscilloscope screen. The introduction of a variable delay unit as shown in Figure 2.6 enables the strain, time pattern to be moved with respect to a reference point on the oscilloscope screen; this facility simplifies the measurement of time

intervals represented by the separation of any two points in the stress pattern. The performance of the individual components of apparatus is described in Chapter 3.

2.2. THE STRAIGHT ROD

A straight cylindrical rod of silver steel 366 cm. long and 1·27 cm. ($\frac{1}{2}$ inch) in diameter was used in preliminary experiments with the PZT-5 ceramic generating transducers. The end faces of the rod were machined flat so that the transducer elements could be easily coupled to them. The rod was supported on adjustable brass V-blocks which were clamped onto aluminium holders. These holders were fixed to a Dexion structure which stood on foam rubber pads. The rod rested in the V-blocks on a soft padding. The V-blocks could be adjusted by unclamping from the holders and adjusting the screw positions and then reclamping (see Figure 2.8). The backing rod with the generating transducer attached was similarly supported in adjustable V-blocks. The backing rod was electrically insulated from the V-blocks and the 200 volt signal applied to it: the specimen rod was earthed. The position and orientation of the backing rod, and hence the generating transducer, could be altered by adjusting the V-blocks as indicated above. In this way the transducer could be positioned on any part of the cross section of the waveguide

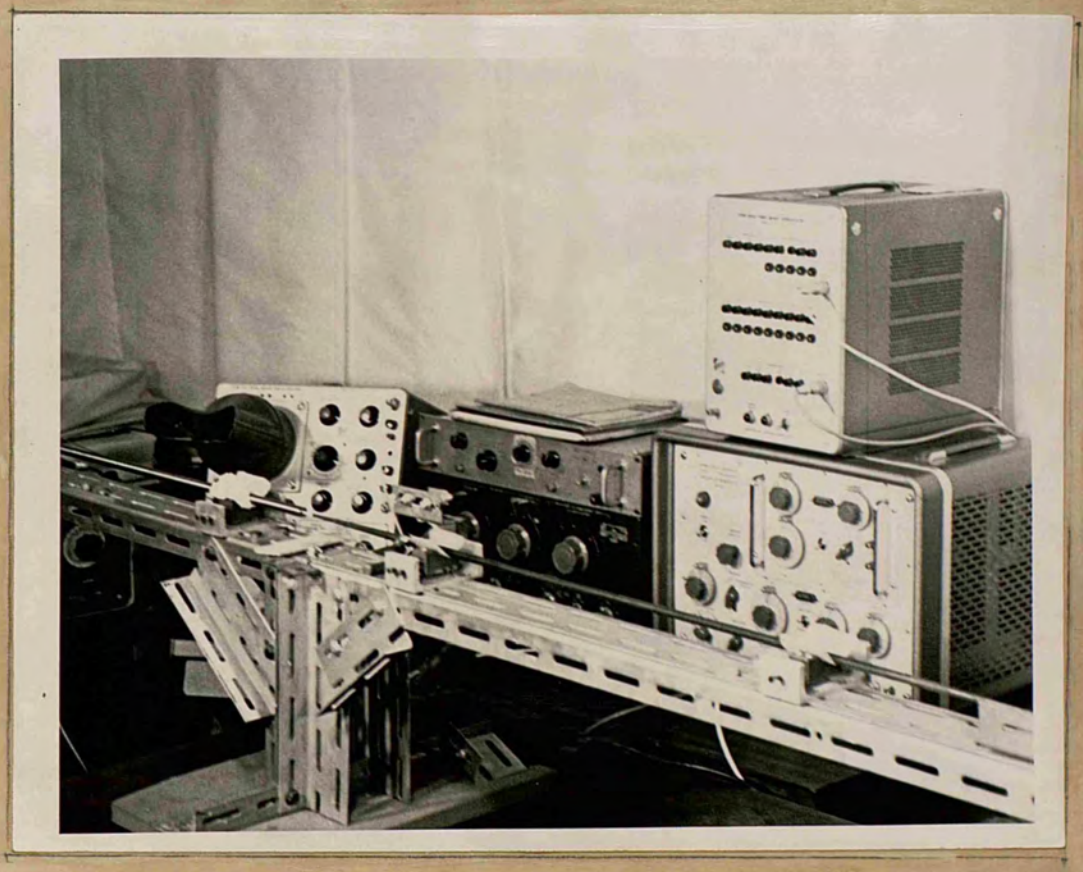

The supporting structure for the mechanical waveguide and the backing rod.

FIGURE 2.8

under investigation. For the preferential excitation of the first longitudinal mode the transducer is placed so that its axis coincides with that of the waveguide (see Figure 2.1).

A straight cylindrical rod of silver steel 234.7 cm long and 0.64 cm (¼ inch) in diameter was used in later work on flexural waves. This rod was supported in the same way as the 1.27 cm diameter rod. The magnetostrictive wire method of generation was used in this case (see Figure 2.2). The long nickel wire was supported in retort clamps and all the kinks in the wire were removed so that spurious reflections within the wire were kept to a minimum. Figure 2.9 shows the pulse obtained in the nickel wire by applying a 60 volt square pulse of 6.4 μsecs duration to the 3.5 cm coil. It is seen that spurious ripple is well below the main pulse height. Any bending of the wire was done smoothly so that no reflections appeared due to sudden change of curvature of the wire. [Britton 1957, Filipczynski 1962]

In both the above cases it was necessary to check that the position of the supporting V-blocks did not affect the stress pattern received by the strain gauges. The positions of the V-blocks were altered but no change in the observed stress pattern could be detected.

The mechanical pulse obtained in the nickel wire

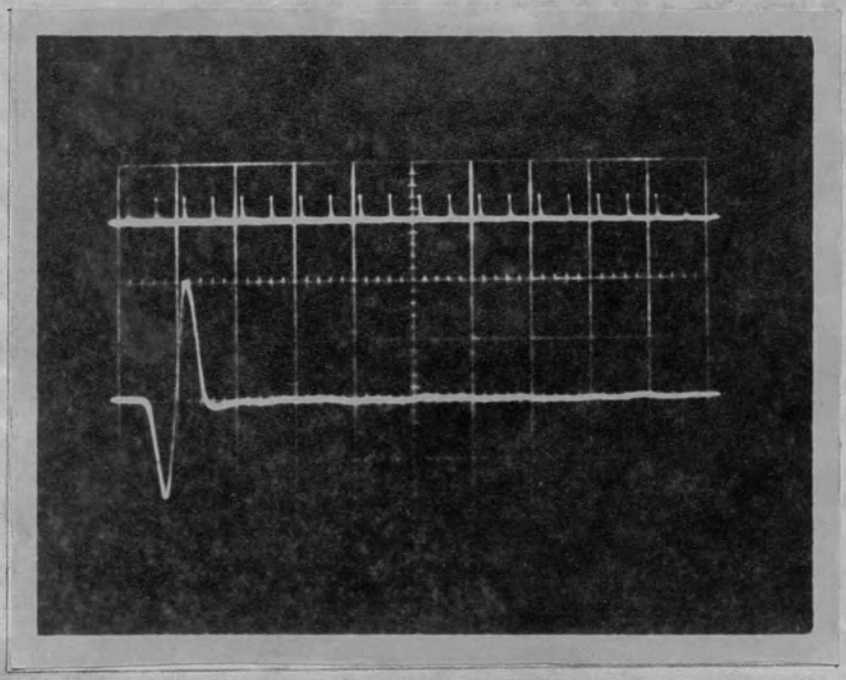

Upper trace - Time markers 10 μsecs. apart

Lower trace - By applying a 6·4 μsec. pulse to a 3·5 cm. coil

FIGURE 2.9

2.3 THE HELICAL SPRING

As already stated, the purpose of this work is to investigate the effects of curvature of a mechanical waveguide on the dispersion characteristics of various modes of vibration. The theoretical work described in chapter 5 indicates that in order to show distinctly the effects of curvature on the first flexural mode, guides of pronounced curvature should be used. Theory also shows that, in the case of the lowest flexural mode, the effect of curvature is greatest for the relatively slow, long period waves. It was therefore necessary to obtain long springs of pronounced curvature. A long spring is necessary so that reflections from the end of the spring do not interfere with slower waves making their first transit. THE HELICAL SPRINGS WERE MADE OF A HARD STEEL.

The experimental set-up for exciting the slower flexural mode is shown in Figure 2.10. The helical spring rests on a soft padding which lies on adjustable brass V-blocks and again the holders for the V-blocks are fastened to the Dexion structure which is placed on foam rubber pads. For excitation of the other modes the transducer was orientated as indicated in Figure 2.5 and the spring remained in the same position. As already mentioned a 4Kc/s high-pass filter unit is included in the apparatus to eliminate signals due to resonance effects caused by repeated reflections from end to end of the waveguide. In the case of helical springs the effect of repeated

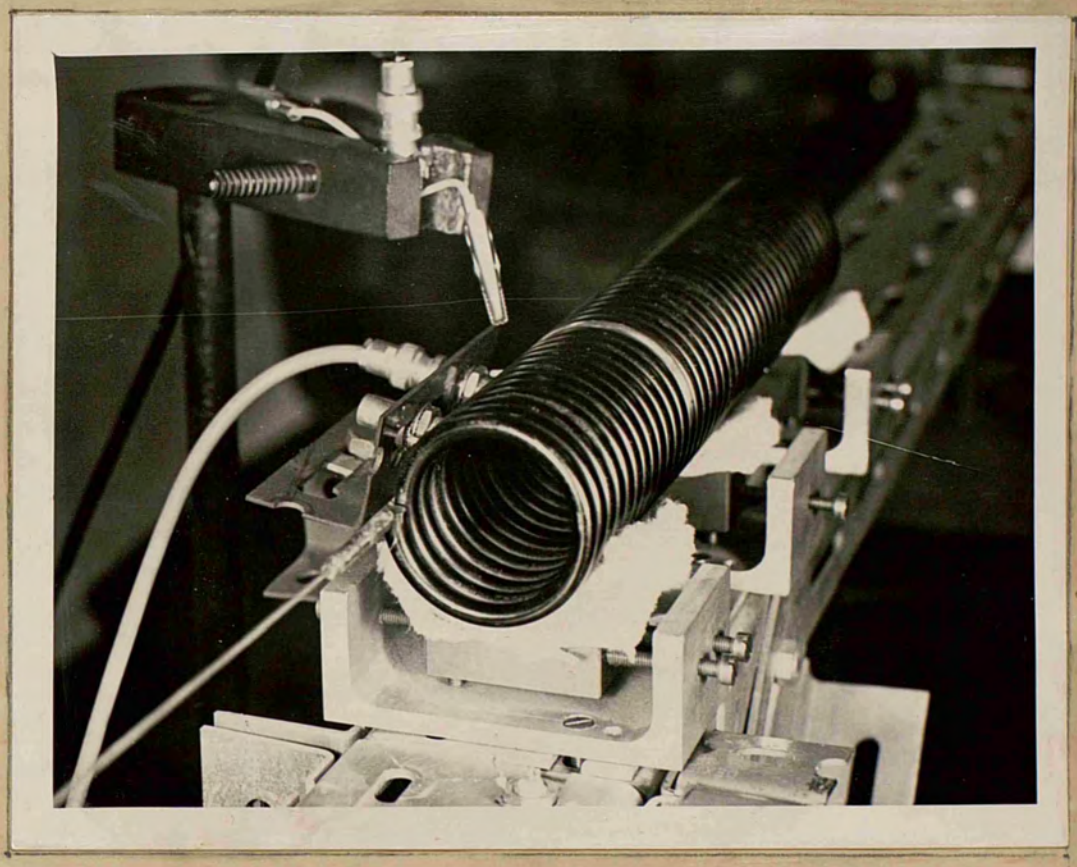

Flexural mode (slower wave) excitation in a helical spring using the magnetostrictive generation technique.

FIGURE 2.10

reflections was found to be more pronounced than in a straight rod and this limits the pulse repetition frequency that can be used because a second pulse is initiated before the effects of the first have damped out. However, by wrapping plasticine around the end of the spring remote from the generating transducer the reflections were sufficiently reduced. This permitted a reasonable pulse repetition frequency to be used and therefore, due to the persistence of the trace on the oscilloscope screen, a steady strain time pattern was obtained with little flicker. As in the case of the straight rod the supports for the spring were moved but again there was no detectable change in the stress pattern.

The dimensions of the springs used in the experiments described here are shown in the table below together with the estimated variation. A diagram of a helical spring is shown in Figure 2.11. In the diagram a is the radius of the rod, R the mean radius of the spring, p the pitch of the spring and α the pitch angle. To find the distance, x, from the end of the spring along the central elastic line after n turns we assume that the central elastic line can be regarded as being wound on a straight circular cylinder of radius R then obviously,

$$x = n(p^2 + 4\pi^2R^2)^{\frac{1}{2}} \qquad 1)$$

Also the pitch angle

$$\alpha = \tan^{-1} {}^{p}/_{2\pi R} \qquad 2)$$

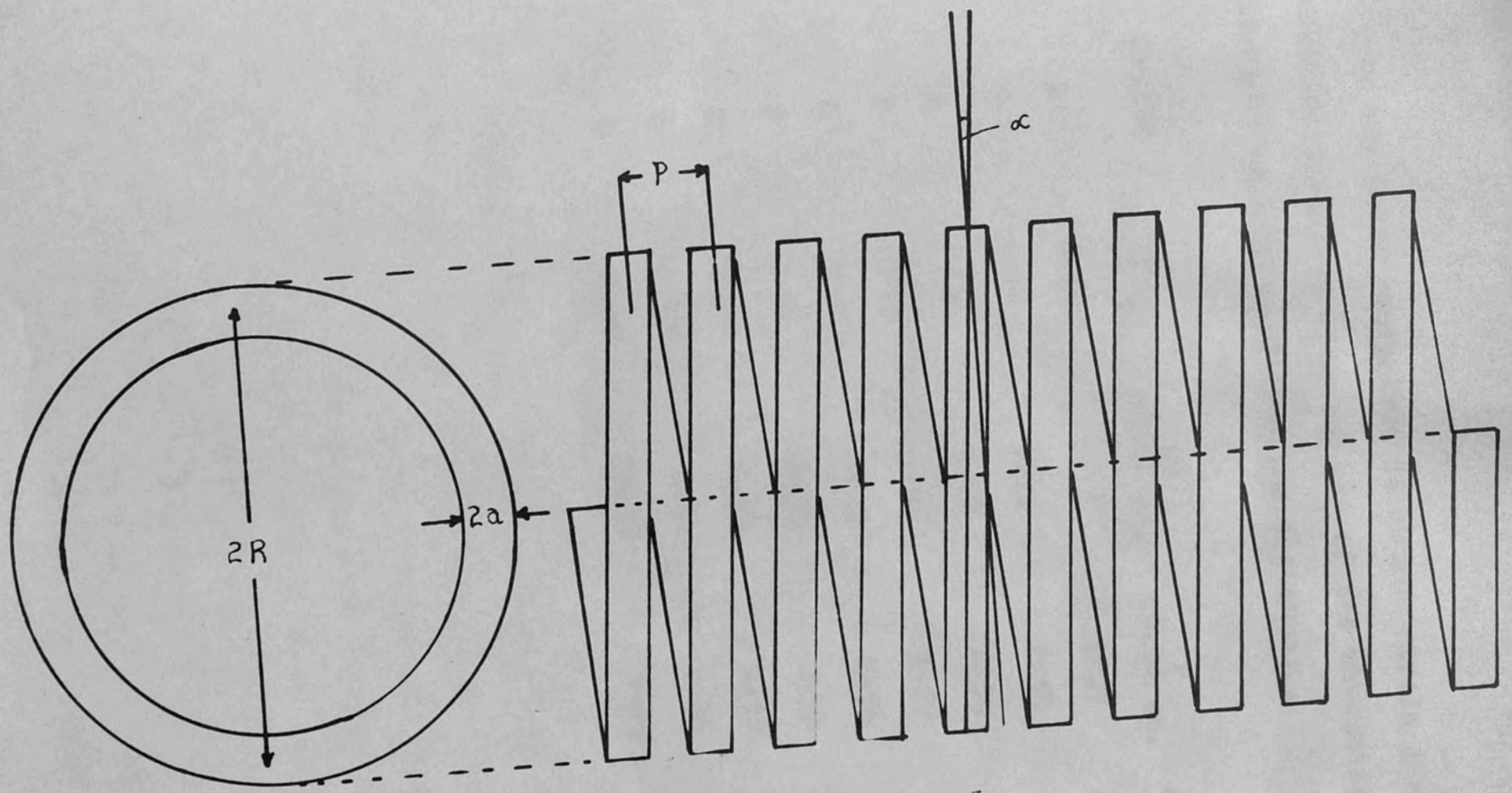

The helical spring

FIGURE 2.11

It was found convenient to attach strain gauges after a number of turns, n, from the end of the waveguide and then to use equation 1 to calculate the distance x.

SPRING	2a ±0.01 cm.	2R ±0.10 cm.	P ±0.10 cm.	α°	NO. OF TURNS
A	0.64	6.10	1.27	3.9	12
B	0.64	6.10	2.54	7.7	12
C	0.64	5.08	0.79	2.8	40
D	0.64	5.08	1.27	4.6	40
E	0.64	5.08	2.54	9.0	36
F	0.64	2.54	0.79	5.7	80
G	0.64	2.54	1.27	9.0	70
H	0.64	2.54	1.91	13.4	50
I	0.64	10.16	0.79	1.4	20

CHAPTER THREE

RECORDING TECHNIQUES

3.1 TRANSDUCER ELEMENTS

As stated in the previous chapter the dispersed stress pulse, after travelling a distance x along the waveguide, is recorded by means of small surface strain gauges. The strain gauges used consist of small elements of PZT-5 ceramic, polarised in a direction indicated in Figure 3.1. The length of such a strain gauge is a limiting factor on the shortest wavelength that it can faithfully record [Davies 1956]. Small PZT-5 strain gauges of dimensions $\frac{1}{8}$ inch long x 1/16 inch wide x 0.035 inch thick were specially made for us by Brush Clevite Company. These elements were coated with silver on their upper and lower surfaces, to our requirements, as shown in Figure 3.1. Leads of 40 s.w.g. enamelled copper wire were soldered onto the gauges with a low melting point solder (Indium/Tin alloy) which melts at about 117°C which is well below the Curie temperature of the PZT-5 ceramic. With these strain gauge elements on a $\frac{1}{4}$ inch diameter rod the stress wave dispersion curve can be studied up to a value where a/λ is approximately 0·2, this value being doubled for a $\frac{1}{2}$ inch

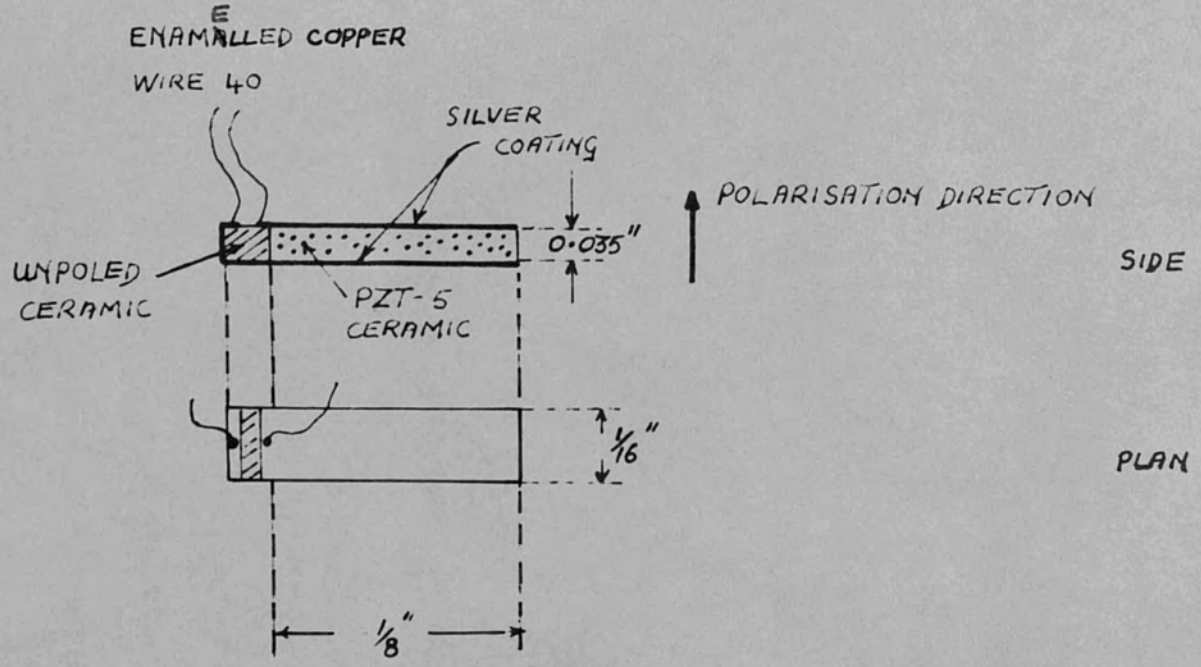

The strain gauge element

FIGURE 3.1

diameter rod. The lowest flexural modes can therefore be studied over their most dispersive region. The ceramic gauges have a much higher sensitivity than the resistance gauges used by previous investigators and the low mechanical Q (broad bandwidth) of PZT-5 ceramic makes it a suitable transducer for recording the dispersed stress pulses. The ceramic element is electrostrictive in nature so that when it is strained in a given direction a charge is built up on the surface of the element and a potential difference appears between its upper and lower surfaces. The reverse effect is used for the generating transducer described in Chapter 2. Here the voltage applied across the end faces of the element results in straining of the element. The strain S produced is related to the voltage V, approximately, by the equation

$$S = K_o V^2 \qquad 3)$$

where K_o is considered constant for a small region about the origin of the strain-voltage characteristic. Thus if a small sinusoidal voltage is applied across the element the resulting stress wave is not sinusoidal. Suppose we now apply a fixed voltage V_p to the element then

$$S_1 = K V_p^2 \qquad 4)$$

where K is a new constant for a small region of the strain-voltage characteristic. If we now apply a small voltage V to

the element then;

$$S_2 = K(V_p + V)^2$$

and therefore the change in strain due to a small voltage V is

$$\Delta s = S_2 - S_1 = (2KV_p)V + K^2V^2$$

or if $V \ll V_p$

$$\Delta s = (2KV_p)V \qquad 5)$$

The strain produced is now proportional to the voltage V applied. The sensitivity of the element is obviously increased as V_p is increased but it is also necessary to choose a region of the strain-voltage characteristic where the value of K can be considered constant over the required range. During manufacture the PZT-5 elements are polarised by heating them above their Curie temperature and then allowing them to cool in a high electric field. Any subsequent heating above the Curie temperature will disturb this polarisation. The surface strain gauge elements are also polarised in this way. The potential difference between the upper and lower surfaces of the strain gauge, resulting from a small strain of the element, is then proportional to the applied strain. The charge appearing on the surface of the gauge when it is in a strained state leaks away fairly rapidly and therefore these gauges are only useful for observing rapidly changing waveforms (i.e. above 20 c/s). The gauges are also incapable of supplying current while maintaining the potential difference

between their surfaces (i.e. electrically they have a high output impedance). If we wish to pre-amplify the signal from the strain gauge elements it is necessary to use a source follower, which is a high input impedance, low output impedance device, to increase the power of the signal. The high input impedance of the device is necessary to limit the flow of charge between the upper and lower faces of the strain gauge which would distort the voltage signal being investigated and the low output impedance is necessary to enable amplification of the signal, with an A.C. amplifier (supplied by Levell Electronics Ltd.,), without introducing electrical noise. Using such sensitive strain gauges, low amplitude initial stress pulses can be used in the rod corresponding to strains of less than 10^{-6}. Therefore many of the difficulties associated with bullet impact experiments do not arise (e.g. plastic flow, exceeding the elastic limit).

3.2 FIXING THE STRAIN GAUGE ELEMENTS

The strain gauges are attached to the waveguides with phenyl salicylate (salol). This chemical melts at 60°C and if allowed to cool forms a supercooled liquid. When seeded the liquid crystallizes and forms into a solid which bonds the gauges to the waveguide very effectively. If the bonding between the gauge and the waveguide is sufficiently good any

straining of the surface of the guide will be faithfully recorded by the strain gauges. To test reproducibility of the stress pattern the following procedure was followed. A photograph of a stress pattern recorded by a gauge was taken and the gauge removed from the waveguide. The gauge was then rebonded in the same position on the waveguide and the stress patterns compared. No difference in the stress patterns could be detected. This test was carried out on several different guides and results indicated that the method of bonding the gauges to the waveguides is sufficiently reproducible. The surface of the specimen rod was cleaned with fine abrasive paper and acetone before attachment of the gauges.

As mentioned earlier, the length of a strain gauge is a limiting factor on the shortest wavelength that it can faithfully record and short gauges were ordered to ensure that the wavelengths of the stress pulses recorded were large compared with the length of the gauge. Another advantage of short gauges is that they are easier to bond to rods of pronounced curvature.

3.3 CIRCUIT COMPONENTS

The general operation of the generating and receiving systems is discussed in section 2.1 and a block diagram of the apparatus is shown in Figure 2.5. We now consider the use of

the receiving apparatus when making quantitative measurements on the stress pattern recorded by the surface strain gauges. As indicated in Figure 2.6 the voltage signal from the strain gauge element is fed into the high impedance input of the source-follower unit. The signal from the low impedance output of the source-follower is then fed into the high input impedance A.C. amplifier. The reason for using the source-follower was discussed in section 3.1. The signal from the A.C. amplifier is then passed through a variable filter, a 4Kc/s high pass filter and a 50 c/s hum rejector before being applied to the oscilloscope preamplifier.

The source-follower unit makes use of two C95 field-effect-transistors (supplied by Semitron Ltd.). The input impedance of the device is above 10MΩ over a frequency range from 1Kc/s to 1Mc/s and the output impedance is about 2KΩ. The unit was tested in two ways. A sinusoidal signal was applied simultaneously to both beams of the oscilloscope and it was found that the traces were in phase. The amplitudes and positions of the traces were then adjusted so that they were completely coincident on the oscilloscope screen. The sinusoidal signal was then applied to the input of the source-follower unit and also to one trace of the oscilloscope. The output from the unit was then applied to the other trace and the two signals compared. The frequency of signal was changed

from 1Kc/s up to 1Mc/s. Below 4Kc/s there was a detectable phase difference between the two traces. This decreased as the frequency was increased until at 4Kc/s and above no phase change could be detected. The second test involved the introduction of a flexural stress pulse into a straight rod of $\frac{1}{4}$ inch diameter using the magnetostrictive generation technique. The receiving strain gauge was at 150 cm. along the rod from the excitation end. The low frequency, long predominant period, portion of the stress pattern has a relatively large amplitude compared with the higher frequency portion (see Chapter 4). It was found possible to observe this low frequency section of the dispersed pulse by feeding the signal from the strain gauge directly into the oscilloscope which was set for maximum sensitivity. The source-follower was then inserted between the strain gauge and the oscilloscope and the resulting stress pattern was compared with the direct signal. There was no detectable difference in the stress patterns for predominant periods of less than 200 μsecs. Above this period a slight difference could be detected. It was assumed from these tests that the source-follower unit does not affect the signal at frequencies between 5Kc/s and 1Mc/s.

The A.C. (Level) amplifier was used to amplify the small amplitude parts of the stress pattern which were to be

investigated. The amplifier has a broad bandwidth (± 0.3 db up to 1Mc/s on the highest amplification setting used) thus enabling the high frequency parts of the stress pattern to be amplified before entering the oscilloscope. The oscilloscope amplifier used had a bandwidth of only 0.3 Mc/s on the highest sensitivity range and therefore less sensitive settings were used which had bandwidths of above 1Mc/s. The input impedance of the A.C. amplifier is about 5MΩ and the output impedance is about 600Ω . This enables the output from the A.C. amplifier to be fed directly into the variable filter which has a 600Ω input impedance. It is worth noting that the strain gauge signal should not be fed directly into the low impedance input of the variable filter for the reasons discussed in section 3.1. On testing the amplifier, using the techniques described above for the source-follower unit, it was found that the only effect of the amplifier was to invert the signal.

The variable filter circuit could be used as a high-pass, low-pass or band-pass system although only the high-pass and low-pass systems were used in this work. The input and output impedance of the filter is 600Ω . The high and low pass cut-off frequencies can be varied between 9Kc/s and 675Kc/s. The filter was mainly used to attenuate high frequency signals which appear simultaneously with lower frequency components of

the stress wave being studied. The high frequency signals could be due to modes other than the one being studied or due to reflections from the end of the waveguide. The low-pass system was used in this case and care was taken to ensure that the filter did not affect the low frequency components of the signal being investigated. The variable filter was adjusted as follows. A part of the stress pattern which was relatively free from interference was selected. The cut-off frequency of the filter was then reduced until troublesome interference was removed from the lower frequency parts of the pattern. It was then assumed that if the predominant period of the selected part of the stress pattern was unaffected by the filter, used in this way, then parts of the pattern having longer predominant periods were also unaffected.

The filter was also used as a high-pass system in some cases. This system was used when we wished to attenuate the lower frequency parts of the stress pattern and observe the higher frequency parts.

The high-pass filter system shown in Figure 2.6 is used to attenuate low frequency signals caused by random mechanical disturbances of the rod. This system attenuates signals below 4Kc/s and therefore reduces movement of the oscilloscope trace. The high frequency components of the flexural stress pattern are generally of low amplitude and therefore the receiving apparatus must have a high sensitivity when making measurements

on these components. The 4Kc/s filter is therefore especially useful when observing the high frequency portion of the trace. Since the low frequency components are of relatively large amplitude the sensitivity of the receiving apparatus can be reduced and in this case the random mechanical disturbances are less troublesome. The high-pass filter system was tested using the techniques described above for the source-follower and A.C. amplifier. No phase change was observed when signals of 10Kc/s and above were passed through the filter and no change in the stress wave pattern for predominant periods of less than 100 μsecs could be detected when the high-pass filter system was inserted between the variable filter and the oscilloscope. When making measurements on signals of frequency 10Kc/s and below (i.e. predominant periods of 100 μsecs and above) the 4Kc/s filter was removed.

The 50c/s hum rejector is used to cut cut signals due to elec tromagnetic pick-up at mains frequency. This system was tested for phase changes in the same way as those described above. No phase change or attenuation was observed at frequencies of 4Kc/s and above. The 50c/s pick-up is introduced at the strain gauge element and is therefore amplified with the signal. The hum rejector is therefore essential if accurate measurements are to be made on the stress pattern.

3.4 ARRIVAL TIME MEASUREMENTS

The variable delay generator is used in conjunction with the time markers from the time mark generator to make accurate measurements of arrival time t and predominant period T_p of a signal arriving at a strain gauge element after travelling a distance x, from the point of initiation, along the central elastic line of the waveguide.

The sweep rate of the oscilloscope trace was first calibrated using the time mark generator, which had been calibrated against a standard frequency. This was done by setting the time marks to be coincident with the graticule lines of the oscilloscope. The sweep rates used varied from 5 μsecs/cm to 200 μsecs/cm, the sweep rate being calibrated on each occasion. When making measurements on the stress wave pattern it was found convenient to use the upper trace of the oscilloscope to display the time markers and the lower to display the stress pattern. The two traces were checked on all time base ranges to ensure that they had the same sweep rate. This was done by simultaneously applying the time mark signal to both traces and checking for coincidence.

Figure 3.2 represents the oscilloscope trace of a dispersed stress pulse together with the time markers from the time mark generator. A signal indicating the instant of

Arrival time measurements

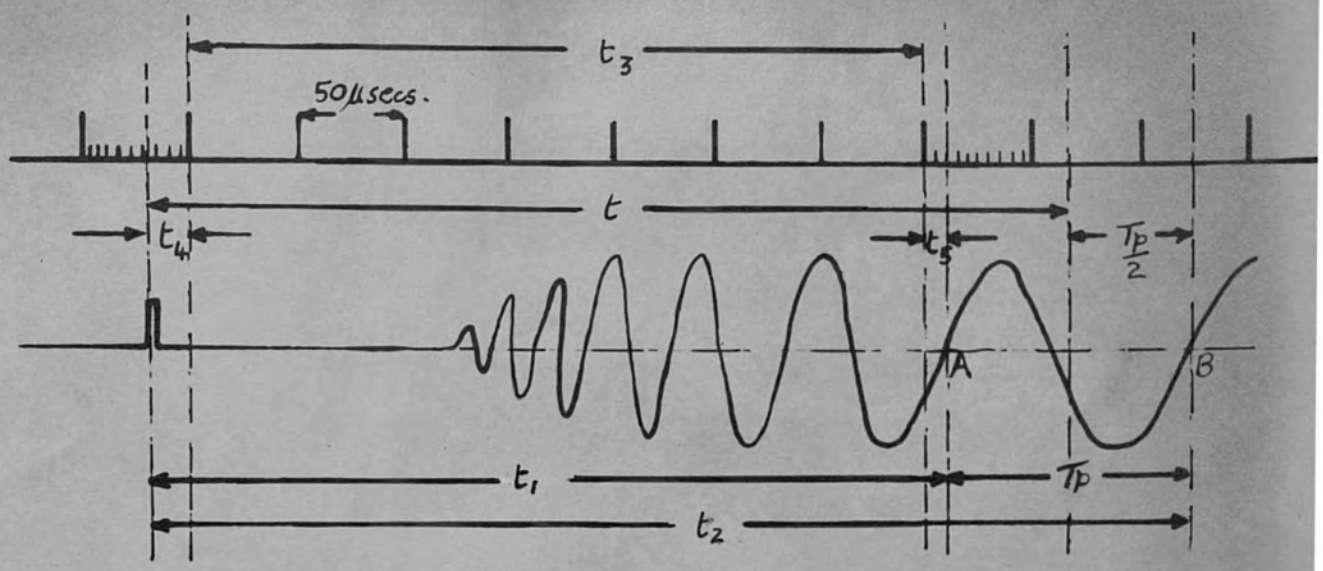

FIGURE 3.2

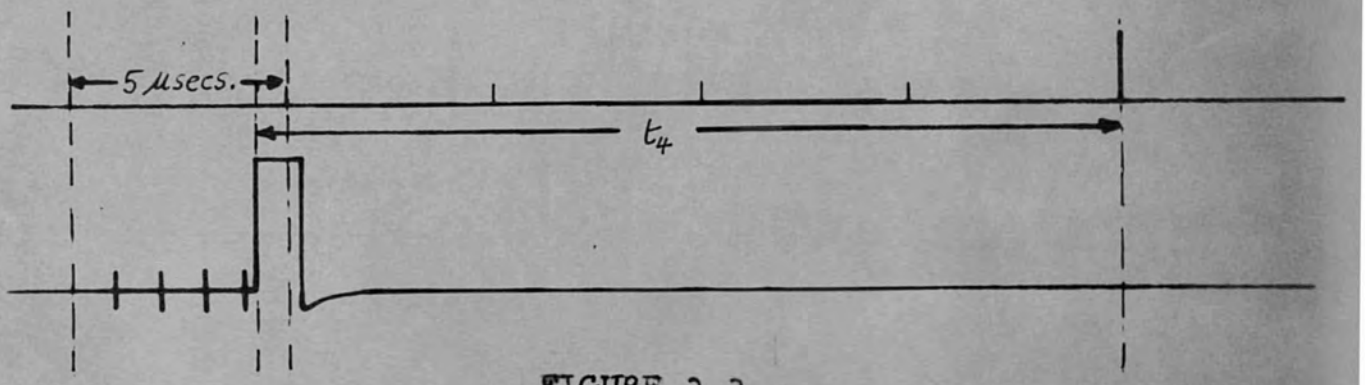

FIGURE 3.3

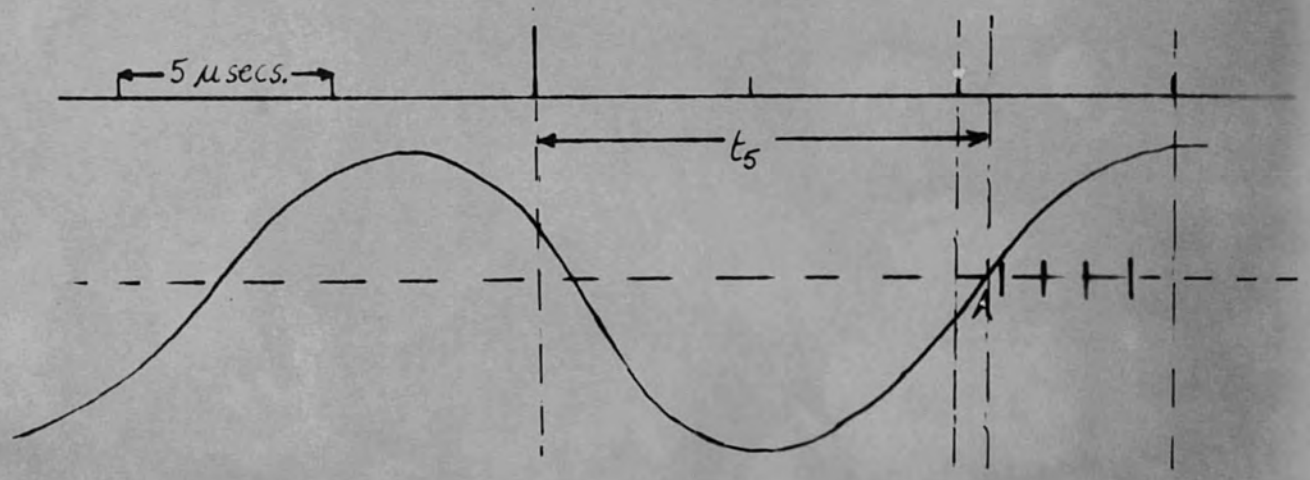

FIGURE 3.4

initiation of the stress pulse appears on the initial portion of each trace. This signal is a direct electromagnetic signal picked up by the strain gauge: a coaxial cable was connected from the pulse generator to a point near the strain gauge so that a clear pick-up signal was obtained. To measure the arrival time t and the predominant period T_p of a portion of the signal the time intervals t_1 and T_p must be measured accurately. To measure time interval t_1, the number of 50 μsec time markers contained between the pick-up signal and the cross-over point A were counted and therefore the time interval t_3 was accurately known. It was found convenient to measure to a cross-over point of the stress pattern; that is where the stress pattern intersects the line of zero strain amplitude. It then remained to measure accurately times t_4 and t_5. To do this the sweep rate was set to 5 μsecs/graticule division and the pick-up signal was brought onto the screen by adjusting the variable delay generator. One of the horizontal lines of the oscilloscope graticule had markings at intervals of $^1/_5$ of a graticule division and therefore each of these small divisions corresponded to a time duration of 1 μsec. The zero strain line of the stress pattern was positioned to coincide with the divided graticule line. The time interval t_4 could then be estimated to within 0·25 μsecs as indicated in Figure 3.3. The variable delay generator was then adjusted to bring the cross-over point A

onto the screen. The time interval t_5 could then be estimated to within 0·25 μsecs as indicated in Figure 3.4. The time interval t_1 is therefore known to within 0·5 μsecs. The time interval between cross-over points A and B was measured directly using the 5 μsec/graticule division sweep rate. Cross-over point A was positioned to coincide with a graticule line. The time interval between this graticule line and cross-over point B could then be estimated to within 0·25 μsecs. This time interval was taken to be the predominant period T_p of a group of waves arriving at the strain gauge a time $t = t_1 + \frac{T_p}{2}$ after the initiation of the stress pulse. Further into the stress pattern of the first flexural mode the predominant period increases to over 100 μsecs and therefore, in order to measure the predominant period the sweep rate of the oscilloscope trace was reduced. The validity and interpretation of this method of measurement is discussed in Chapter 6.

3.5 PHOTOGRAPHIC RECORDS

Experimental readings of arrival time and predominant period were taken directly from the oscilloscope screen. Photographic records of the stress pattern for various waveguides were taken using a polaroid camera. For this purpose the aperture of the camera was fully opened. The camera shutter

could be opened and closed by successive operations of the shutter control lead. The sweep repetition frequency was set to one sweep per second. Since the trace could not be seen when the camera was attached to the oscilloscope, use was made of the neon indicator lights on the delay generator unit which flashed each time the oscilloscope time base was triggered. In this way a single sweep of the stress pattern could be photographed.

CHAPTER FOUR

EXPERIMENTAL RESULTS

In this chapter the experimental results obtained using the techniques described in chapters 2 and 3 are discussed and photographic records of the resulting stress pulses are shown.

4.1 THE STRAIGHT ROD

a) THE LONGITUDINAL MODE

Preliminary experiments on straight rods were carried out in order to try different techniques and also to assess the general accuracy of the methods used.

The first experimental records were taken from the 1.27 cm. ($\frac{1}{2}$ inch) diameter rod of silver steel. A record of the pulse obtained at 300 cm. along the rod, when excited by the electrostrictive transducer using the techniques described in section 2.1, is shown in the lower trace of Figure 4.1. The transducer was excited by a 200 volt square pulse of 3 μsec. duration and positioned for the preferential excitation of the longitudinal modes. The upper trace of Figure 4.1 shows the time markers which are 10 μsecs. apart. It can be seen from this record that the predominant period decreases with increase

The dispersed longitudinal pulse in the ½ inch diameter straight rod

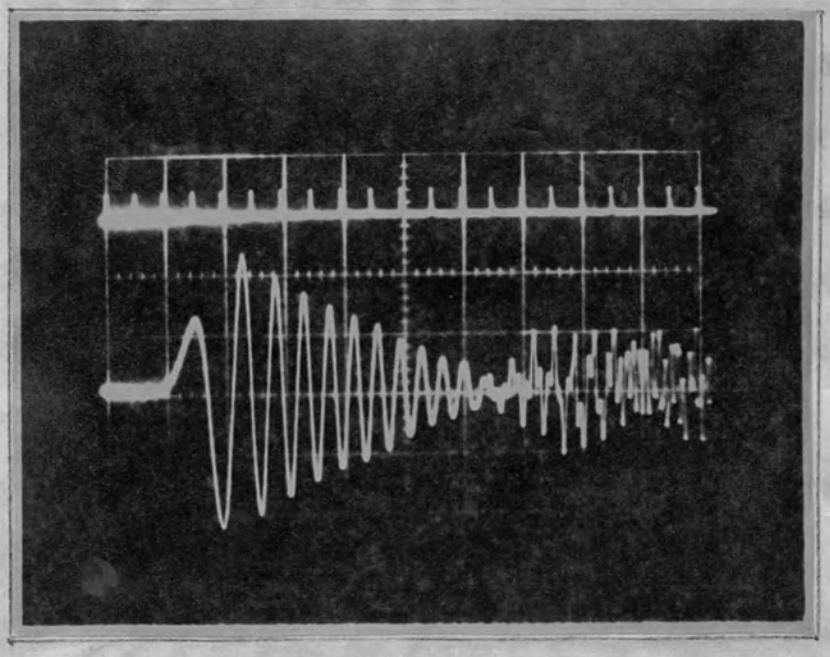

Upper trace - Time markers 10 μsecs. apart

Lower trace - Pulse received at x = 300 cm.

FIGURE 4.1

of arrival time. Approximately 100 μsecs. after the beginning of the dispersed pulse, interference begins and from this point it appears that at least two modes of vibration are present. This agrees with the results obtained by other investigators [Oliver 1957]. It can also be seen from the record that most of the dispersion of the longitudinal modes in a ½ inch diameter straight rod occurs in a region where the predominant period is less than 20 μsecs. which, according to the exact theory, corresponds to a region where $a/\lambda > 0.4$. The wavelengths of the most dispersive part of the stress pulse are therefore comparable with the length of the strain gauge and, as indicated in section 3.1, it is advisable to use shorter strain gauges to study this short wavelength dispersion pattern. The effect of curvature of the waveguide on the first longitudinal mode is expected to be pronounced at much longer wavelengths; that is, in a region where there is very little dispersion for the case of a straight guide. It is, however, worth recording the above trace for comparison purposes.

b) THE FLEXURAL MODE

To study the dispersion of the first flexural mode in a straight rod the 0.64 cm. (¼ inch) diameter rod of silver steel was used and the magnetostrictive wire method of generation employed (Figure 2.2). Figure 4.2 shows the mechanical pulse received by a strain gauge attached close to the generation end

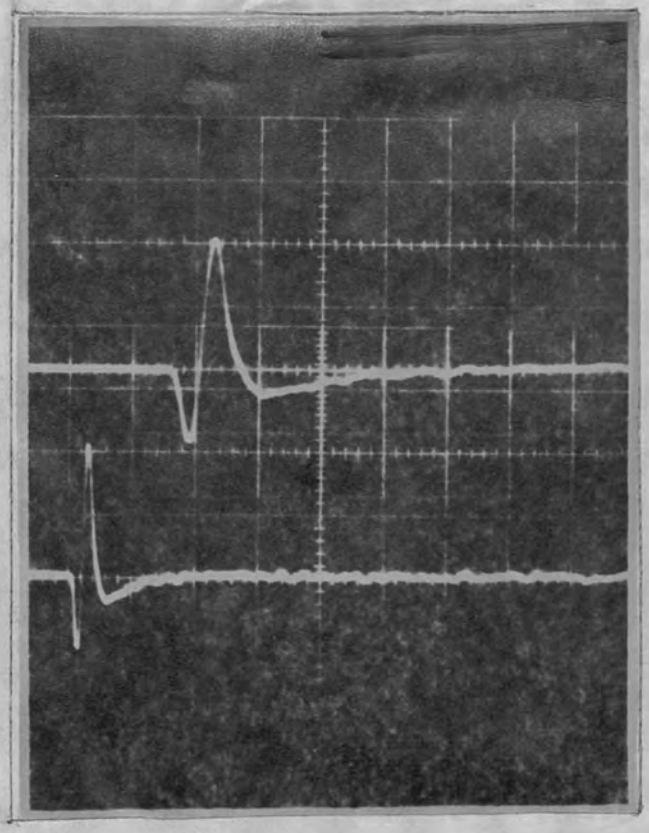

Upper trace -

20 μsecs./graticule division

Lower trace -

50 μsecs./graticule division

The initial pulse in the rod
FIGURE 4.2

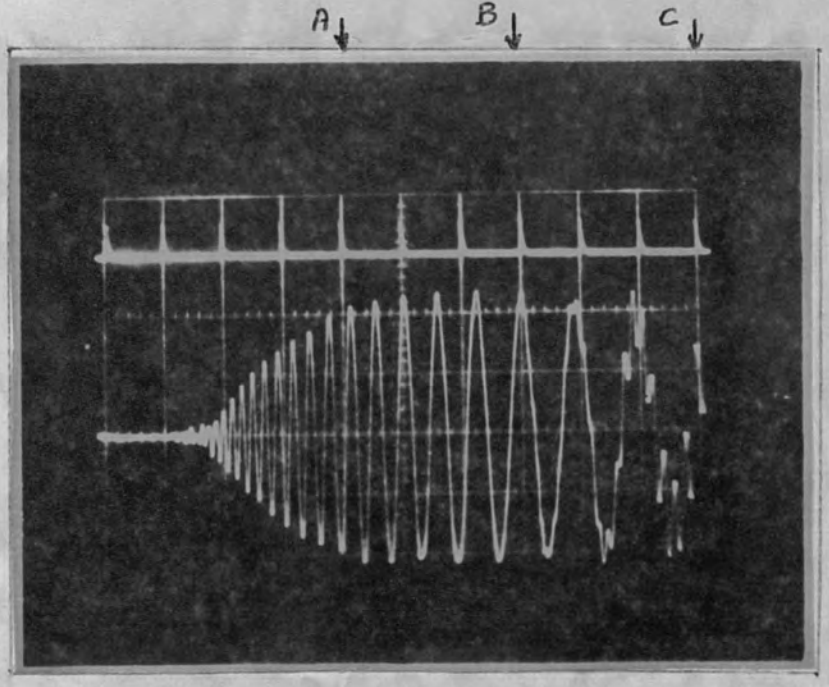

Upper trace - Time markers 100 μsecs. apart

Lower trace - Pulse received at x = 150 cm.
FIGURE 4.3

of the rod when a square electrical pulse of 6·4 μsecs. duration was applied to the 3·5 cm. transducer coil. The sweep rates of the upper and lower traces were 20 and 50 μsecs/graticule division respectively. The gauge was attached to the opposite side of the rod from the generating transducer.

It is seen that the initial flexural pulse in the rod differs slightly from the mechanical pulse in the nickel wire (Figure 2.9). The main pulse is still of about 20 μsecs. duration but there is also a tail to the pulse of about 30 μsecs. duration. This could be due to the very slow, long period, flexural waves or to end resonance effects of the rod. It can be seen from the lower trace of Figure 4·2 that the spurious ripple is well down on the main pulse height.

The mechanical pulse was also received at a distance of 150 cm. from the generation end of the rod, this distance being measured to the mid-point of the strain gauge. The pulse profile received is shown in Figure 4·3; the time markers are 100 μsecs. apart. It can be seen immediately that the predominant period increases with increase of arrival time and that reflections from the end of the rod, or other modes of propagation, make their appearance about 600 μsecs. after the initial part of the flexural stress pattern. Figure 4.4 shows the direct electromagnetic pick-up pulse which is used as a zero time marker and also a small disturbance which arrives about 300 μsecs. after

The flexural pulse in the $\frac{1}{4}$ inch diameter straight rod

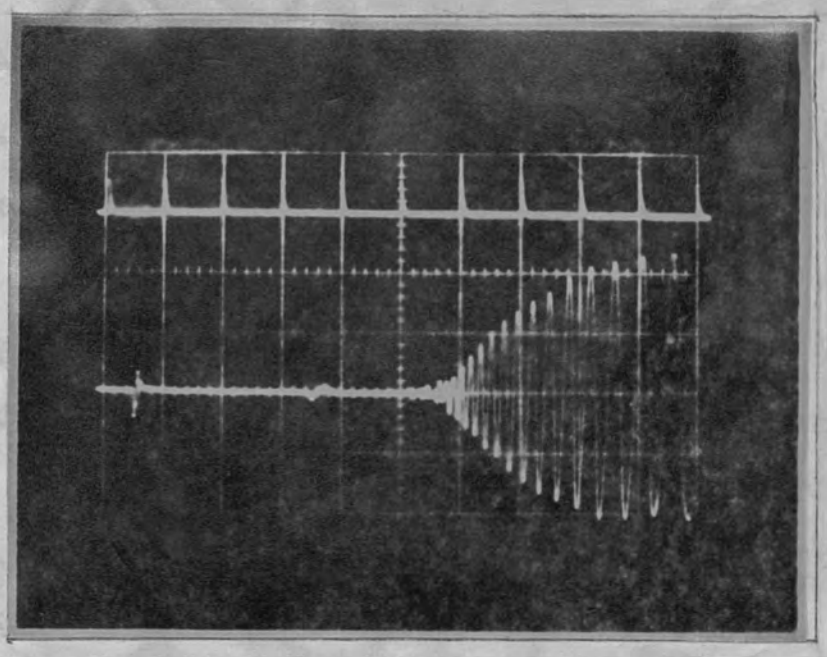

Upper trace - Time markers 100 μsecs. apart
Lower trace - Pulse received at x = 150 cm. together with the direct electrical pick-up pulse.

FIGURE 4.4

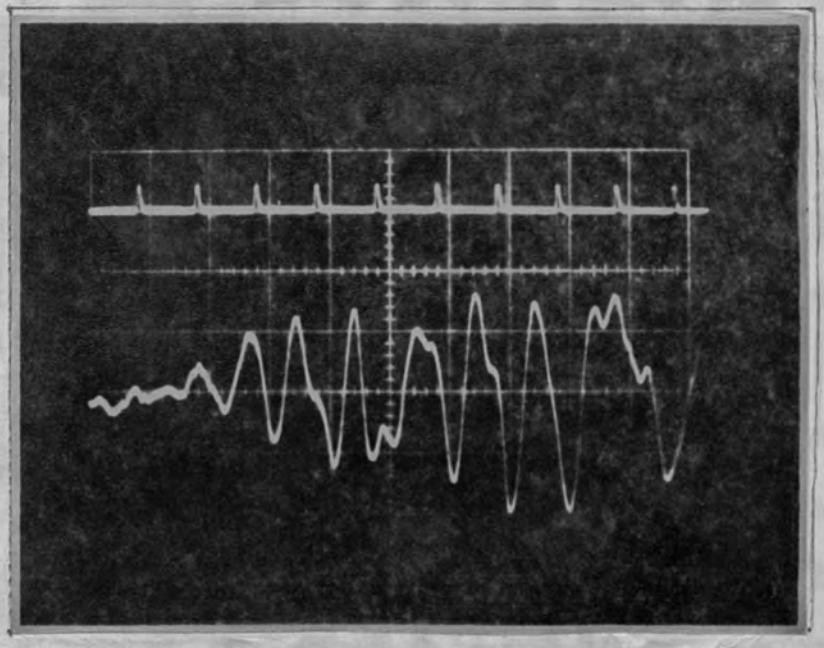

Upper trace - Time markers 5 μsecs. apart
Lower trace - Initial section of pulse at x = 150 cm.

FIGURE 4.5

the pick-up pulse. This disturbance is probably due to the faster longitudinal modes which are unavoidably excited but since they are of small amplitude they do not affect measurements on the flexural stress pattern. Figure 4.5 shows the initial portion of the dispersed pulse of Figure 4.3 on a much increased amplification setting of the receiving apparatus; the time markers are 5 μsecs. apart. It is seen that at least two components are present. The predominant period of one appears to increase with increased arrival time while that of the other appears to decrease. The initial predominant period is about 4 μsecs. and this, according to the exact theory, corresponds to a region where a/λ is about 0.2. For values of $a/\lambda > 0.2$ the wavelength becomes comparable with the length of the strain gauge and therefore no quantitative measurements were made on the high frequency component where the predominant period was less than 4 μsecs.

Figure 4.6 shows a portion of the flexural stress pattern of Figure 4.3 which is free from interference due to other modes and reflections from the end of the rod; the time markers are 10 μsecs. apart. Figure 4.7 illustrates the use of the variable filter to cut out unwanted interference from the record. The top trace shows a portion of the flexural stress pattern of Figure 4.3 where interference begins to appear and the lower trace shows the signal after passing

The flexural pulse in the $\frac{1}{4}$ inch diameter straight rod

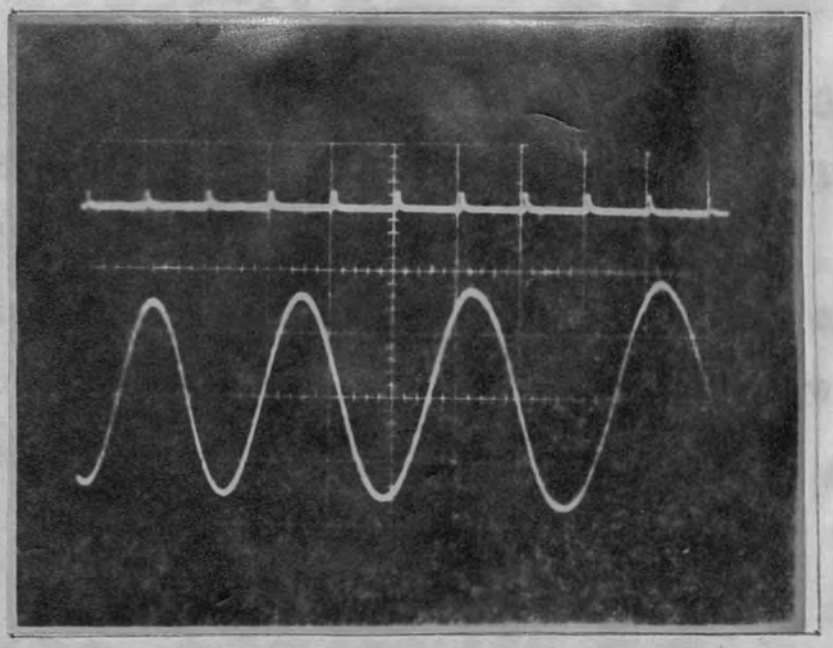

Upper trace - Time markers 10 μsecs. apart
Lower trace - A section of the pulse at x = 150 cm. which is free from interference. THE TRACE CORRESPONDS TO A SECTION OF THE PULSE BETWEEN A AND B IN FIGURE 4.3.

FIGURE 4.6

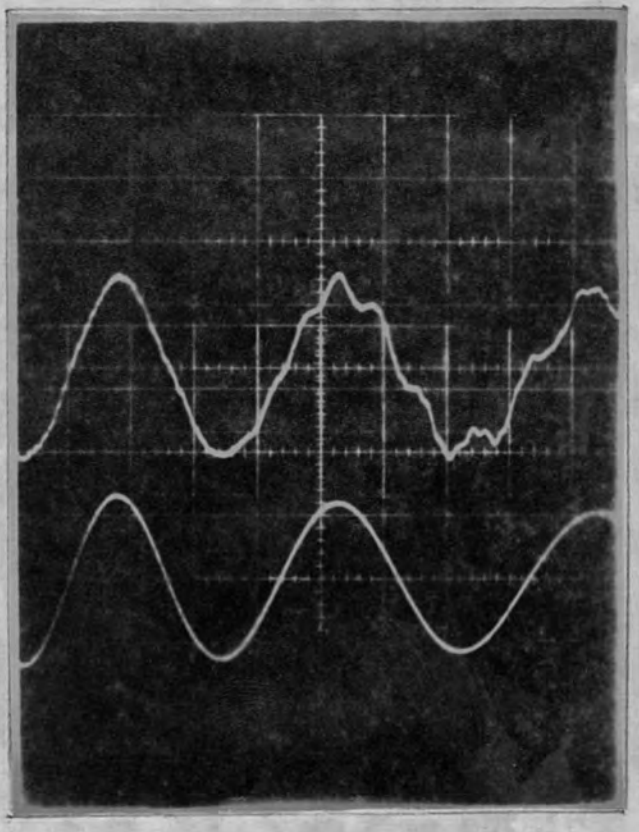

Upper trace - Without the variable filter

Lower trace - obtained using the variable filter

A section of the dispersed pulse at x = 150 cm. THE TRACE CORRESPONDS TO A SECTION OF THE PULSE BETWEEN B AND C FIGURE 4.3

FIGURE 4.7

through the variable filter; the sweep rate was 20 μsecs/ graticule division. In this case the variable filter was used as a low pass system.

Experimental results were taken from traces similar to those shown in the above records. The results are interpreted and discussed in Chapter 6.

4.2. THE HELICAL SPRING

a) THE LONGITUDINAL MODE

When studying the dispersed longitudinal mode we wish to make quantitative measurements on the low frequency (i.e. long period) portion of the stress pattern where the dispersion characteristics for the helical spring and the straight rod are expected to differ most. At high frequencies little difference is expected between the dispersion characteristics for the two cases and since we wish to study the lower frequency portion of the dispersed pulse the higher frequency disturbances are filtered out in the records shown unless otherwise stated.

Longitudinal pulses were introduced into helical springs using the magnetostrictive wire generation technique. For the preferential excitation of the longitudinal modes, the generating transducer was orientated in direction 1 Figure 2.5. Initial pulses similar to that shown for flexural waves in a straight rod (Figure 4.2) could be obtained by this method.

Figure 4.8 shows the dispersed pulse picked-up at a position $7\frac{3}{4}$ turns (148·9 cm.) from the excitation end of spring A, for which a/R = 0·106, P = $\frac{1}{2}$ inch and α = 3·9°; the initial pulse was of approximately 20 μsecs. duration. The electromagnetic pick-up pulse is shown on the left-hand portion of the trace and the time markers are 50 μsecs. apart. A difference can be seen immediately between this record and that for longitudinal waves in a straight rod (Figure 4.1). For a straight rod the lowest frequency longitudinal waves are the first to arrive. It is seen that this is not the case for longitudinal waves in a helical spring. Quantitative measurements were made on the record shown in Figure 4.8.

Longitudinal pulses were introduced into different springs in order to invesitgate the effects of changes of curvature and changes of pitch on the dispersion characteristics.

To investigate the effect of pitch the 20 μsec. mechanical pulse was introduced into springs C (a/R = $\frac{1}{8}$, P = $\frac{5}{16}$ inch α = 2·8°) and E (a/R = $\frac{1}{8}$, P = 1 inch, α = 9·0°). These springs have the same value of a/R but different pitches. Figure 4.9 shows the dispersed pulse at a position $12\frac{3}{4}$ turns (203·7 cm) from the excitation end of spring C; the time markers are 50 μsecs. apart. It can be seen that this record is similar to that obtained from spring A (Figure 4.8) and that about 200 μsecs. after the appearance of the fastest longitudinal

The dispersed longitudinal pulse in spring A

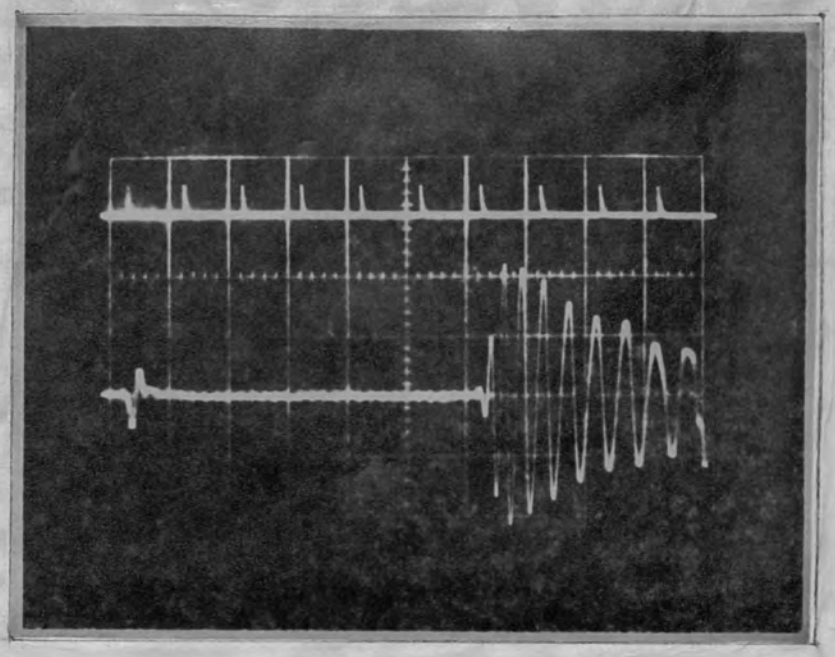

Upper trace - Time markers 50 μsecs. apart
Lower trace - The dispersed pulse at x = 148.9 cm.

FIGURE 4.8

The dispersed longitudinal pulse in spring C

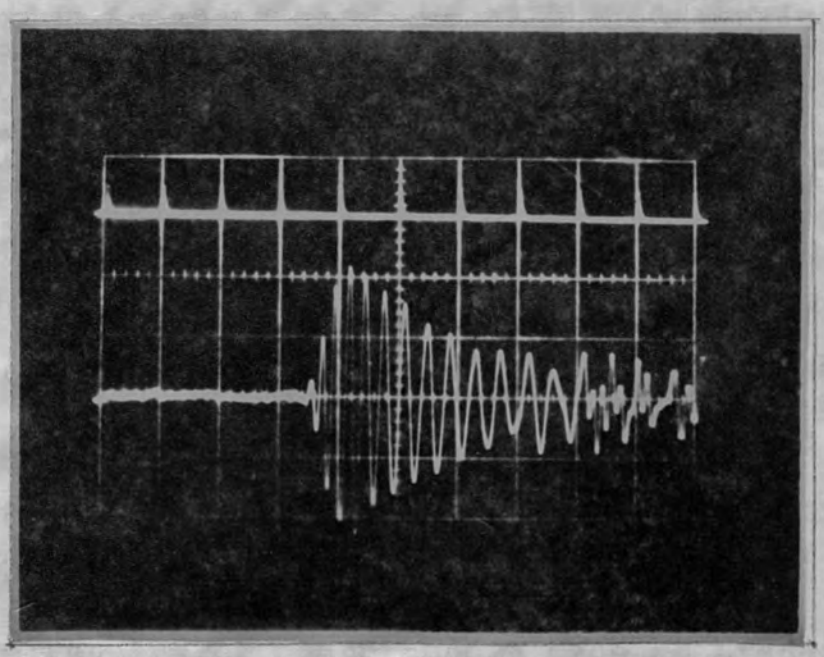

Upper trace - Time markers 50 μsecs. apart
Lower trace - The dispersed pulse at x = 203.7 cm.

FIGURE 4.9

mode other modes begin to arrive at the strain gauge. Figure 4.10 shows the dispersed pulse at a position 12¾ turns (206.1 cm.) from the excitation end of spring E. This record is similar to that shown in Figure 4.9 and therefore quantitative measurements on the records shown in Figures 4.9 and 4.10 were necessary in order to show any effect of increased pitch angle

•

To investigate the effect of curvature, the 20 μsec. mechanical pulse was introduced into spring I ($a/R = 1/16$, $P = 5/16$ inch, $\alpha = 1.4^{\circ}$). Figure 4.11 shows the dispersed pulse at a position 6¾ turns (215.5 cm.) from the excitation end of the spring; the time markers are 50 μsecs. apart. The predominant period of the fastest longitudinal mode in this spring is about the same as that in springs A, C and E but the predominant period increases much more rapidly with arrival time. Quantitative measurements were made on the record shown in Figure 4.11.

It will be remembered that in all the above records the high frequency components of the first longitudinal mode have been filtered out. Figure 4.12 is included to show the form of the pulse, corresponding to that shown in Figure 4.8, when the variable filter is not in use.

The results of measurements made on traces similar to those shown in the above records are interpreted and discussed

The dispersed longitudinal pulse in spring E

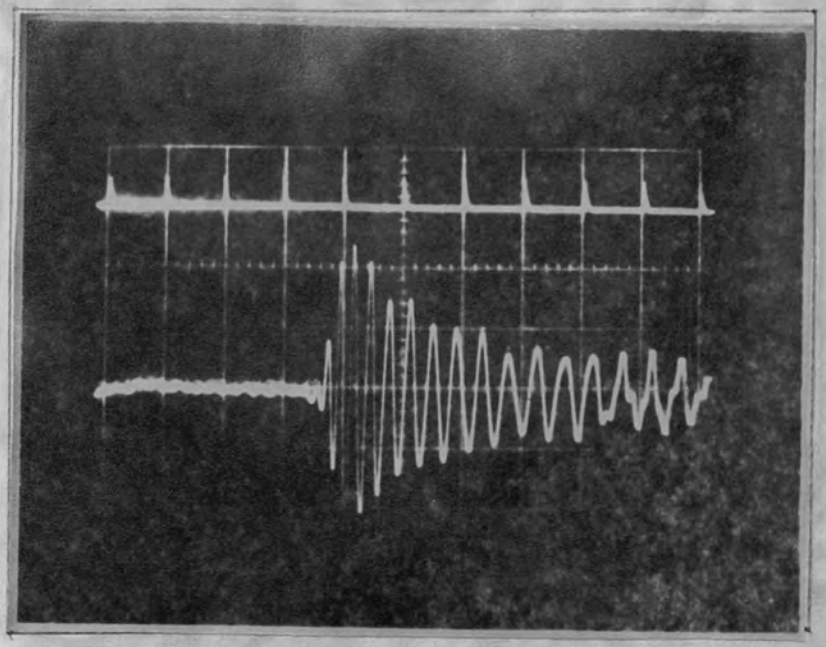

Upper trace - Time markers 50 μsecs. apart
Lower trace - The dispersed pulse at x = 206.1 cm.

FIGURE 4.10

The dispersed longitudinal pulse in spring I

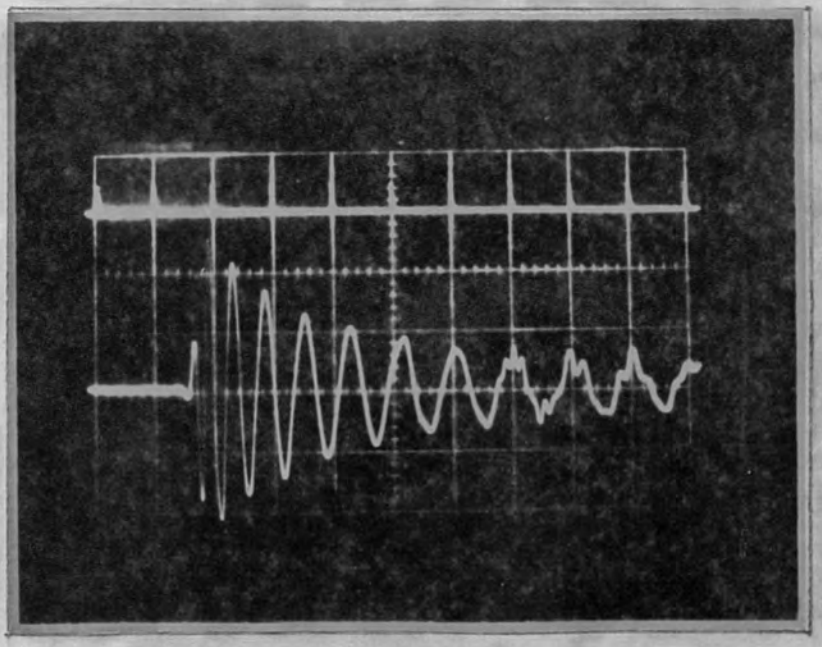

Upper trace - Time markers 50 μsecs. apart
Lower trace - The dispersed pulse at x = 215.5 cm.

FIGURE 4.11

The dispersed longitudinal pulse in spring A obtained without using the variable filter

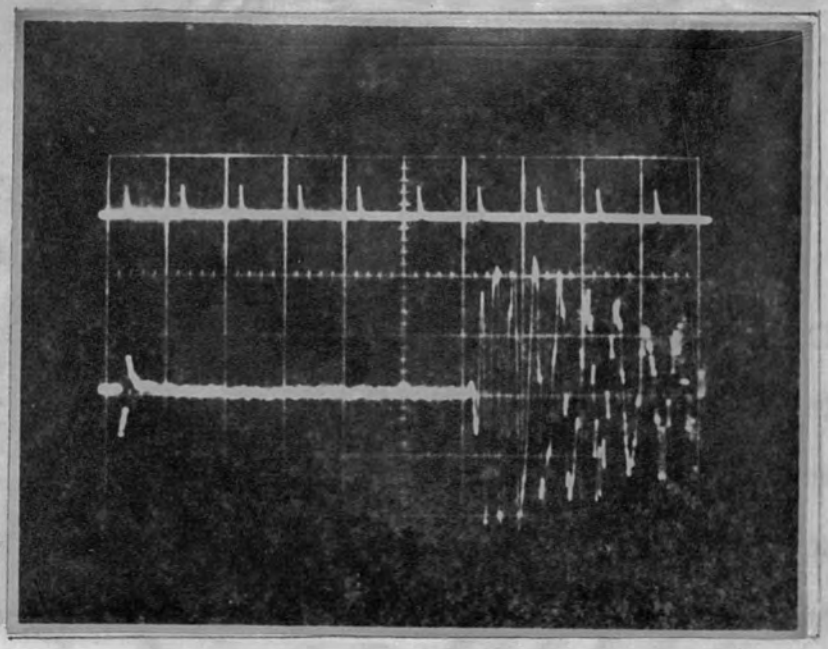

Upper trace - Time markers 50 μsecs. apart
Lower trace - The dispersed pulse at x = 148.9 cm.

FIGURE 4.12

Flexural pulse in spring A excited in direction 2 Fig. 2.5

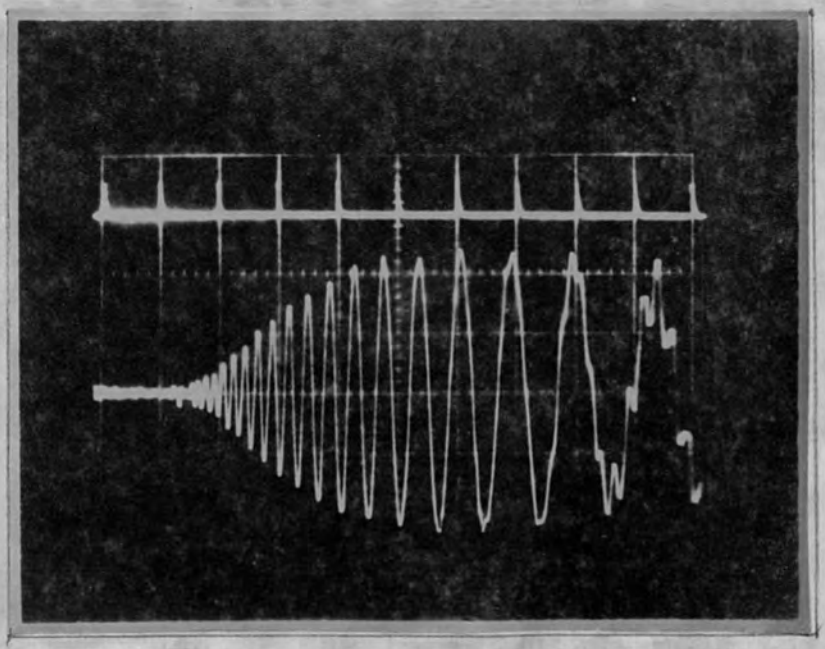

Upper trace - Time markers 100 μsecs. apart
Lower trace - The dispersed pulse at x = 153.7 cm.

FIGURE 4.13

in Chapter 6.

b) THE FLEXURAL MODE - FASTER WAVE (VIBRATIONS IN THE PLANE OF THE RING)

The magnetostrictive wire method of generation was again used to excite flexural modes in the helical springs. For preferential excitation of the faster flexural mode the generating transducer was orientated in direction 2 Figure 2.5. The initial pulses in the springs were similar to that shown for flexural waves in a straight rod (Figure 4.2).

Figure 4.13 shows the dispersed pulse at a position 8 turns (153.7 cm.) from the excitation end of spring A (a/R = 0.106, P = ½", α = 3.9°); the time markers are 100 μsecs. apart. The initial pulse in the rod was again of approximately 20 μsecs. duration. It is seen that generally the dispersion pattern is similar to that obtained for a straight rod (Figure 4.3). Qualitatively it seems that, in the case of spring A, the predominant period increases more rapidly with increasing arrival time than in the case of the straight rod but a more quantitative analysis is required. Measurements of predominant period and arrival time were made on the record shown in Figure 4.13.

As in the case of the longitudinal mode the flexural pulses were introduced into different springs in order to test the

effect of curvature and pitch on the dispersion characteristics.

To investigate the effects of pitch the 20 μsec. mechanical pulse was introduced into springs C ($a/R = \frac{1}{8}$, P = $5/16$ inch, $\alpha = 2.8^{\circ}$), D ($a/R = \frac{1}{8}$, P = $\frac{1}{2}$ inch, $\alpha = 4.6^{\circ}$) and E ($a/R = \frac{1}{8}$, P = 1 inch, $\alpha = 9.0^{\circ}$). Again the generating transducer was orientated for the preferential excitation of the faster flexural mode. Springs C, D and E are much longer than spring A and therefore the receiving strain gauge can be positioned much further from the excitation end of the spring without decreasing the portion of the stress pattern that can be studied before reflections from the far end of the spring make their appearance. Figure 4.14 shows the dispersed stress pulse at a position 13 turns (207.7 cm.) from the excitation end of spring C; the time markers are 100 μsecs. apart. It can be seen that generally there is little difference between this trace and that for spring A (Figure 4.13) apart from a small pulse which preceeds the main flexural pattern. This small pulse could be due to beating between two disturbances of nearly equal period. Theory predicts that, in the initial part of the flexural pattern, two waves of nearly equal frequency are present, one being due to the lower frequency part of the dispersion curve and the other due to a comparatively short high frequency region (see chapter 5). Quantitative measurements were made on the lower frequency component of the trace shown in Figure 4.14.

Flexural pulse in spring C excited in direction 2 Fig. 2.5

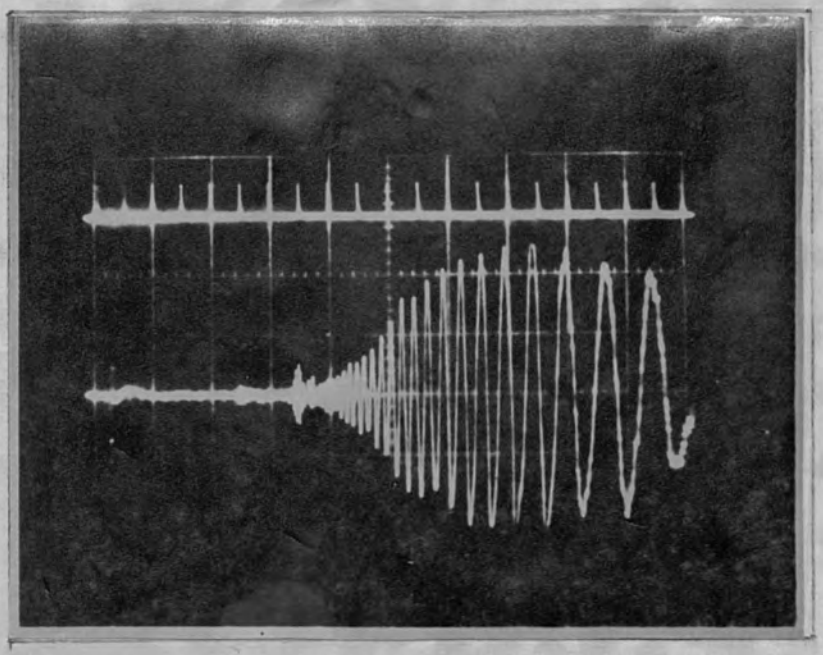

Upper trace - Time markers 100 μsecs. apart
Lower trace - The dispersed pulse at x = 207.7 cm.

FIGURE 4.14

Flexural pulse in spring D excited in direction 2 Fig. 2.5

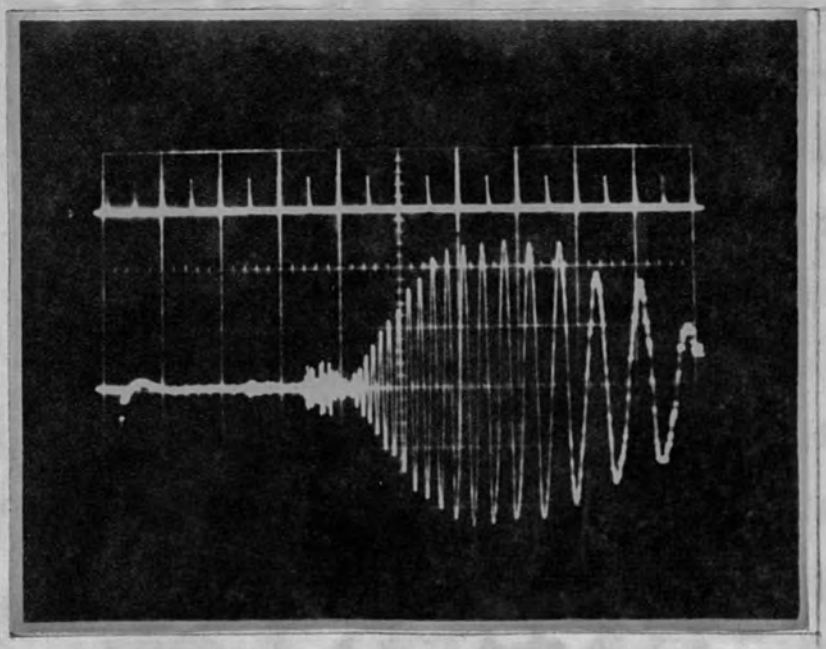

Upper trace - Time markers 100 μsecs. apart
Lower trace - The dispersed pulse at x = 208.1 cm.

FIGURE 4.15

Figure 4.15 shows the dispersed pulse at a position 13 turns (208·1 cm.) from the excitation end of spring D; the time markers are 100 μsecs. apart. Generally there is little difference between the low frequency dispersion patterns obtained from springs C and D and therefore quantitative measurements were necessary in order to show the effects of pitch angle α. It is observed, however, that in the case of spring D the amplitude of the stress pattern falls more rapidly from the maximum than in the case of spring C. This effect will be discussed further in chapter 6.

Figure 4.16 shows the dispersed stress pulse at a position 13 turns (210·1 cm.) from the excitation end of spring E; the time markers are 100 μsecs apart. It is seen immediately that about 600 μsecs. after the arrival of the initial part of the flexural mode pattern the amplitude falls rapidly. The amplitude then increases to a second maximum about 600 μsecs. later. It appears from this record that two modes of similar predominant period are arriving simultaneously at the strain gauge over the entire section of the stress pattern shown. This would indicate the presence of two modes with dispersion characteristics which are very close over the whole range of frequencies considered; this will be discussed further in chapter 6. Quantitative measurements were made on the trace shown in Figure 4.16.

Flexural pulse in spring E excited in direction 2 Fig. 2.5

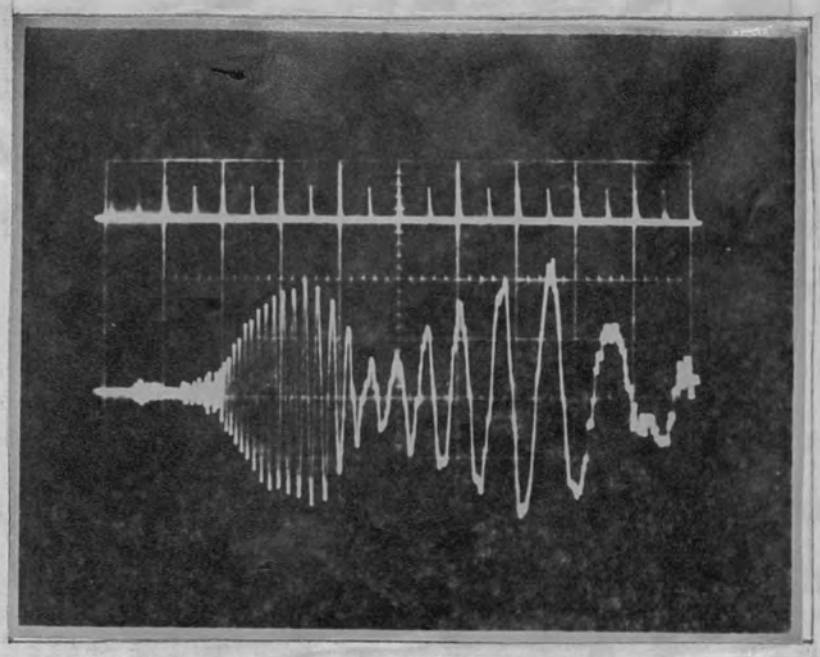

Upper trace - Time markers 100 usecs. apart
Lower trace - The dispersed pulse at x = 210.1 cm.

FIGURE 4.16

Flexural pulse in spring F excited in direction 2 Fig. 2.5

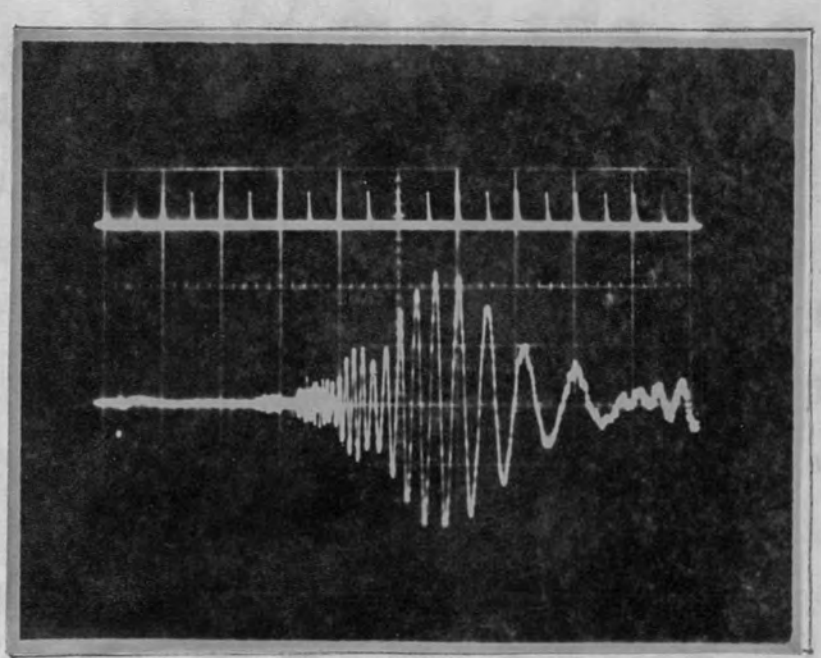

Upper trace - Time markers 100 usecs. apart
Lower trace - The dispersed pulse at x = 200.5 cm.

FIGURE 4.17

To investigate the effects of pronounced curvature on the faster flexural wave dispersion curve for a helical spring the 20 μsec. mechanical pulse was introduced into spring F ($a/R = \frac{1}{4}$, P = $5/16$ inch, $\alpha = 5{\cdot}7^{\circ}$). Figure 4.17 shows the dispersed pulse received at a position 25 turns (200·5 cm.) from the excitation end of the spring; the time markers are 100 μsecs. apart. The dispersed pulse is much shorter than those received at similar distances from the ends of straight rods and helical springs of less pronounced curvature. The predominant period increases more rapidly with increasing arrival time and there is more irregularity in the trace. For large values of α it is difficult to excite only the faster flexural mode and therefore in the case of a spring where $a/R = \frac{1}{4}$ other modes are likely to be excited in appreciable amplitude. Quantitative measurements were made on the trace shown in Figure 4.17.

The 20 μsec. mechanical pulse was also introduced into springs G ($a/R = \frac{1}{4}$, P = $\frac{1}{2}$ inch, $\alpha = 9{\cdot}0^{\circ}$) and H ($a/R = \frac{1}{4}$, P = $\frac{3}{4}$ inch, $\alpha = 13{\cdot}4^{\circ}$). In both cases the stress pattern recorded, after 25 turns of the spring, had the same general characteristics as that obtained from spring F (Figure 4.17). Quantitative measurements were made on the stress patterns received in springs G and H.

The interpretation of the results obtained from

measurements on traces similar to those shown in the above records is discussed in chapter 6 where the effect of decreased radius (R) of the spring and increased pitch angle (α) is analysed.

c) THE FLEXURAL MODE - SLOWER WAVE (VIBRATIONS PERPENDICULAR TO THE PLANE OF THE RING)

In this case the 20 μsec. mechanical pulse, from the magnetostrictive wire, was introduced into the springs by orientating the transducing system in direction 3 Figure 2.5. We are now preferentially exciting the slower flexural wave by the application of stresses parallel to the axis of the spring, this will also tend to produce some torsion in the spring.

Figure 4.18 shows the dispersed pulse received at a position 8 turns (153·7 cm.) from the excitation end of spring A (a/R = 0·106, P = $\frac{1}{2}$ inch, α = 3·9°). For this record the variable filter was used as a low pass system to attenuate unwanted high frequency signals which interfere with the low frequency section of the dispersed pulse being studied; the time markers are 100 μsecs apart. It appears from the record that at least two modes are present over the whole range recorded. Figure 4.19 shows the initial part of the pattern on an expanded time base; the time markers are 10

Flexural pulse in spring A excited in direction 3 Fig. 2.5

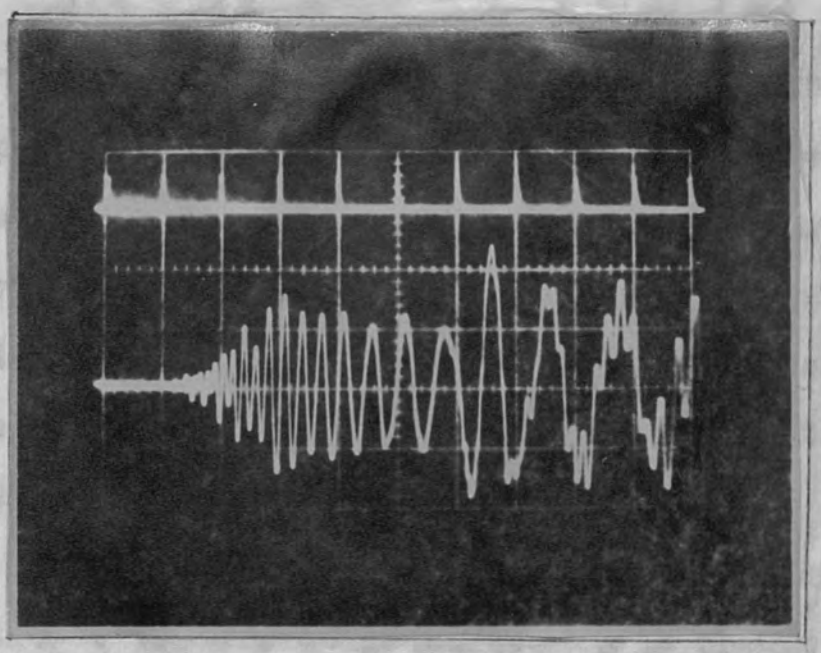

Upper trace - Time markers 100 μsecs. apart
Lower trace - The dispersed pulse at x = 153·7 cm.

FIGURE 4.18

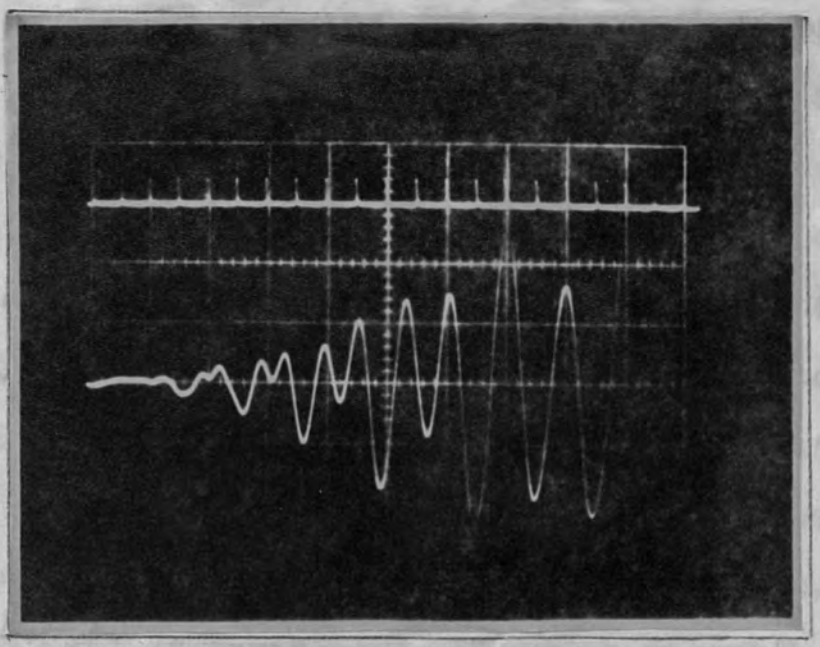

Upper trace - Time markers 10 μsecs. apart
Lower trace - Initial part of pulse at x = 153·7 cm.

FIGURE 4.19

μsecs apart. It is clear that the initial flexural pattern is accompanied by a signal of about twice its period. This low frequency signal was studied by reducing the cut-off frequency of the variable low pass filter so that the flexural oscillations were removed. Quantitative measurements were then made on the low frequency pattern. The interpretation of the results is discussed in chapter 6.

The latter part of the pulse, shown in Figure 4.18, indicates that there are at least two modes of similar period arriving simultaneously at the strain gauge over a large section of the dispersed pulse pattern. Quantitative measurements were made on the dispersed flexural pulse shown in Figure 4.18.

In order to check that the general shape of the stress pattern was not due to the initial pulse shape a $1/16$ inch diameter steel sphere was used to introduce the mechanical pulse into the spring. This was done by allowing the sphere to roll down a tube which was shaped so that the impact direction of the ball on the spring was in direction 3 Figure 2.5. The trigger pulse for the oscilloscope was obtained from a strain gauge placed near the impact end of the spring. The dispersed pulse at a position 8 turns (153·7 cm.) from the excitation end of spring A is shown in Figure 4.20. It is seen that the general shape of the pulse is independent of the

Flexural pulse in spring A excited in direction 3 Fig. 2.5 by the ball impact technique

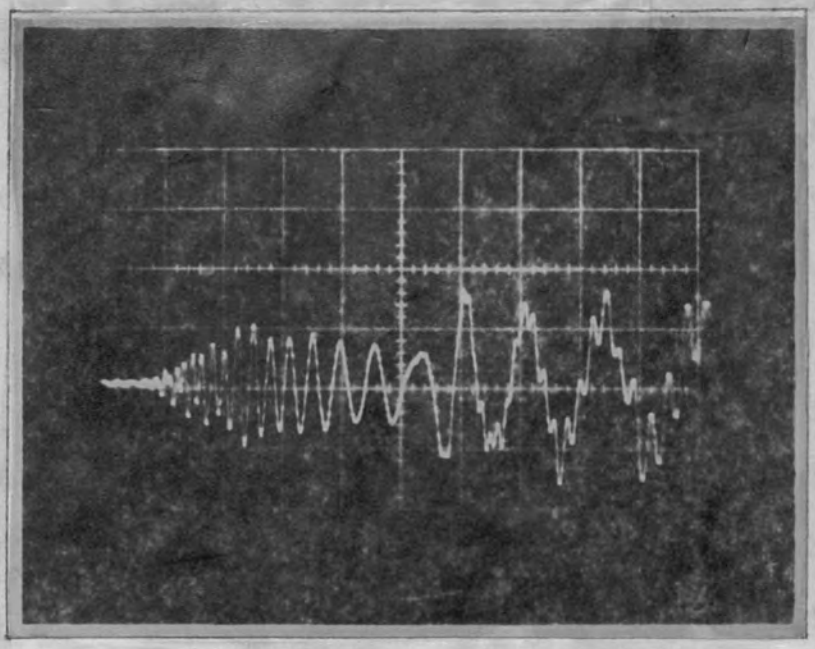

Sweep rate - 100 μsecs. per graticule division
The dispersed pulse at x = 153.7 cm

FIGURE 4.20

Flexural pulse in spring D excited in direction 3 Fig. 2.5

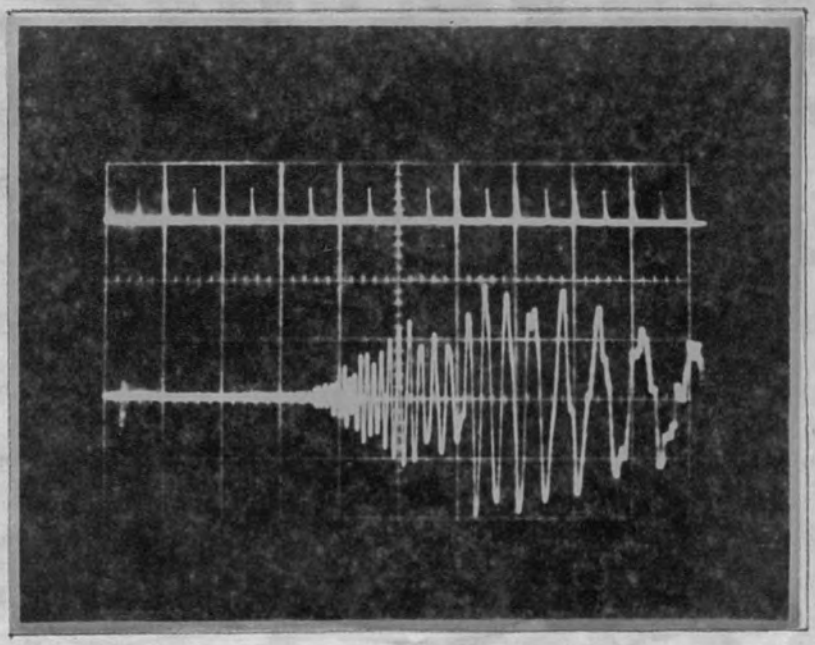

Upper trace - Time markers 100 μsecs. apart
Lower trace - The dispersed pulse at x = 208.1 cm.

FIGURE 4.21.

initial pulse shape. No filter was used for the record shown in Figure 4.20 which was obtained at a much earlier date than those recorded using the magnetostrictive wire technique.

To investigate further the low frequency oscillations appearing in the initial section of the dispersed pulse, which may be due to dispersion of the lowest torsional mode, the 20 μsec. mechanical pulse from the magnetostrictive wire was introduced into spring D ($a/R = \frac{1}{8}$, P = $\frac{1}{2}$ inch, $\alpha = 4.6^{\circ}$). Figure 4.21 shows the dispersed pulse at a position 13 turns (208.1 cm.) from the excitation end of the spring; the time markers are 100 μsecs. apart. It is seen that the pulse has the same general features as the pulse obtained from spring A (Figure 4.18). The initial part of the dispersed pulse again indicates the presence of two modes, one of which is about twice the frequency of the other, and the latter part again indicates that at least two modes of similar period arrive simultaneously at the strain gauge over a large section of the stress pattern shown. Quantitative measurements were made on the trace shown in Figure 4.21, the higher frequency flexural mode being filtered out when studying the low frequency component present in the initial section of the dispersed pulse. The results of the above measurements are discussed in chapter 6.

Figure 4.22 shows the dispersed pulse at a position 25

Flexural pulse in spring G excited in direction 3 Fig. 2.5

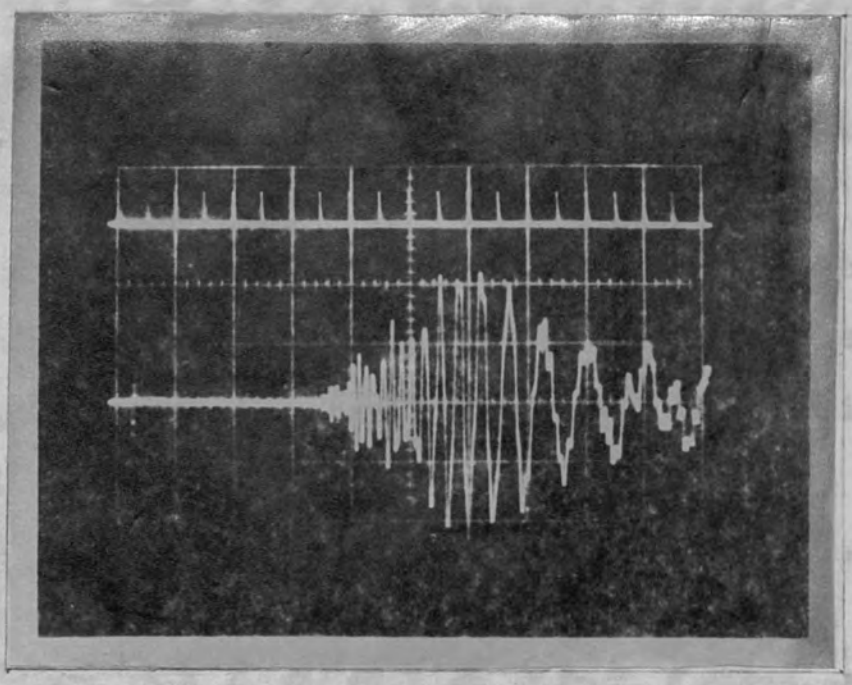

Upper trace - Time markers 100 μsecs. apart
Lower trace - The dispersed pulse at x = 202.0 cm.

FIGURE 4.22

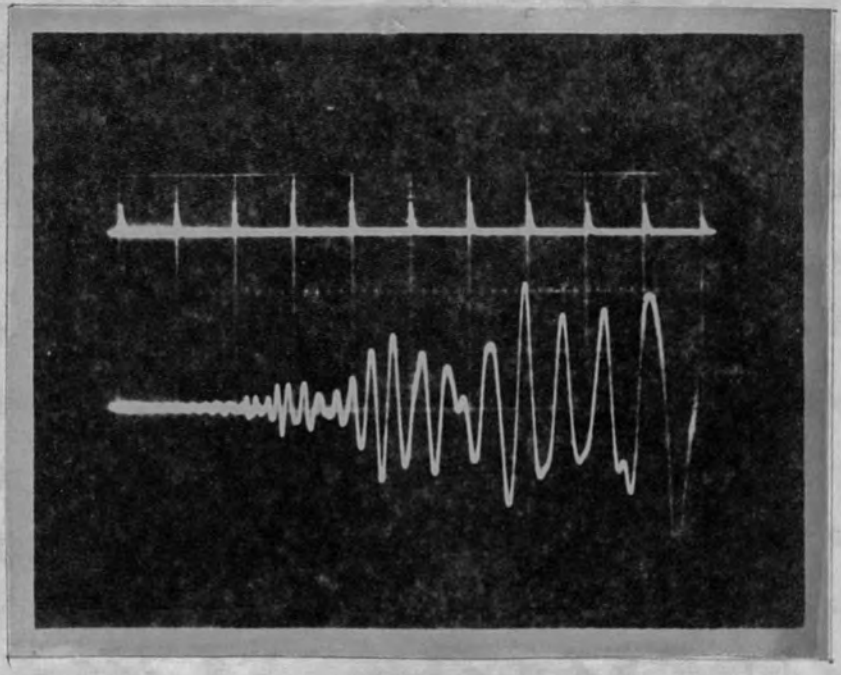

Upper trace - Time markers 50 μsecs. apart
Lower trace - The initial pulse at x = 202·0 cm.

FIGURE 4.23

turns (202·0 cm.) from the end of spring G ($a/R = \frac{1}{4}$, P = $\frac{1}{2}$ inch, $\alpha = 13{\cdot}4^{\circ}$); the initial mechanical pulse in the guide was again of approximately 20 μsecs. duration. The time markers shown on the upper trace of Figure 4.22 are 100 μsecs. apart. Again it is seen that the dispersed pulse is irregular which indicates the presence of at least two modes of similar period arriving simultaneously at the strain gauge. The initial section of the dispersed pulse pattern is shown in Figure 4.23; the time markers are 50 μsecs. apart. As discussed above, the corresponding section of the flexural stress pattern obtained in spring A (Figure 4.19) is accompanied by a component of longer predominant period; this low frequency component was also observed in spring D. The record shown in Figure 4.23, however, gives no indication of this longer predominant period component but there is evidence of a mode which has a similar predominant period to the flexural mode over the initial section of the dispersed pulse pattern. This undefined mode has a dispersion pattern which increases in period with increase of arrival time but at a much slower rate than the flexural pattern. The predominant period then becomes fairly constant with increasing arrival time. In order to study this mode in more detail the lower frequency (longer period) flexural modes were filtered out using the variable filter as a high pass system. Figure 4.24 shows the portion of the stress pattern where the

The high frequency component of the pulse in spring G excited in direction 3 Figure 2.5

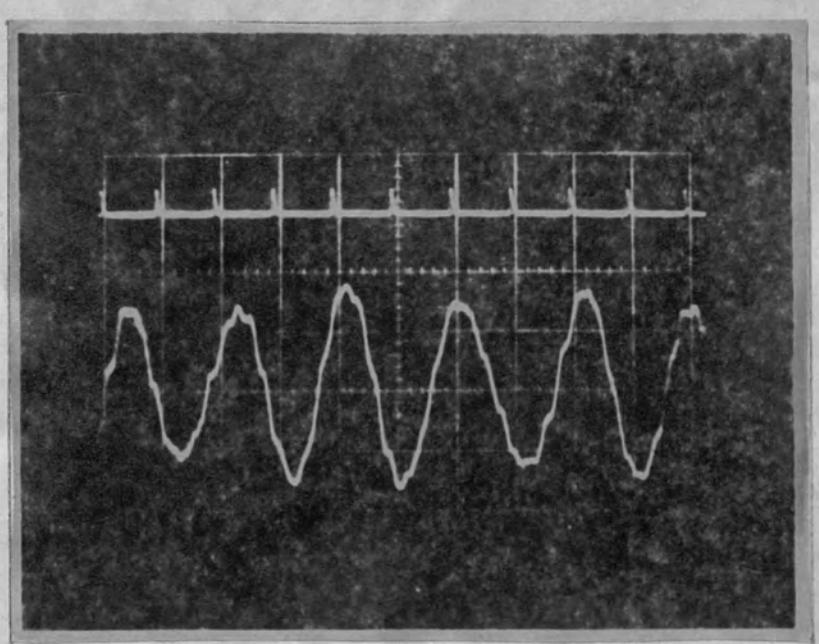

Upper trace - Time markers 10 μsecs. apart

Lower trace - The dispersed pulse at x = 202·0 cm.

FIGURE 4.24

undefined mode has an almost constant predominant period; the time markers are 10 μsecs. apart. The predominant period of the undefined mode in the region shown is therefore about 19 μsecs. Since this mode has almost constant predominant period, apart from in the initial section of the pattern where the period was comparable with that of the flexural modes, no further quantitative measurements were made. Quantitative measurements were made on the flexural mode pattern shown in Figure 4.22. The results of these measurements are discussed in chapter 6.

The stress patterns obtained from springs A, D and G (Figures 4.18, 4.21 and 4.22 respectively) all indicate that at least two modes of similar predominant period arrive simultaneously at the strain gauge over the whole section of the dispersed pulse considered. By exciting the springs in direction 3, Figure 2.5, both the faster and slower flexural modes may be excited in appreciable amplitude and there is also evidence of another dispersive mode. In order to attach the receiving strain gauge in the position indicated in Figure 2.5 it was necessary to use springs of at least $\frac{1}{2}$ inch pitch and, for these springs, it was not found possible to excite only the slower flexural mode. For this reason the effect of pitch angle (α) on the slower flexural dispersion characteristic was not investigated.

As discussed in chapter 3, the dispersed stress pulses are detected by means of surface strain gauges. The records discussed above therefore give no indication of the variation of stress amplitude over the cross-section of the waveguide which depends on the mode and frequency of the propagated wave [Davies 1948]. However, we are concerned with dispersion rather than stress amplitude measurements and the surface strain gauges should be satisfactory for our purposes especially in the low frequency region of the dispersed pulse patterns on which our quantitative measurements were made.

CHAPTER FIVE

THE THEORY OF THE PROPAGATION OF STRESS WAVES IN BOUNDED MEDIA

5.1 GENERAL

In general the propagation of elastic waves in a waveguide is a dispersive phenomena. One aim of the theory is to derive the characteristic, or dispersion, equations of the wave motion; these equations represent the relation between the phase velocity of the wave, the wavelength, the lateral dimensions of the solid and the mechanical properties of the material. In the exact theory the characteristic equations are derived by using the equations of motion of a solid from the general theory of elasticity and applying the boundary conditions appropriate to the geometry of the waveguide. The method is so complex that only in a few cases have the exact characteristic equations been obtained. A number of approximate theories have therefore been developed which can give a useful prediction of the dispersion characteristics of the lower modes of propagation in guides of various geometries. Some of the approximate theories, relevant to this work, are discussed below.

In order to assess the accuracy of the techniques used to obtain experimental values of predominant period and arrival time for various modes in a curved waveguide, preliminary experiments were carried out on a straight cylindrical rod. The exact theory equations have been solved for this case [Bancroft 1941, Hudson 1943, Abramson 1957] and therefore the experimental results obtained from the straight rod can be compared directly with the exact theory. It is also possible to compare the results of the approximate and exact theories in this case.

5.2 THE STRAIGHT ROD

a) FLEXURAL WAVES

For flexural waves in a straight rod three degrees of approximation are generally used. In the elementary theory it is assumed that the motion of the elements of the solid is a pure translation in a direction perpendicular to the direction of propagation of the wave. The next degree of approximation assumes that the elements undergo rotation as rigid bodies in addition to their lateral translation; the modification due to rotation is often called the rotary inertia correction. Finally there is an approximate theory, the Timoshenko theory [Timoshenko 1921 and 1922] , in which it is assumed that the elements are subject to shearing stresses in addition to lateral translation and rigid body rotation. This approach

leads to a characteristic equation which is a quadratic in $(C/Co)^2$ for each fixed value of a/λ, where C is the phase velocity of the stress wave and Co is the velocity of extensional waves of infinitely long wavelength in the guide. $Co = \left\{\frac{E}{\rho}\right\}^{\frac{1}{2}}$ where E is Young's modulus and ρ is the density of the material of the rod . The characteristic equation is given below.

$$\frac{E}{\kappa^2 G}\left(\frac{C}{Co}\right)^4 - \left[\frac{\lambda^2}{4\pi^2 Ko^2} + 1 + \frac{E}{\kappa^2 G}\right]\left(\frac{C}{Co}\right)^2 + 1 = 0 \qquad 6)$$

where G is the shear modulus, Ko is the radius of gyration of an element of the rod about an axis perpendicular to the plane of flexure and passing through the central elastic line of the rod and κ^2 is a constant whose value depends on the distribution of shear over the cross-section of the rod. For a rod of circular cross-section $Ko^2 = a/4^2$ (a is the radius of cross-section of the rod).

The exact characteristic equations have been derived for a cylindrical rod of infinite length. It is found that, for flexural waves, there is a double infinity of possible modes of propagation all of which are dispersive [May 1964] . The Timoshenko theory predicts only two modes but in the case of the lower mode there is close agreement with the lowest mode given by the exact theory. If the shear correction is not made, agreement is only close for wavelengths which are large

compared with the lateral dimensions of the rod. The lower mode of the Timoshenko theory has values of phase velocity which increase continuously from zero, when $a/\lambda = 0$, to a value which asymptotically approaches $\left(\frac{E}{\kappa^2 G}\right)^{-\frac{1}{2}} \cdot Co$ at infinite a/λ and therefore $\frac{C}{Co}$ is equal to $\left(\frac{E}{\kappa^2 G}\right)^{-\frac{1}{2}}$ when a/λ is infinite. The value of κ^2 thus determines the short wavelength limit of the lower mode phase velocity as computed from the Timoshenko theory. The higher mode of the Timoshenko theory has values of phase velocity which decrease continuously with decrease of wavelength from a value which is infinite for $a/\lambda = 0$ to a value Co when a/λ is infinite. This mode does not agree well with a higher mode of the exact theory.

The phase velocity curves for the Timoshenko theory are shown in Figure 5.1. The value of $\frac{E}{G} = 2(1+\nu)$, where ν is poisson's ratio, was calculated assuming $\nu = 0.29$ which is a typical value for hard steel. The value of κ^2 used was 0.9. The reason for choosing this value of κ^2 is discussed below. The dispersion curves are presented in non-dimensional form by plotting $\frac{C}{Co}$ against a/λ

The experimental results, discussed in chapter 4, are analysed according to Kelvin's method of stationary phase. This method of analysis is discussed in chapter 6. For the comparison of experimental results with theory it is convenient to present the theoretical curves in non-dimensional form by

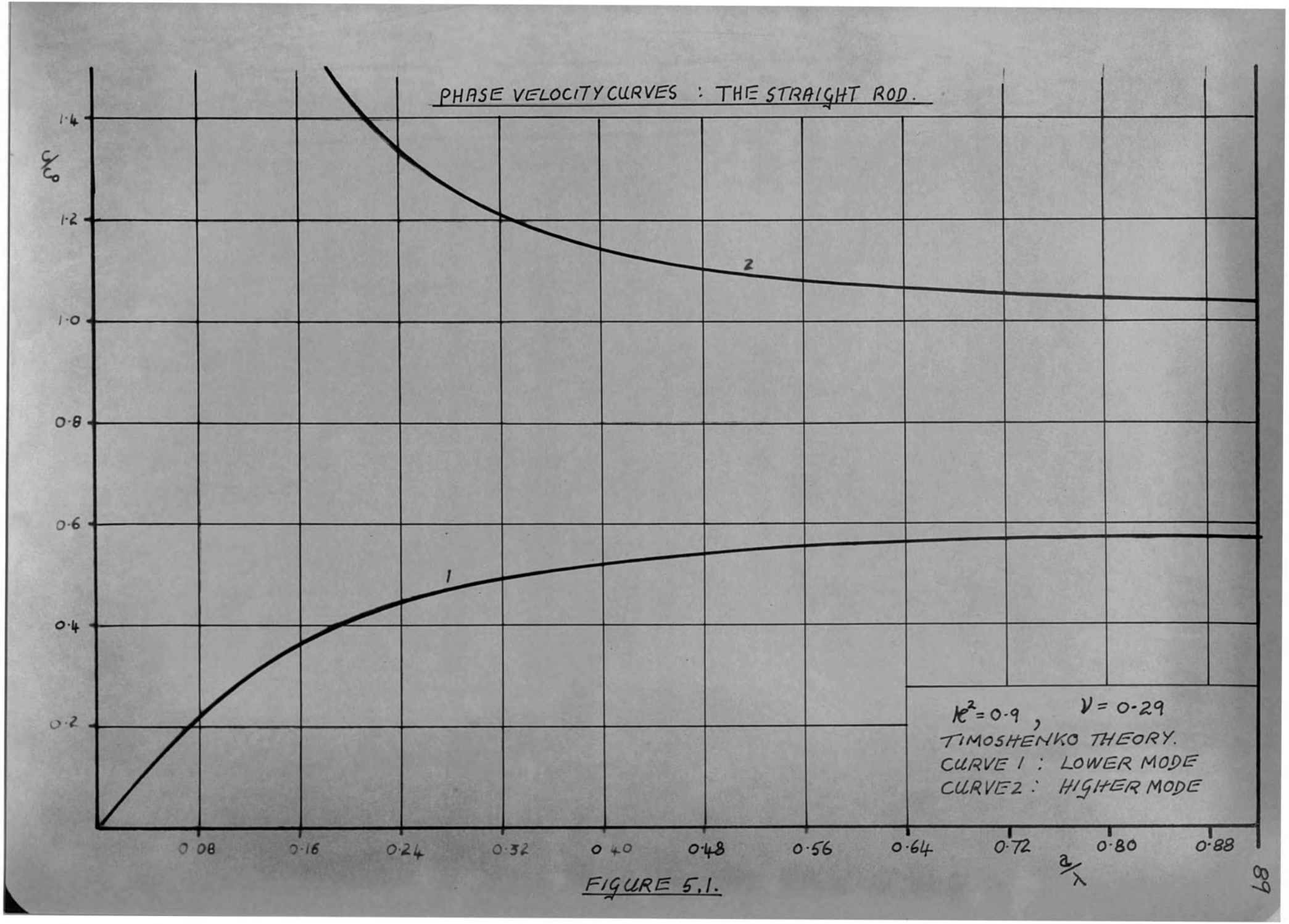
PHASE VELOCITY CURVES : THE STRAIGHT ROD.
c/c0
1·4
1·2
1·0
0·8
0·6
0·4
0·2
1
2
0·08
0·16
0·24
0·32
0·40
0·48
0·56
0·64
0·72
0·80
0·88
a/λ
ν² = 0·9 , ν = 0·29
TIMOSHENKO THEORY.
CURVE 1 : LOWER MODE
CURVE 2 : HIGHER MODE

FIGURE 5.1.

plotting $\frac{Tp}{Ta}$ against $\frac{t}{To}$, where Tp is the predominant period of a small group of waves which arrive at a distance x from the excitation end of the rod at a time t after the intiation of the pulse. The $\left(\frac{Tp}{Ta}, \frac{t}{To}\right)$ curves are referred to as arrival curves. The values of $\frac{Tp}{Ta}$ and $\frac{t}{To}$ are given by the equations

$$\frac{Tp}{Ta} = \frac{\lambda}{a} \cdot \frac{Co}{C} \qquad 7)$$

$$\frac{t}{To} = \frac{Co}{Cg} \qquad 8)$$

WHERE $Ta = \frac{a}{Co}$, $To = \frac{x}{Co}$ AND

where Cg is the group velocity of the stress wave of wavelength λ and phase velocity C (see chapter 6). To plot the theoretical arrival curves it is therefore necessary to know the value of $\frac{Cg}{Co}$, as well as the value of $\frac{C}{Co}$, for different values of a/λ. The group velocity Cg is the velocity of a small group of waves having wavelengths which are spread over a very small spectrum and, as discussed by Boit [1957], the rate of transmission of energy is equal to the group velocity rather than the phase velocity. The group velocity Cg is given by the equation

$$\frac{Cg}{Co} = \frac{C}{Co} - \lambda \frac{d\left(\frac{C}{Co}\right)}{d\lambda} \qquad 9)$$

Thus knowing the phase velocity, the group velocity can be calculated. Figure 5.2 shows the variation of $\frac{Cg}{Co}$ with a/λ for the two flexural waves in a straight rod as obtained from the Timoshenko theory using the values of ν and ke^2 given above.

To decide on the value of ke^2 to be used in the calculations from the Timoshenko theory the arrival curves for the lowest flexural mode in a straight rod, assuming $\nu = 0.29$, were plotted using three different value of ke^2. These curves are shown in Figure 5.3. Curves 1, 2 and 3 were calculated with ke^2 equal to 0.99, 0.9 and 0.847 respectively. The lowest mode arrival curve obtained from the exact theory is shown in Figure 5.4 for comparison. It was decided that the curve assuming $ke^2 = 0.9$ is sufficiently close to the exact theory curve for the purposes of this work. According to the exact theory the fastest flexural waves arrive at $t/T_o = 1.568$ whereas from the Timoshenko theory using $ke^2 = 0.9$ these waves arrive at $t/T_o = 1.589$. Comparing figures 5.3 and 5.4 it is seen that the discrepancy between the two theories is very small for values of $\frac{Tp}{Ta}$ greater than 20. It can also be seen from these figures that, according to both theories, there is a small region of the initial part of the dispersed stress pattern where the lowest flexural mode in the straight rod contributes two predominant periods for any given arrival time.

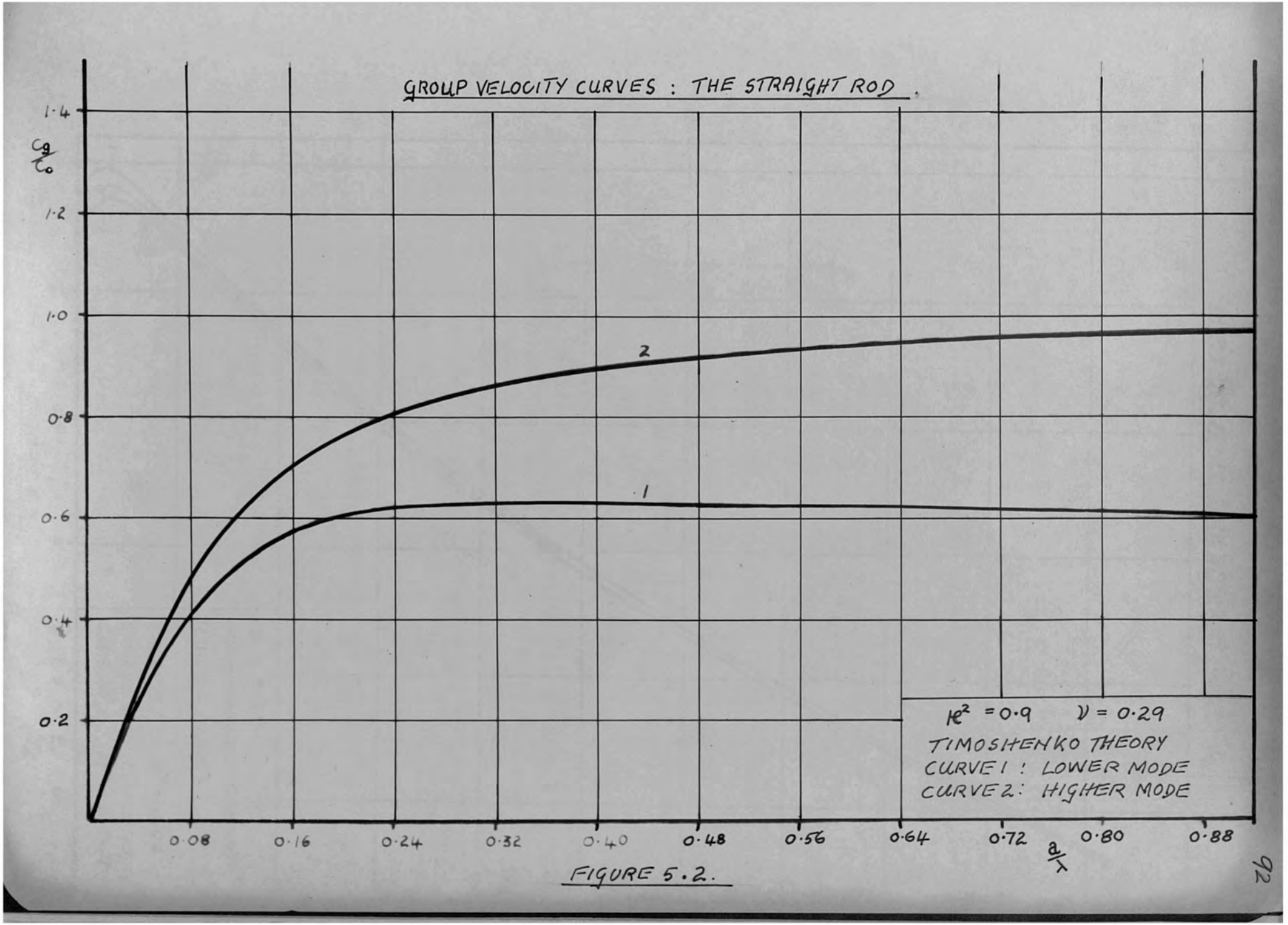
GROUP VELOCITY CURVES : THE STRAIGHT ROD.
$\frac{c_g}{c_0}$
1·4
1·2
1·0
0·8
0·6
0·4
0·2
0·08
0·16
0·24
0·32
0·40
0·48
0·56
0·64
0·72
0·80
0·88
$\frac{a}{\lambda}$
1
2
$k^2 = 0.9$ $\nu = 0.29$
TIMOSHENKO THEORY
CURVE 1 : LOWER MODE
CURVE 2: HIGHER MODE

FIGURE 5.2.

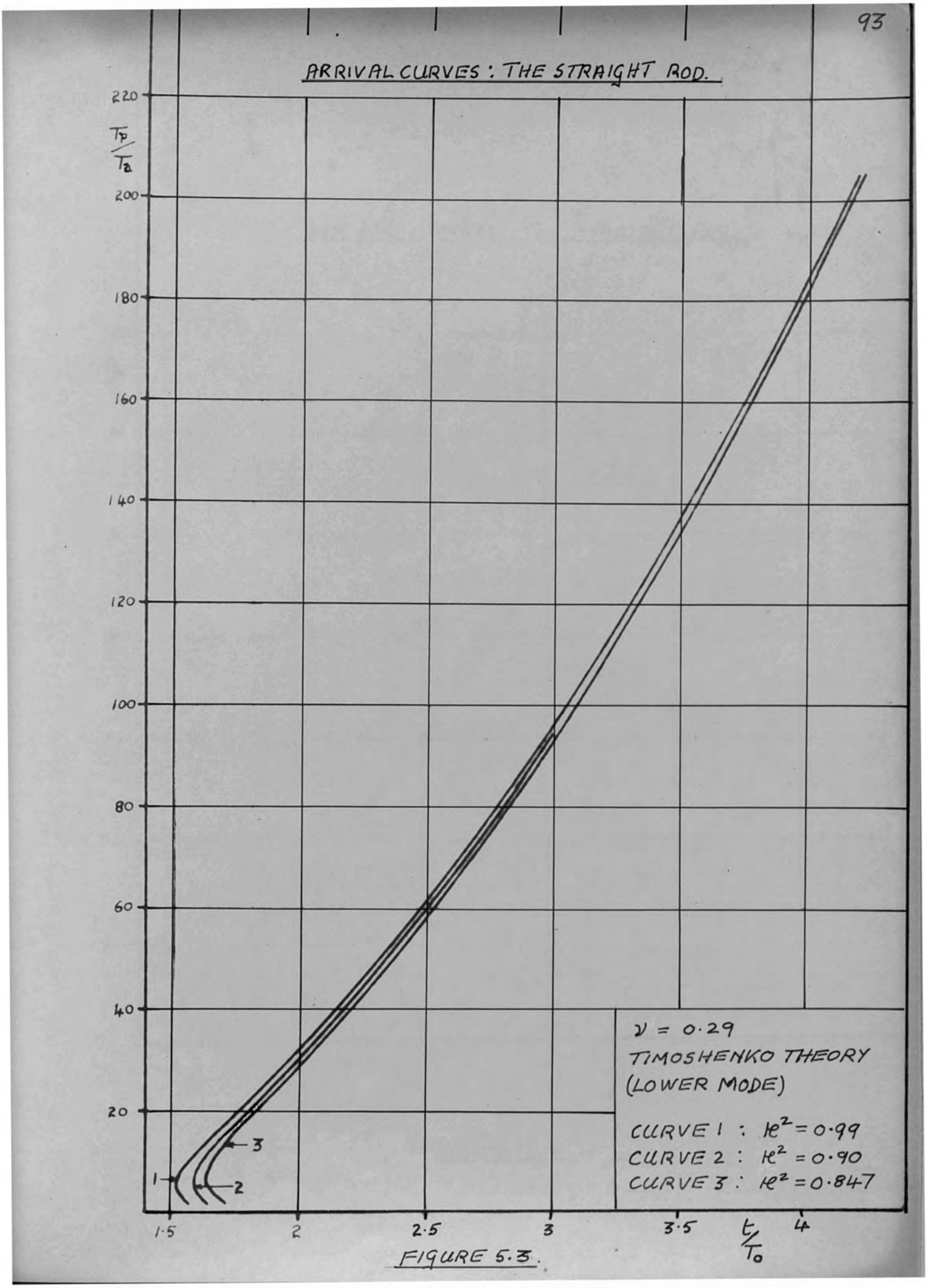
ARRIVAL CURVES : THE STRAIGHT ROD.
220
200
180
160
140
120
100
80
60
40
20
$\frac{T_p}{T_2}$
1·5
2
2·5
3
3·5
4
$\frac{t}{T_0}$
1
2
3
$\nu = 0.29$
TIMOSHENKO THEORY
(LOWER MODE)
CURVE 1 : $k^2 = 0.99$
CURVE 2 : $k^2 = 0.90$
CURVE 3 : $k^2 = 0.847$

FIGURE 5.3.

ARRIVAL CURVES: THE STRAIGHT ROD.

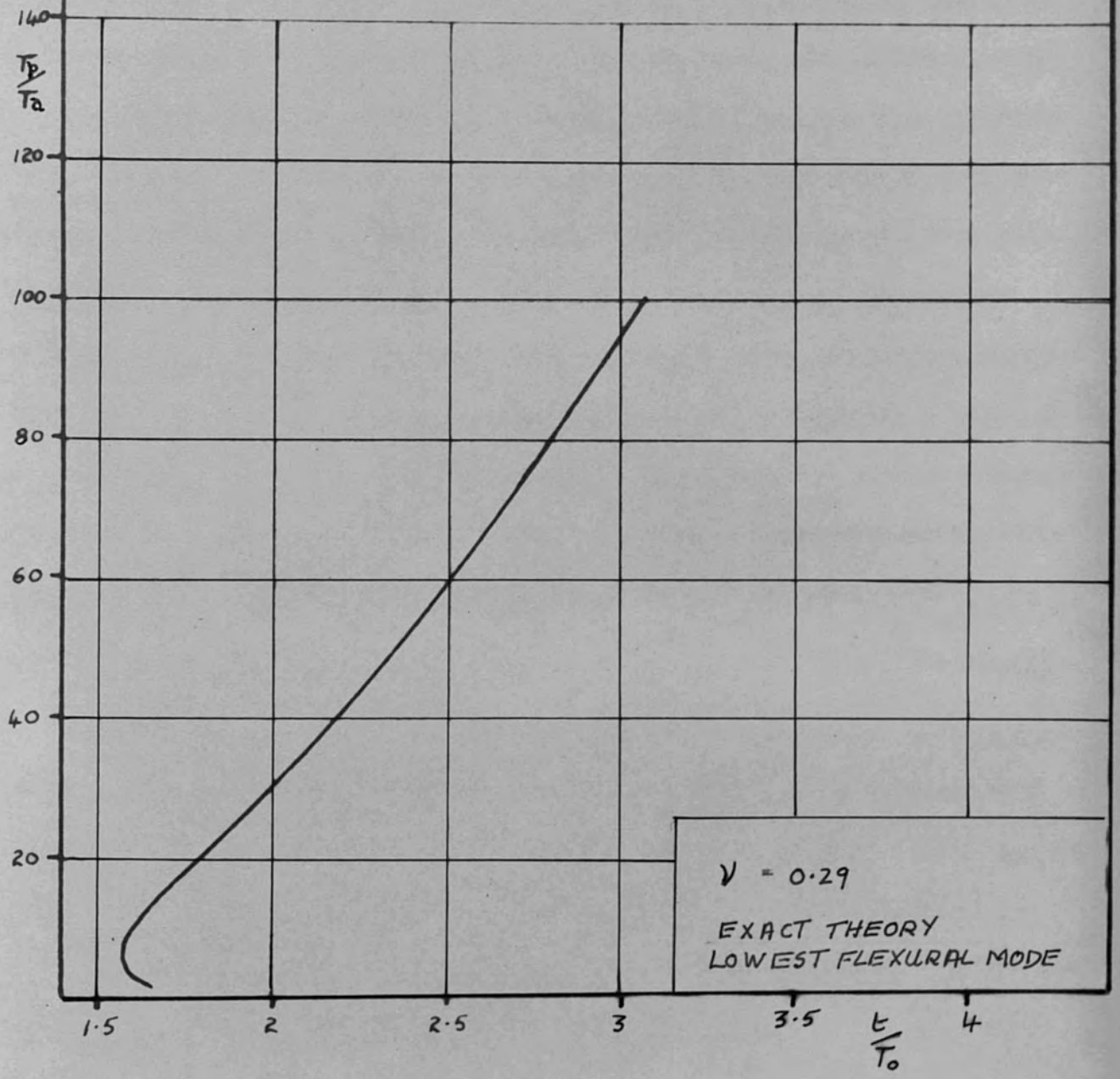

FIGURE 5.4

In one case the predominant period increases with arrival time and for the other case it decreases with arrival time.

b) LONGITUDINAL WAVES

Approximate theories have also been put forward for longitudinal waves in a cylinder. Again it is found that these theories postulate only one or two modes whereas exact theory gives an infinity of possible modes, all of which are dispersive. Agreement between the lowest mode of the exact and approximate theories is good for all wavelengths only when shear has been taken into account [Abramson, Plass and Ripperger 1958] . If a shear correction is not included the agreement is only good at long wavelengths where there is very little dispersion for the case of a straight rod. The agreement between the second modes is not so good even when shear has been taken into account. [Mindlin and Herrmann 1951, Herrmann 1954]

c) THE TORSIONAL MODE

It is worth noting that for torsional waves in cylinders an elementary approach gives a result which is in agreement with the lowest (zeroth) mode of the exact theory. This mode is non-dispersive with phase velocity $C_T = \left(\frac{G}{\rho}\right)^{\frac{1}{2}}$ where G is the shear modulus and ρ the density of the material of the rod. For the case of a material of Poisson's ratio $\nu = 0.29$,

$$\frac{C_T}{Co} = 0.622$$

5.3 THE CURVED GUIDE

It would be extremely difficult to derive dispersion equations for a helical waveguide by exact theory and in fact only approximate theories are available. As already mentioned the curved waveguides used in the work reported here were rods of radius of cross-section, a, wound as helical springs of mean radius R and pitch angle α. Before proceeding to the approximate theories for such a guide it is instructive to consider the case of a plane circular ring which can be regarded as a spring of zero pitch angle α. The theoretical treatment is, in this case, simplified in that it becomes possible to consider independently vibrations and waves which involve flexure 1) in the plane of the ring and 11) perpendicular to the plane of the ring. We will consider the two cases separately.

5.3a. THE CIRCULAR RING: FLEXURE IN THE PLANE OF THE RING

This has been dealt with by Lamb [1931] using the elementary approach but taking into account the extension of the central elastic line. He showed that two types of wave are possible, one being mainly extensional, the other flexural. If the extension of the elastic line is neglected an expression is found for the flexural wave velocity and it is not difficult to allow for rotary inertia in this case [Britton 1957].

Philipson [1956] has taken into account rotary inertia and central elastic line extension. However, as indicated earlier, the correction for radial shear becomes important at high frequencies and such a correction has been made in a theory given by Morley [1961] . Morley considers vibrations in the plane of a circular ring which has a central elastic line of natural radius of curvature R. It is assumed in the Morley theory that the thickness perpendicular to the plane of the ring is so small that plane stress exists throughout this thickness. It is also assumed that the radial stress σ_r is negligible compared with other stresses. Figure 5.5 represents an element of the curved rod. The thickness of the guide in the plane of the ring is not considered slight and therefore the equations of motion of an element δs must be obtained by considering an elementary strip and then integrating over the cross-sectional area, A, of the guide (see Figure 5.5). The resultant stresses and bending moment acting on the element δs must also be obtained by integrating over the area of cross-section A. The strains of the elementary strip can be given in terms of the radial and tangential displacements at the strip, the assumptions as to the nature of these displacements follow those of the Timoshenko theory for a straight rod. By substituting the resultant stresses and bending moment acting on the element δs into the equations of motion of the

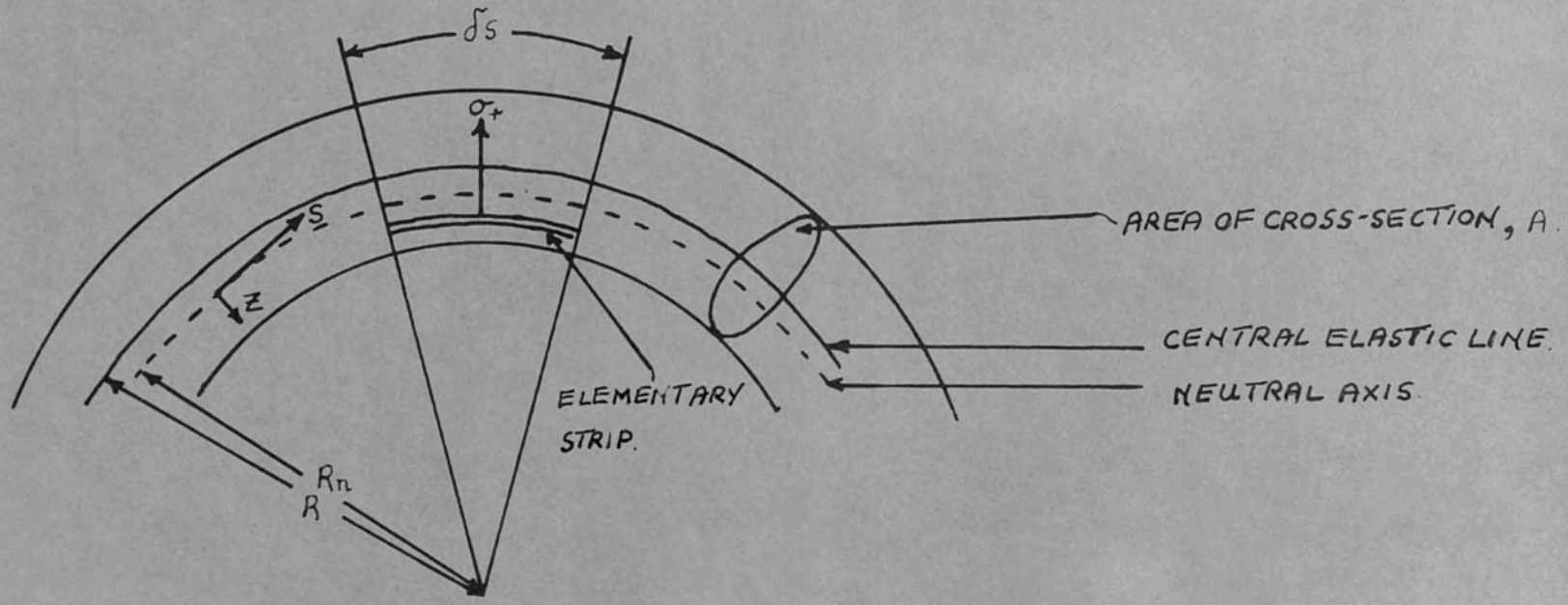

The curved rod

FIGURE 5.5

element, differential equations of motion in terms of displacements at the neutral axis are obtained. From these equations a single equation in one of these displacements can be found. It is then assumed that this displacement, ω say, takes the form

$$\omega = W\exp\left\{i(Pt - \frac{L\varsigma}{R_n})\right\} \qquad 10)$$

where ς is the tangential co-ordinate measured around the neutral axis of a plane ring, $i = \sqrt{-1}$, W is a constant, amplitude P is the pulsatance and

$$L = \frac{2\pi R_n}{\lambda} \qquad 11)$$

where R_n is the radius of the neutral axis and λ is the wavelength of the stress wave measured along the neutral axis. A characteristic equation relating phase velocity to wavelength is then obtained by substituting equation 10 into the equation of motion. The Morley characteristic equation for pronounced curvature is given below:

$$K^2(L^2-1)^2 - \left(\frac{C}{C_o}\right)^2\left[1 + M_1 + L^2\left\{1 - M_3 + K^2(1+K^2)(1+\frac{E}{Ie^2\varsigma})\right\}\right.$$
$$\left.+L^4\left\{K_2{}^2 + K^2(1+K^2)(1+\frac{E}{Ie^2\varsigma})\right\}\right] + \left(\frac{C}{C_o}\right)^4\left[L^2\left\{(1+K^2)(1+M_1) + M_2\frac{E}{Ie^2\varsigma}\right\}\right.$$
$$\left.+L^4\left\{M_2 + (1+K^2)(K^2+K_2{}^2)\frac{E}{Ie^2\varsigma}\right\}\right] - \left(\frac{C}{C_o}\right)^6 L^4(1+K^2)M_2\frac{E}{Ie^2\varsigma} = 0 \qquad 12)$$

where $$K^2 = \frac{1}{A} \iint_A \frac{\frac{z^2}{R_n^2}\, dA}{\left(1 - \frac{z}{R_n}\right)} \qquad 13)$$

$$K_1^2 = -\frac{1}{A} \iint_A \frac{z}{R_n} \left(1 - \frac{z}{R_n}\right) dA \qquad 14)$$

$$K_2^2 = \frac{1}{A} \iint_A \frac{z^2}{R_n} \left(1 - \frac{z}{R_n}\right) dA \qquad 15)$$

and where z is the radial co-ordinate measured along the inward drawn normal to the neutral axis of the ring. The values of M_1, M_2 and M_3 are given by

$$M_1 = K^2 + 2K_1^2 + K_2^2$$

$$M_2 = K_2^2 + K^2K_2^2 - K_1^4$$

$$M_3 = 2K_1^2 + 2K_2^2 - K^2$$

It remains to find the values of K^2, K_1^2, K_2^2 and R_n in terms of measurable dimensions of the guide under investigation. The magnitude of Rn can be determined as in the usual static theory [Timoshenko 1941] by using the equation

$$\iint_A \frac{\frac{z}{R_n}\, dA}{\left(1 - \frac{z}{R_n}\right)} = 0 \qquad 16)$$

Assuming a circular cross-section and performing the above integral

$$R_n = \frac{a/2}{\frac{R}{a} - \left(\frac{R^2}{a^2} - 1\right)^{\frac{1}{2}}} \qquad 17)$$

where R is the radius of curvature of the central elastic line of the ring.

Also performing the integrals of equations 13, 14 and 15

$$K^2 = \frac{2R}{a}\left[\frac{R}{a} - \left(\frac{R^2}{a^2} - 1\right)^{\frac{1}{2}}\right] - 1 \qquad 18)$$

$$K_1^2 = K^4 + K^2 + \frac{a^2}{4R_n^2} \qquad 19)$$

$$K_2^2 = K_1^2 - K^2 + \frac{3K^2a^2}{4R_n^2} + K^6 \qquad 20)$$

For a slightly curved guide, where $\frac{z}{R} \ll 1$ over the cross-section of the rod, it is a simple matter to show that

$$K_n^2 = R_n^2 K^2 \qquad 21)$$

where K_n is the radius of gyration of the cross-section of the rod about an axis which is perpendicular to the plane of curvature and which passes through the neutral axis of the guide. Thus, for slight curvature, since $\frac{K_n^2}{R_n^2} \ll 1$ then $K^2 \ll 1$. If we make $K^2 \ll 1$ in equation 12 it is seen that the characteristic equation for slight curvature is

$$K^2(L-1)^2 - \left(\frac{C}{Co}\right)^2\left[1 + L^2 + L^4K^2\left(2 + \frac{E}{\kappa^2 G}\right)\right]$$

$$+\left(\frac{C}{Co}\right)^4\left[L^2 + L^4K^2\left(1 + \frac{2E}{\kappa^2 G}\right)\right] - \left(\frac{C}{Co}\right)^6 L^4K^2\frac{E}{\kappa^2 G} = 0 \qquad 22)$$

Equation 12 was solved for various values of a/R . The phase velocity dispersion curves for a/R equal to $\frac{1}{8}$ and $\frac{1}{4}$ are shown in Figures 5.6 and 5.7 respectively assuming a material of Poisson's ratio $\nu = 0{\cdot}29$ and a value of $\kappa^2 = 0.9$. The characteristic equation is a cubic in $(\frac{C}{Co})^2$ resulting in three branches to the dispersion curves which can be associated with predominantly flexural, longitudinal and radial shear modes as indicated in the diagrams.

It is seen from these curves that the longitudinal mode is dispersive, according to the above theory, at very long wavelengths. However, because of the assumptions relating to the distribution of stress over the cross-section of the guide, made in the Morley theory, the dispersion curve for the longitudinal mode is equivalent to an elementary-type theory and therefore this curve can only give an accurate representation of the dispersion phenomena in the long wavelength region where, it will be remembered, there is very little dispersion in the case of a straight rod.

The dispersion curve for flexural modes indicates a zero value of phase velocity at a value of a/λ given by

$$a/\lambda = \frac{a}{2\pi R_n} \qquad 23)$$

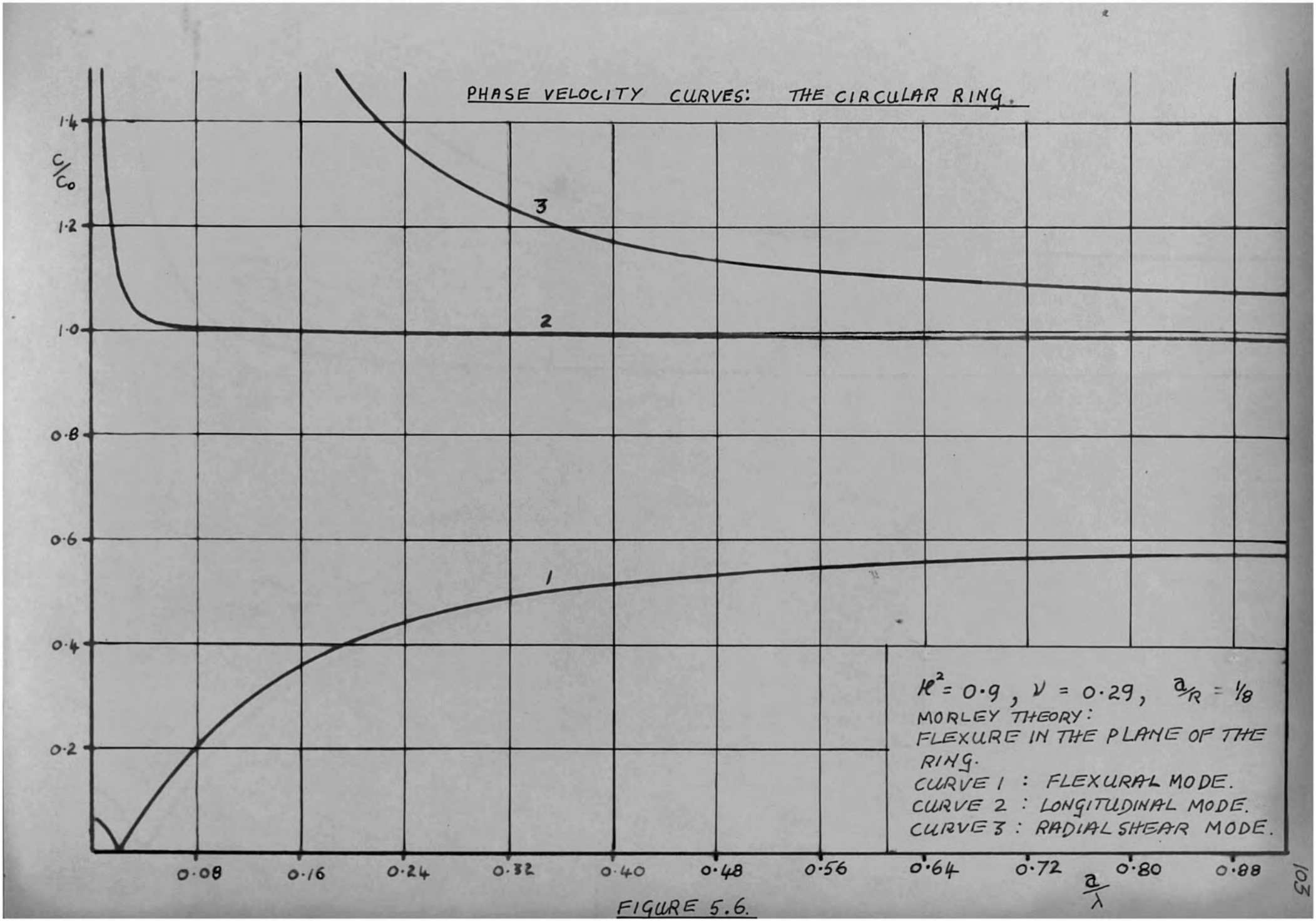
PHASE VELOCITY CURVES: THE CIRCULAR RING.
C/C0
1·4
1·2
1·0
0·8
0·6
0·4
0·2
0·08
0·16
0·24
0·32
0·40
0·48
0·56
0·64
0·72
0·80
0·88
a/λ
1
2
3
k² = 0·9 , ν = 0·29, a/R = 1/8
MORLEY THEORY:
FLEXURE IN THE PLANE OF THE RING.
CURVE 1 : FLEXURAL MODE.
CURVE 2 : LONGITUDINAL MODE.
CURVE 3 : RADIAL SHEAR MODE.

FIGURE 5.6.

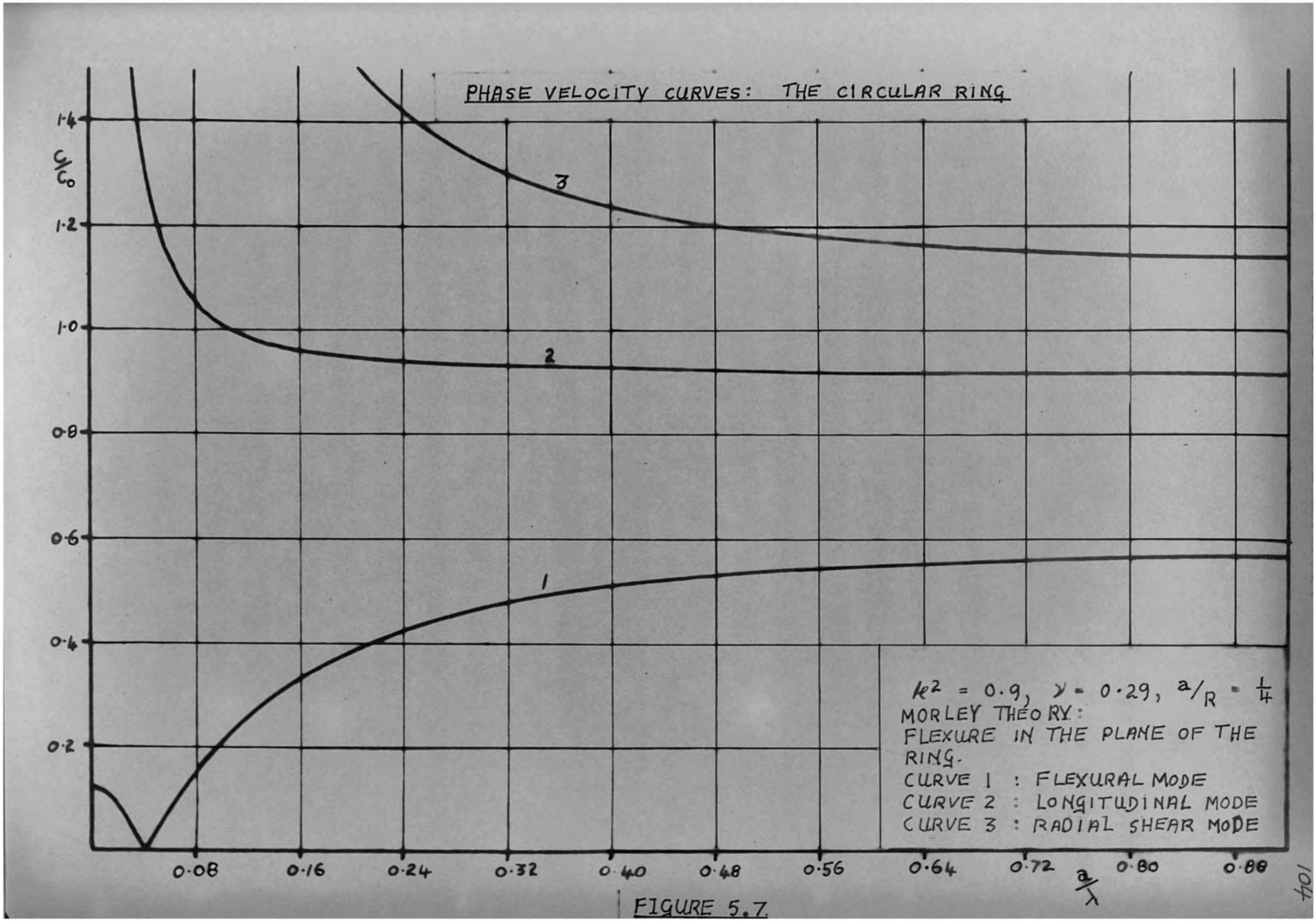
PHASE VELOCITY CURVES: THE CIRCULAR RING
C/C0
1·4
1·2
1·0
0·8
0·6
0·4
0·2
0·08
0·16
0·24
0·32
0·40
0·48
0·56
0·64
0·72
0·80
0·88
a/λ
1
2
3
k² = 0.9, ν = 0.29, a/R = 1/4
MORLEY THEORY:
FLEXURE IN THE PLANE OF THE RING.
CURVE 1 : FLEXURAL MODE
CURVE 2 : LONGITUDINAL MODE
CURVE 3 : RADIAL SHEAR MODE

FIGURE 5.7.

It can be seen from equations 12 and 22 that this condition is equivalent to $L^2 - 1 = 0$ and therefore one of the roots of the characteristic equation is zero. In this case $\lambda = 2\pi R_n$, that is, the wavelength of the stress wave is equal to the circumference of the ring measured along the neutral axis. The physical interpretation of this result is obtained by considering the displacements due to a sinusoidal wave motion of the above wavelength; it is found that the ring oscillates as a whole, in its plane of curvature, without deformation in this case. The effect of curvature on the flexural wave dispersion curve can be clearly seen in Figures 5.6 and 5.7.

The third mode (the radial shear mode) is similar to the higher velocity mode of the Timoshenko theory for a straight rod (Figure 5.1).

Equation 22 is the Morley theory equation for slight curvature. If we rearrange this equation we have, remembering $K^2 = \frac{K_n^2}{R_n^2}$ and $L = \frac{2\pi R_n}{\lambda}$,

$$K_n^2\left[\frac{4\pi^2 R_n^2}{\lambda^2} - 1\right]^2 - \left(\frac{C}{C_0}\right)^2\left[1 + 4\frac{\pi^2 R_n^2}{\lambda^2} + 16\frac{\pi^4 R_n^2 K_n^2}{\lambda^4}\left(2 + \frac{E}{\rho e^2 G}\right)\right]$$

$$+\left(\frac{C}{C_0}\right)^4\left[\frac{4\pi^2 R_n^2}{\lambda^2} + 16\frac{\pi^4 R_n^2}{\lambda^4} K_n^2\right] - \left(\frac{C}{C_0}\right)^6 \frac{16\pi^4}{\lambda^4} K_n^2 \frac{E}{\rho e^2 G} = 0 \qquad 24)$$

If $R_n \to \infty$ we have

$$1 - \left(\frac{C}{C_o}\right)^2\left[\frac{\lambda^2}{4\pi^2 K_n^2} + \left(2 + \frac{E}{ie^2\zeta}\right)\right] + \left(\frac{C}{C_o}\right)^4\left[\frac{\lambda^2}{4\pi^2 K_n^2} + 1\right] - \left(\frac{C}{C_o}\right)^6 \frac{E}{ie^2\zeta} = 0$$

which can be written as

$$\left\{\frac{E}{ie^2\zeta}\left(\frac{C}{C_o}\right)^4 - \left[\frac{\lambda^2}{4\pi^2 K_n^2} + \left(1 + \frac{E}{ie^2\zeta}\right)\right]\left(\frac{C}{C_o}\right)^2 + 1\right\}\left\{\left(\frac{C}{C_o}\right)^2 - 1\right\} = 0 \qquad 25)$$

This is the Morley theory characteristic equation for the case of infinite radius of curvature. From this equation it can be seen that one solution is

$$\left(\frac{C}{C_o}\right)^2 - 1 = 0$$

which is the elementary theory result for longitudinal waves in a straight rod. The other possible solutions are given by the equation

$$\frac{E}{ie^2\zeta}\left(\frac{C}{C_o}\right)^4 - \left[\frac{\lambda^2}{4\pi^2 K_n^2} + \left(1 + \frac{E}{ie^2\zeta}\right)\right]\left(\frac{C}{C_o}\right)^2 + 1 = 0$$

which is the Timoshenko theory for flexural waves in a straight rod.

The Morley theory group velocity dispersion curves for the two rings having values of a/R equal to $\frac{1}{8}$ and $\frac{1}{4}$ are shown in Figures 5.8 and 5.9 respectively. It is found that for a small range of a/λ, in the long wavelength region of the flexural mode dispersion curve, the phase and group velocity have opposite sign. This result can be interpreted in three ways. Either a) the Morley theory does not hold in this region,

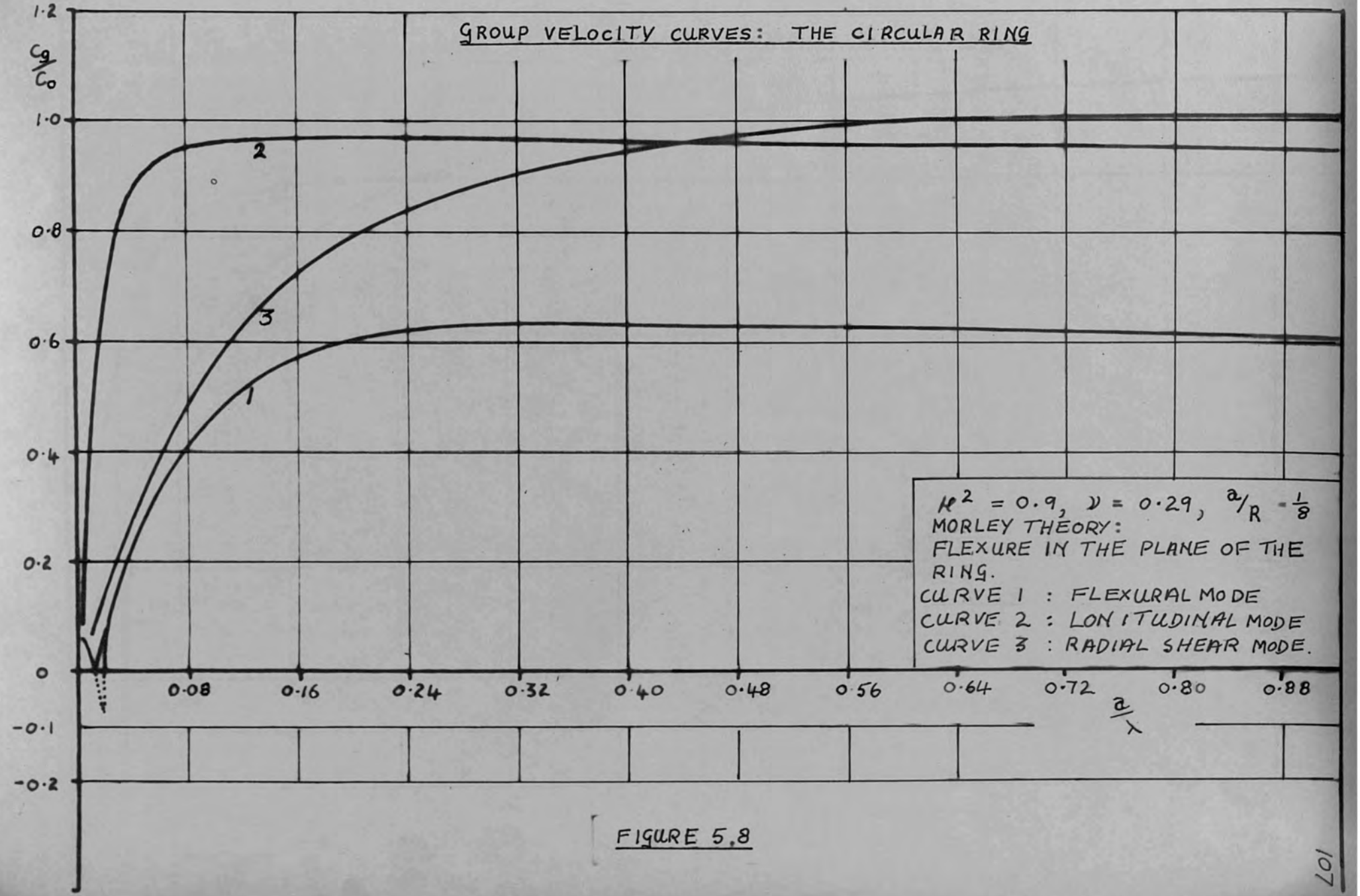
GROUP VELOCITY CURVES: THE CIRCULAR RING
c_g/c_0
1·2
1·0
0·8
0·6
0·4
0·2
0
-0·1
-0·2
0·08
0·16
0·24
0·32
0·40
0·48
0·56
0·64
0·72
0·80
0·88
a/λ
1
2
3
$\mu^2 = 0.9$, $\nu = 0.29$, $a/R = \frac{1}{8}$
MORLEY THEORY:
FLEXURE IN THE PLANE OF THE RING.
CURVE 1 : FLEXURAL MODE
CURVE 2 : LONGITUDINAL MODE
CURVE 3 : RADIAL SHEAR MODE.

FIGURE 5.8

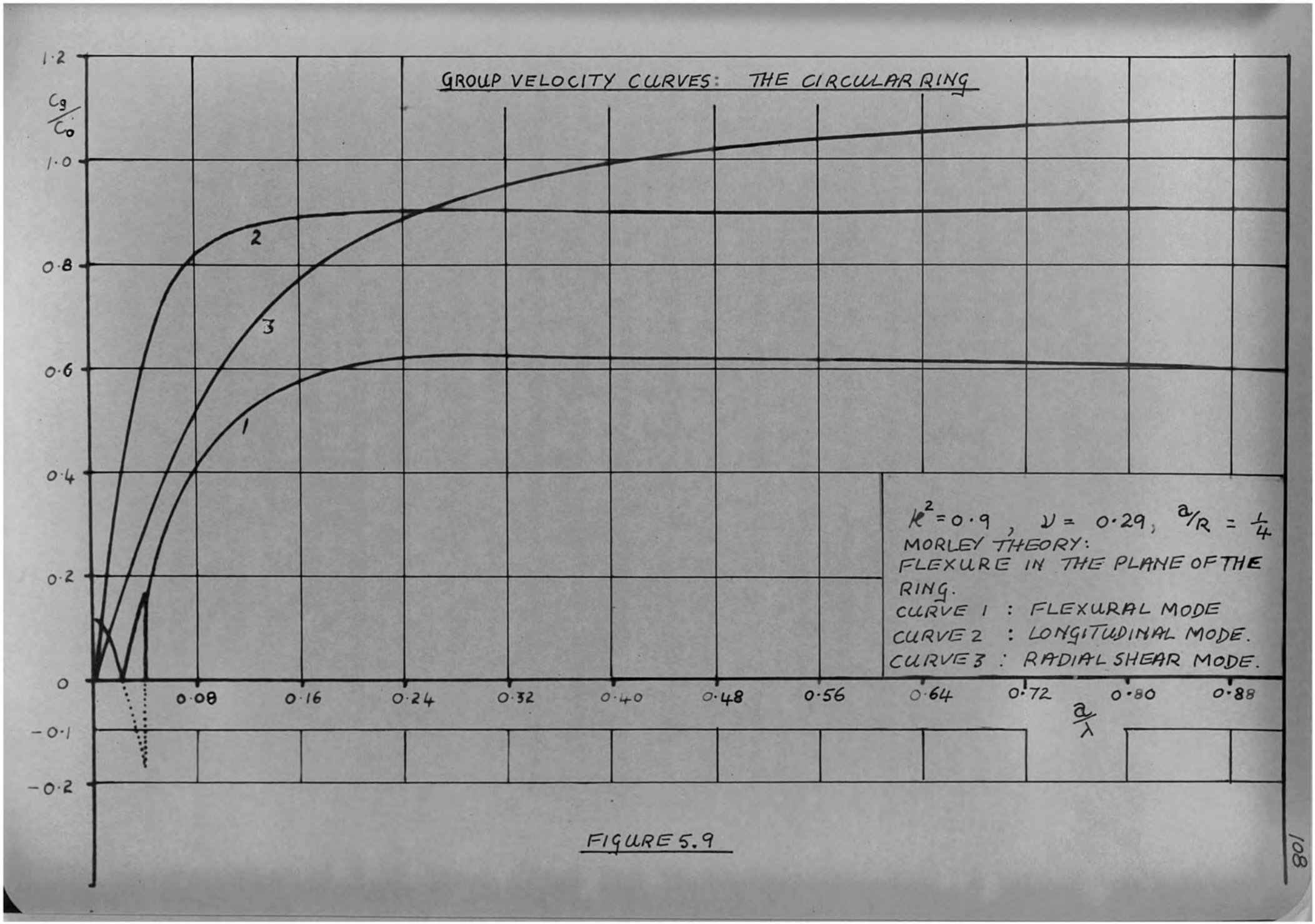
GROUP VELOCITY CURVES: THE CIRCULAR RING
C_g/C_0
1·2
1·0
0·8
0·6
0·4
0·2
0
−0·1
−0·2
0·08
0·16
0·24
0·32
0·40
0·48
0·56
0·64
0·72
0·80
0·88
a/λ
1
2
3
$k^2 = 0·9$, $\nu = 0·29$; $a/R = \frac{1}{4}$
MORLEY THEORY:
FLEXURE IN THE PLANE OF THE RING.
CURVE 1 : FLEXURAL MODE
CURVE 2 : LONGITUDINAL MODE.
CURVE 3 : RADIAL SHEAR MODE.

FIGURE 5.9

or b) the group velocity is negative and the phase velocity positive, or c) the group velocity is positive and the phase velocity negative.

The first alternative can only be eliminated by developing the exact theory. However, it is expected that there would be close agreement between exact and approximate theories over this long wavelength region of the dispersion curve.

The second alternative would indicate that, for a small range of wavelengths, the lowest flexural mode cannot propagate in the waveguide. It has already been mentioned that the rate of transmission of energy is equal to the group velocity and therefore a negative group velocity would mean that no energy, from the generating system, can propagate along the guide. Cut-off phenomena of this type are usually accompanied by an infinite value of phase velocity which is not the case here.

The third alternative would mean that we are dealing with a wave packet in which the crests and troughs of the constituent waves propagate towards the generating system. In this case we take the negative root of the $\left(\frac{C}{Co}\right)^2$ value obtained from the characteristic equation.

The above result is also found when studying the more elementary theories and the interpretation is discussed by Britton [1957] and by Tolstoy and Usdin [1957]. In both cases

a negative phase velocity is assumed over the above region. A negative phase velocity is also assumed in this work although no supporting experimental evidence is presented.

Figure 5.10 shows the arrival curves for the flexural mode in rings having values of a/R equal to $\frac{1}{8}$ and $\frac{1}{4}$ as indicated in the diagram. The Timoshenko straight rod curve is shown for comparison. The effect of curvature of the waveguide on the arrival curves is clearly seen. Figure 5.11 shows the arrival curves of the longitudinal mode for rings of a/R equal to $\frac{1}{4}$, $\frac{1}{8}$ and $1/16$ as indicated in the diagram.

The third mode (the radial shear mode), predicted by the Morley theory, is similar to the higher velocity mode predicted by the Timoshenko theory of a straight rod. This mode has comparatively small values of Tp/Ta over the range of arrival times studied. For an arrival time given by $t/To = 10$ the values of Tp/Ta for a straight rod and a plane ring of $a/R = \frac{1}{4}$ are 5·30 and 5·10 respectively. In both cases the value of Tp/Ta decreases with decrease of t/To over the range $1 < t/To < 10$. This comparatively high frequency mode was not studied experimentally in this work.

Table I shows a comparison of theoretical results obtained, for a spring of a/R equal to $\frac{1}{8}$, using equations 12 and 22. It is seen that the difference is small for this value of a/R and therefore it is assumed that the slight

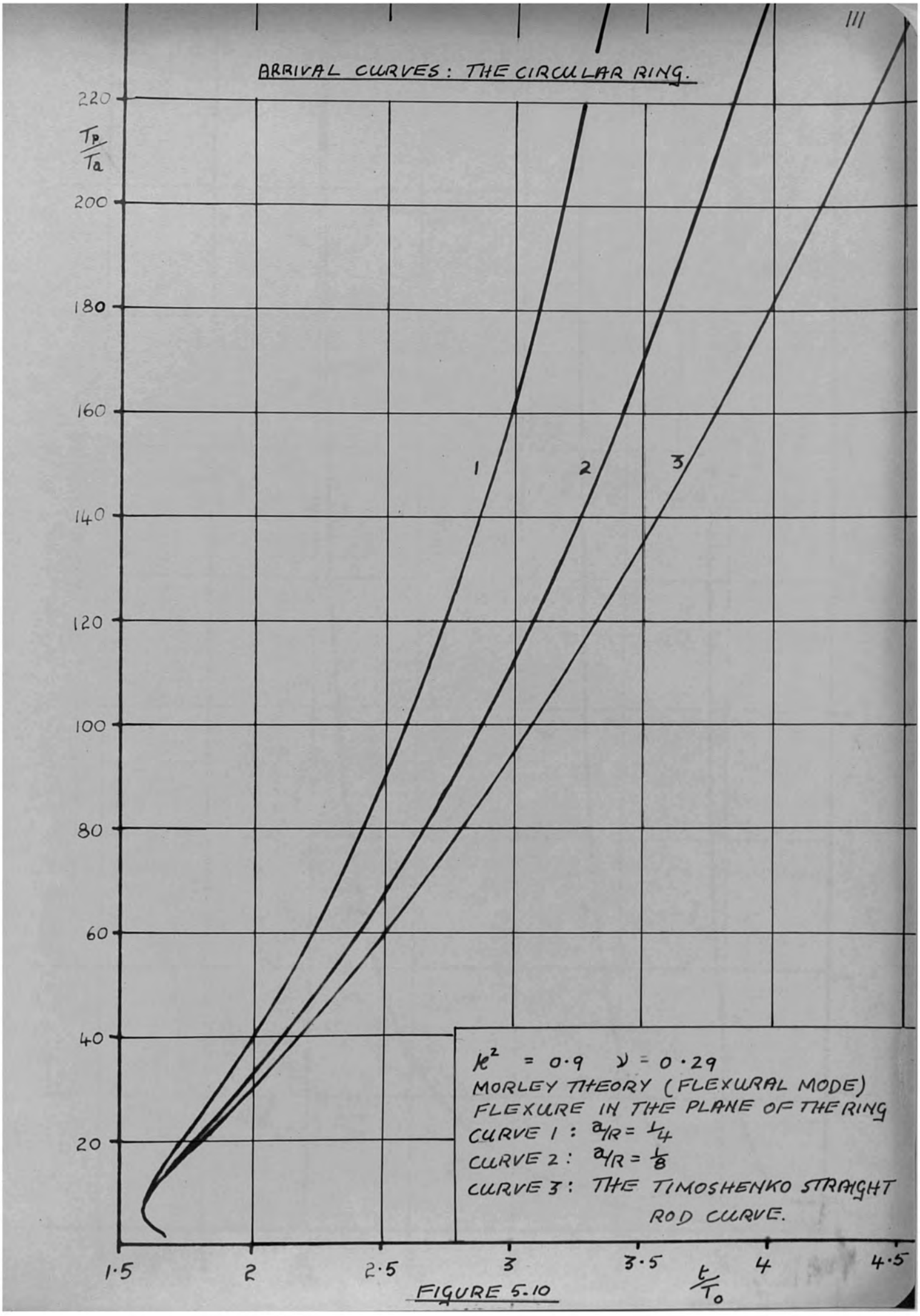
ARRIVAL CURVES: THE CIRCULAR RING.
220
200
180
160
140
120
100
80
60
40
20
Tp/Ta
1
2
3
k² = 0·9 ν = 0·29
MORLEY THEORY (FLEXURAL MODE)
FLEXURE IN THE PLANE OF THE RING
CURVE 1: a/R = 1/4
CURVE 2: a/R = 1/8
CURVE 3: THE TIMOSHENKO STRAIGHT ROD CURVE.
1·5
2
2·5
3
3·5
4
4·5
t/T0

FIGURE 5.10

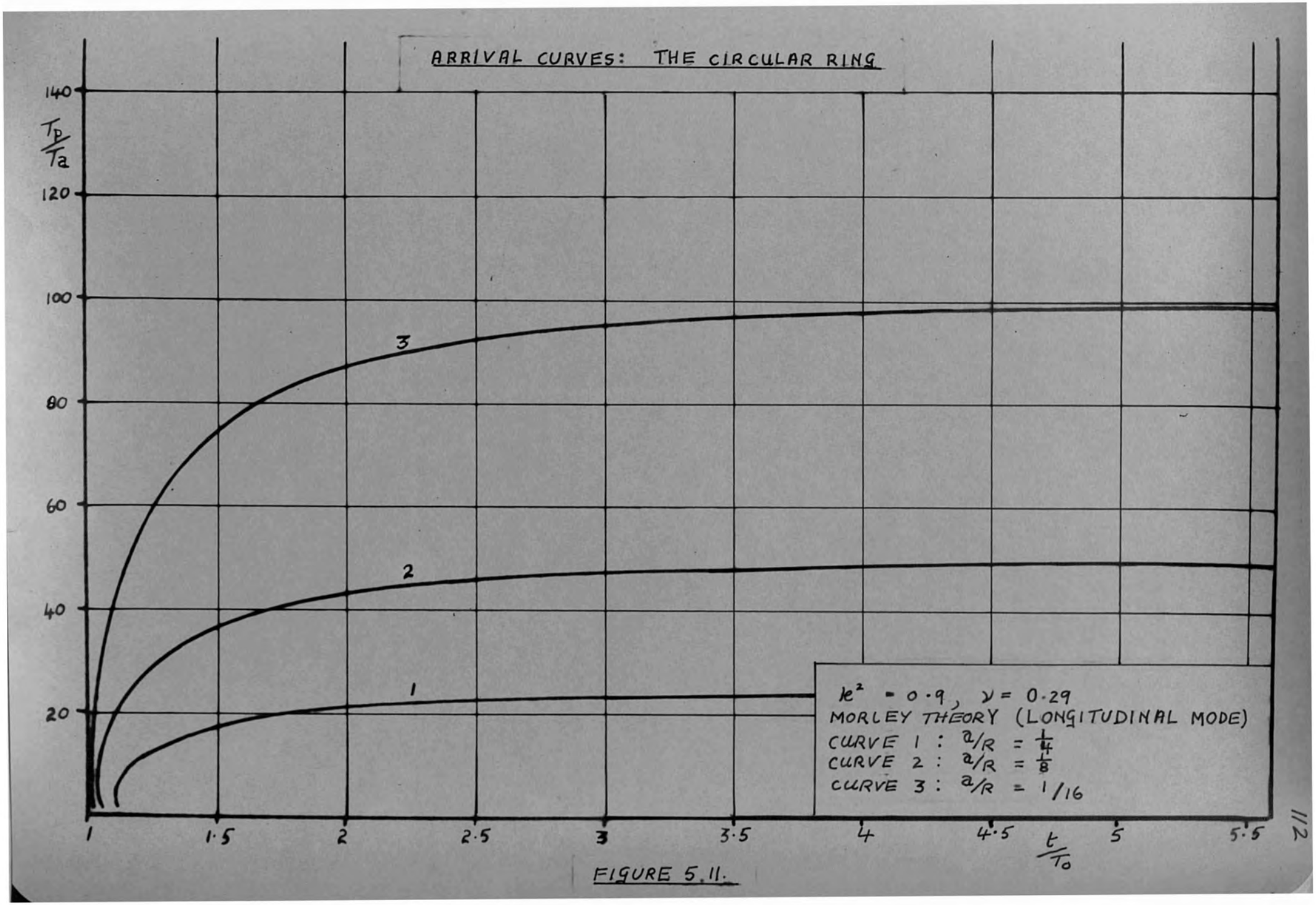
ARRIVAL CURVES: THE CIRCULAR RING
140
120
100
80
60
40
20
T_p/T_a
3
2
1
$k^2 = 0.9$, $\nu = 0.29$
MORLEY THEORY (LONGITUDINAL MODE)
CURVE 1 : $a/R = \frac{1}{4}$
CURVE 2 : $a/R = \frac{1}{8}$
CURVE 3 : $a/R = 1/16$
1
1·5
2
2·5
3
3·5
4
4·5
5
5·5
t/T_0

FIGURE 5.11.

curvature equation (equation 22) adequately describes the dispersion of the lowest flexural mode for rings where $a/R < \frac{1}{8}$. The arrival curves obtained from equations 12 and 22 are so close that it is not possible to show the difference clearly on the scale used in Figure 5.10. The difference between the arrival curves obtained from the Morley theory for a ring of a/R equal to $\frac{1}{8}$ and that obtained from the Timoshenko theory of a straight rod is, however, very clear on this scale.

TABLE I

FLEXURAL MODE, MORLEY THEORY ARRIVAL TIMES

	From equation 12		From equation 22	
a/λ	T_p/T_a	t/T_o	T_p/T_a	t/T_o
0.044	235.11	3.941	234.44	3.945
0.048	188.25	3.630	187.86	3.635
0.052	154.91	3.377	154.67	3.382
0.056	130.22	3.168	130.09	3.173
0.060	111.37	2.992	111.29	2.997
0.064	96.60	2.842	96.57	2.847
0.068	84.80	2.713	84.79	2.718
0.072	75.19	2.601	75.20	2.606
0.076	67.26	2.504	67.28	2.508
0.080	60.63	2.418	60.66	2.422
0.084	55.02	2.342	55.05	2.346
0.088	50.23	2.274	50.26	2.278
0.092	46.10	2.214	46.13	2.217
0.096	42.51	2.159	42.55	2.163
0.100	39.38	2.111	39.41	2.114
0.120	28.30	1.929	28.32	1.931
0.160	17.44	1.738	17.46	1.739
0.200	12.35	1.653	12.35	1.652
0.240	9.48	1.613	9.48	1.611
0.280	7.66	1.596	7.66	1.593
0.320	6.43	1.590	6.42	1.586
0.360	5.53	1.590	5.53	1.586
0.400	4.86	1.594	4.85	1.587
0.440	4.33	1.599	4.32	1.593
0.480	3.91	1.605	3.90	1.599
0.520	3.56	1.611	3.56	1.605
0.560	3.27	1.617	3.27	1.611
0.600	3.03	1.623	3.02	1.617

5.3.b. THE CIRCULAR RING: FLEXURE PERPENDICULAR TO THE PLANE OF THE RING

The vibration is more intricate than that of motion in the plane of the ring since flexure is now accompanied by torsion of the rod. The problem has been solved by Michell [1889] allowing for rotary inertia but there seems to have been no direct Timoshenko-type solution. A Timoshenko-type theory has been put forward, by Wittrick [1966], for a helical spring. This theory, which is discussed in section 5.3.c., takes into account shear but assumes slight curvature of the waveguide. (Curvature is considered slight when $a/R < 0.1$.) The characteristic equation for a helical spring is presented by Wittrick in matrix form. Due to the algebraic complexity it seems impractical to expand the matrix into the form

$$a'\left(\frac{c}{c_o}\right)^{12} + b'\left(\frac{c}{c_o}\right)^{10} + c'\left(\frac{c}{c_o}\right)^{8} + d'\left(\frac{c}{c_o}\right)^{6} + e'\left(\frac{c}{c_o}\right)^{4} + f'\left(\frac{c}{c_o}\right)^{2} + g' = 0 \qquad 34A)$$

where a', b', c', d', e', f', and g' are all functions of λ . However it can be seen from the matrix that, in general, there are six roots giving six values of $\left(\frac{c}{c_o}\right)^2$ for each value of λ . If the condition that $\alpha = 0$ (i.e. the condition for a plane ring) is introduced into the matrix then the resulting matrix represents two distinct sets of three equations (see section 5.3.c.) By applying the condition that the solution to each set of equations is non-zero we obtain two distinct characteristic equations each being a cubic in $\left(\frac{c}{c_o}\right)^2$. The two

equations obtained are

$$\frac{\kappa e^2 G}{E}\left(\frac{L^2-1}{L^4}\right)^2 - \frac{\kappa e^2 G}{EL^4K^2}\left[K^2\left(2+\frac{E}{\kappa e^2 G}\right)L^4+\left(\frac{EK^2}{\kappa e^2 G}+1-K^2\right)L^2+K^2+1\right]\left(\frac{C}{Co}\right)^2$$

$$+\frac{\kappa e^2 G}{L^4 EK^2}\left[K^2\left(1+\frac{2E}{\kappa e^2 G}\right)L^4+\left\{K^2\left(1+\frac{E}{\kappa e^2 G}\right)+1\right\}L^2\right]\left(\frac{C}{Co}\right)^4-\left(\frac{C}{Co}\right)^6=0 \qquad 26)$$

where $K^2R^2 = K_n^2$ for slight curvature, and

$$\frac{\gamma\kappa e^2 G^2}{L^4E^2}(L^2-1)^2 - \frac{\gamma\kappa e^2 G^2}{L^4E^2}\left[\left\{\frac{E}{\kappa e^2 G}+\frac{E}{\gamma G}+1\right\}L^4+\left\{\frac{R^2}{K_p^2}+\frac{K_p^2}{K_T^2}\,\frac{E}{\gamma G}\right.\right.$$

$$\left.\left.-\frac{2E}{\kappa e^2 G}\right\}L^2+\frac{E}{\gamma G}\,\frac{R^2}{K_T^2}\right]\left(\frac{C}{Co}\right)^2+\frac{\gamma\kappa e^2 G^2}{L^4E^2}\left[\left\{\frac{E}{\kappa e^2 G}+\frac{E}{\gamma G}+\frac{E^2}{\kappa e^2\gamma G^2}\right\}L^4\right.$$

$$\left.+\frac{E}{\gamma G}\,\frac{R^2}{K_p^2}L^2\right]\left(\frac{C}{Co}\right)^4-\left(\frac{C}{Co}\right)^6=0 \qquad 27)$$

where K_p is the radius of gyration of the cross-section of the rod about an axis which lies in the plane of curvature and intersects the central elastic line at right angles, K_T is the polar radius of gyration of the cross-section of the rod (see figure 5.17) and γ is a constant for a given cross-section defined by

$$\beta_T = \gamma G A K_T^2 \qquad 28)$$

where β_T is the torsional rigidity of the guide. $\gamma = 1$ for a guide of circular cross-section.

In deriving his general characteristic equation for a

helical spring it was assumed by Wittrick from the outset that a parameter $\gamma^2 >> 1$ where

$$\gamma = \frac{R}{K_T} \sec^2 \alpha \qquad 29)$$

or for the case of a plane ring where $\alpha = 0$

$$\gamma = \frac{R}{K_T}$$

Thus we are assuming that

$$\frac{K_T}{R} << 1$$

i.e. for a circular cross-section

$$\left(\frac{a^2}{2R^2}\right)^{\frac{1}{2}} = \frac{a}{\sqrt{2}R} << 1$$

We are therefore assuming slight curvature and that Rn = R (i.e. the neutral axis and central elastic line coincide).

Also $K^2R^2 = Kn^2$

and for slight curvature $\frac{Kn^2}{R^2} << 1$

and therefore $K^2 << 1$.

If we put the condition $K^2 << 1$ into equation 26 we obtain

$$K^2(L^2-1)^2 - \left[1 + L^2 + L^4K^2\left(2 + \frac{E}{ke^2G}\right)\right]\left(\frac{C}{Co}\right)^2 + \left[L^2 + L^4K^2\left(1 + \frac{2E}{ke^2G}\right)\right]\left(\frac{C}{Co}\right)^4$$

$$- \left(\frac{C}{Co}\right)^6 L^4K^2 \frac{E}{ke^2G} = 0 \qquad 30)$$

This is precisely the equation resulting from the Morley theory for vibrations in the plane of a ring when curvature is considered slight (equation 22). We therefore assume that equation 27 represents vibrations perpendicular to the plane of a plane ring of slight curvature. Equation 27 has been solved for various values of a/R. Figure 5.12 shows the phase velocity dispersion curves for a/R equal to $\frac{1}{5}$. The cubic equation gives three roots which can be associated with flexural, torsional and bending moment waves as shown in the diagram (Figure 5.12).

The torsional mode is seen to be dispersive at long wavelengths, the phase velocity decreasing from infinity at long wavelengths, to a value $(G/\rho)^{\frac{1}{2}}$. Co at short wavelengths. It will be remembered that this mode is non-dispersive in the case of a straight rod.

The flexural mode has the same general characteristics as the flexural mode in the plane of a ring. Again $\left(\frac{C}{Co}\right)^2$ drops to zero when $a/\lambda = \frac{a}{2\pi R}$

i.e. when $L^2 - 1 = 0$ or $\lambda = 2\pi R$

In this case the wavelength is equal to the perimeter of the ring measured around the central elastic line. The physical interpretation of this result is obtained by considering the displacement due to a sinusoidal wave motion of the above wavelength; it is found that the ring rotates about a diameter of the central elastic line and there is no elastic deformation in this case. The effect of curvature on the flexural dispersion

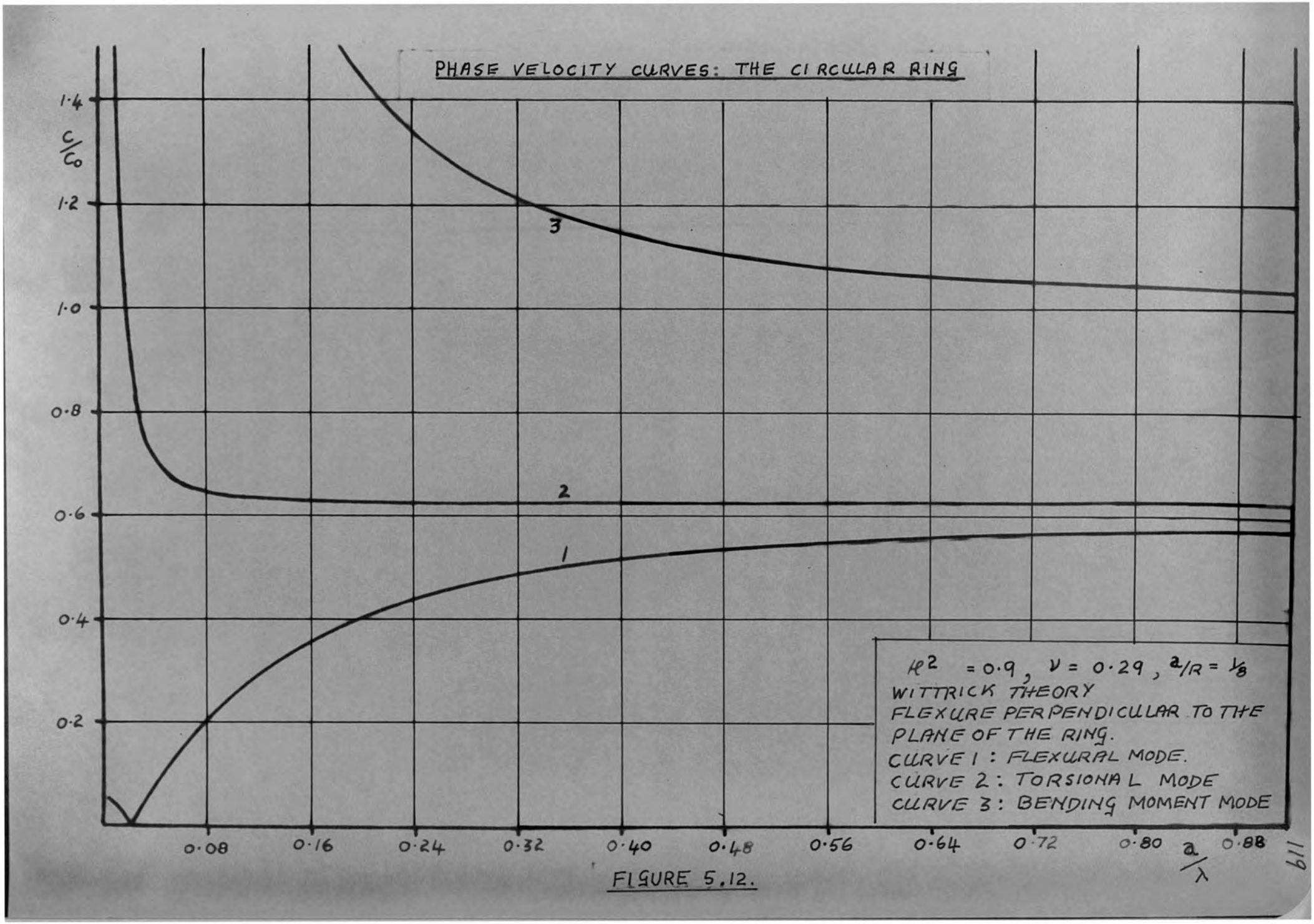
PHASE VELOCITY CURVES: THE CIRCULAR RING
1·4
1·2
1·0
0·8
0·6
0·4
0·2
C/Co
3
2
1
0·08
0·16
0·24
0·32
0·40
0·48
0·56
0·64
0·72
0·80
0·88
a/λ
k² = 0·9, ν = 0·29, a/R = 1/8
WITTRICK THEORY
FLEXURE PERPENDICULAR TO THE PLANE OF THE RING.
CURVE 1 : FLEXURAL MODE.
CURVE 2 : TORSIONAL MODE
CURVE 3 : BENDING MOMENT MODE

FIGURE 5.12.

curve can be clearly seen in Figure 5.12. The third mode (the bending moment mode) is not investigated in detail in this work.

Since the above theory is for slight curvature only it is necessary to consider whether the curves shown in Figure 5.12 are a valid representation of the flexural wave dispersion characteristics for a ring of $a/R = \frac{1}{8}$. Table II shows some of the calculated results for a ring of $\frac{a}{R} = \frac{1}{8}$. Columns A, B and C were calculated from the Morley theory (pronounced curvature), the Morley theory (slight curvature) and the Wittrick theory for vibrations perpendicular to the plane of a ring respectively.

TABLE II

a/λ	$A\left(\frac{C}{C_o}\right)$	$B\left(\frac{C}{C_o}\right)$	$C\left(\frac{C}{C_o}\right)$
0.002	0.0611	0.0615	0.0540
0.004	0.0584	0.0588	0.0518
0.010	0.0417	0.0421	0.0375
0.014	0.0259	0.0263	0.0235
0.020	0.0001	0.0005	0.0004
0.024	0.0176	0.0180	0.0170
0.030	0.0430	0.0433	0.0415
0.034	0.0591	0.0593	0.0574
0.040	0.0821	0.0824	0.0801
0.044	0.0967	0.0969	0.0945
0.050	0.1175	0.1177	0.1152
0.054	0.1307	0.1308	0.1284
0.060	0.1497	0.1498	0.1474
0.064	0.1618	0.1618	0.1595
0.070	0.1791	0.1791	0.1769
0.074	0.1902	0.1902	0.1880
0.080	0.2062	0.2061	0.2040
0.084	0.2164	0.2163	0.2142
0.090	0.2311	0.2310	0.2290
0.094	0.2405	0.2404	0.2383
0.100	0.2540	0.2538	0.2519
0.120	0.2945	0.2943	0.2926
0.160	0.3584	0.3582	0.3569
0.200	0.4050	0.4048	0.4039

The range of a/λ shown in table II covers the region of the flexural mode dispersion curves which were studied experimentally. It is seen from the table that over this range the Morley theory for slight curvature gives results which are very close to those given by the Morley theory equation of pronounced curvature. We can therefore say that the slight curvature equation gives a good approximation to the pronounced curvature equation when rings having values of $a/R < \frac{1}{8}$ are considered. It is therefore expected that the Wittrick theory, for vibrations perpendicular to the plane of the ring, gives results which are sufficiently accurate, within the limitations of the Timoshenko theory, over the range of a/λ shown in table II. The dispersion of the flexural waves in rings with values of $a/R < \frac{1}{8}$ is therefore expected to be adequately described by the slight curvature equations over a range of a/λ from 0 to 0.2. It is also seen from table II that, for the range of a/λ shown, the flexural wave having displacements perpendicular to the plane of the ring is slower than that having displacements in the plane of the ring; the former is therefore called the slower wave and the latter the faster wave. It can be seen from the dispersion curves shown in Figures 5.6 and 5.12 that the two flexural modes are very close over the range of a/λ from 0 to 1.

Figure 5.13 shows the group velocity curves for vibrations perpendicular to the plane of a ring as computed from the

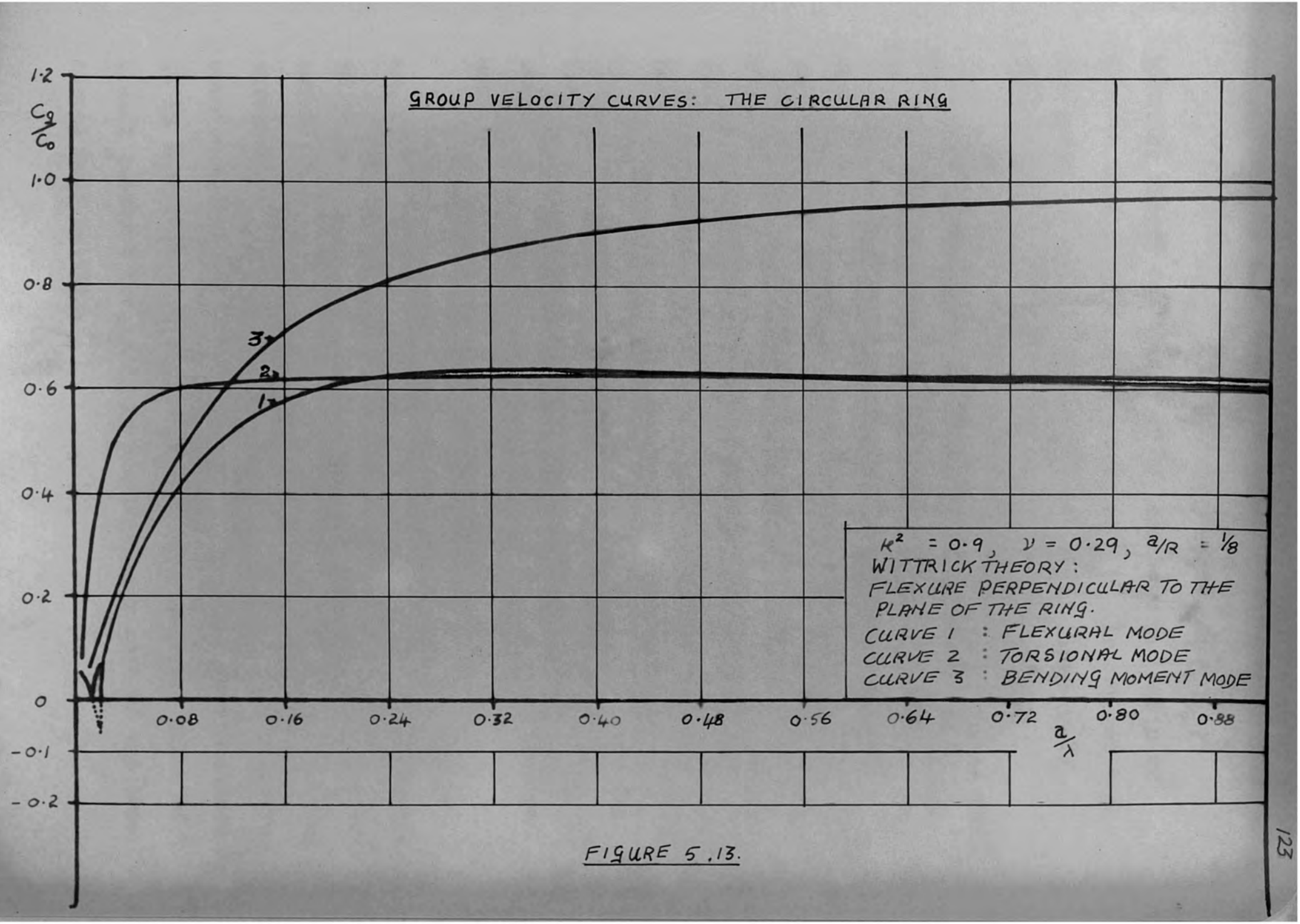
GROUP VELOCITY CURVES: THE CIRCULAR RING
C_g/C_0
1·2
1·0
0·8
0·6
0·4
0·2
0
-0·1
-0·2
0·08
0·16
0·24
0·32
0·40
0·48
0·56
0·64
0·72
0·80
0·88
a/λ
1
2
3
$K^2 = 0.9$, $\nu = 0.29$, $a/R = 1/8$
WITTRICK THEORY:
FLEXURE PERPENDICULAR TO THE PLANE OF THE RING.
CURVE 1 : FLEXURAL MODE
CURVE 2 : TORSIONAL MODE
CURVE 3 : BENDING MOMENT MODE

FIGURE 5.13.

Wittrick theory for a ring of a/R equal to $\frac{1}{8}$. Again we observe that if the positive root of $\left(\frac{C}{Co}\right)^2$ is assumed then the group velocity is negative for a small range of a/λ. This result was discussed in the previous section.

Figure 5.14 shows the corresponding arrival curves for a ring as computed from the Wittrick theory. The Timoshenko straight rod curve is included for comparison purposes. It was seen in section 5.3.a that the flexural mode arrival curves for vibrations in the plane of a ring, as computed from the Morley theory equations for pronounced and slight curvature, are very close, the difference being negligible compared with the difference between the curved and straight rod results. It is therefore assumed that for $a/R < \frac{1}{8}$ the arrival curve for flexural vibrations perpendicular to the plane of a ring, as computed from the Wittrick theory, is a good approximation within the limitations of the Timoshenko theory.

Figure 5.15 shows the arrival curves for a ring of a/R equal to $\frac{1}{4}$ as computed from equation 27. The assumption of slight curvature is no longer valid, however, the arrival curve is expected to give a good indication of the effect of curvature on the stress pulse pattern. The effect of curvature on the torsional mode arrival curve is very pronounced and it is seen from Figure 5.15 that a long dispersed pulse of almost constant frequency is predicted for most of the torsional mode pattern.

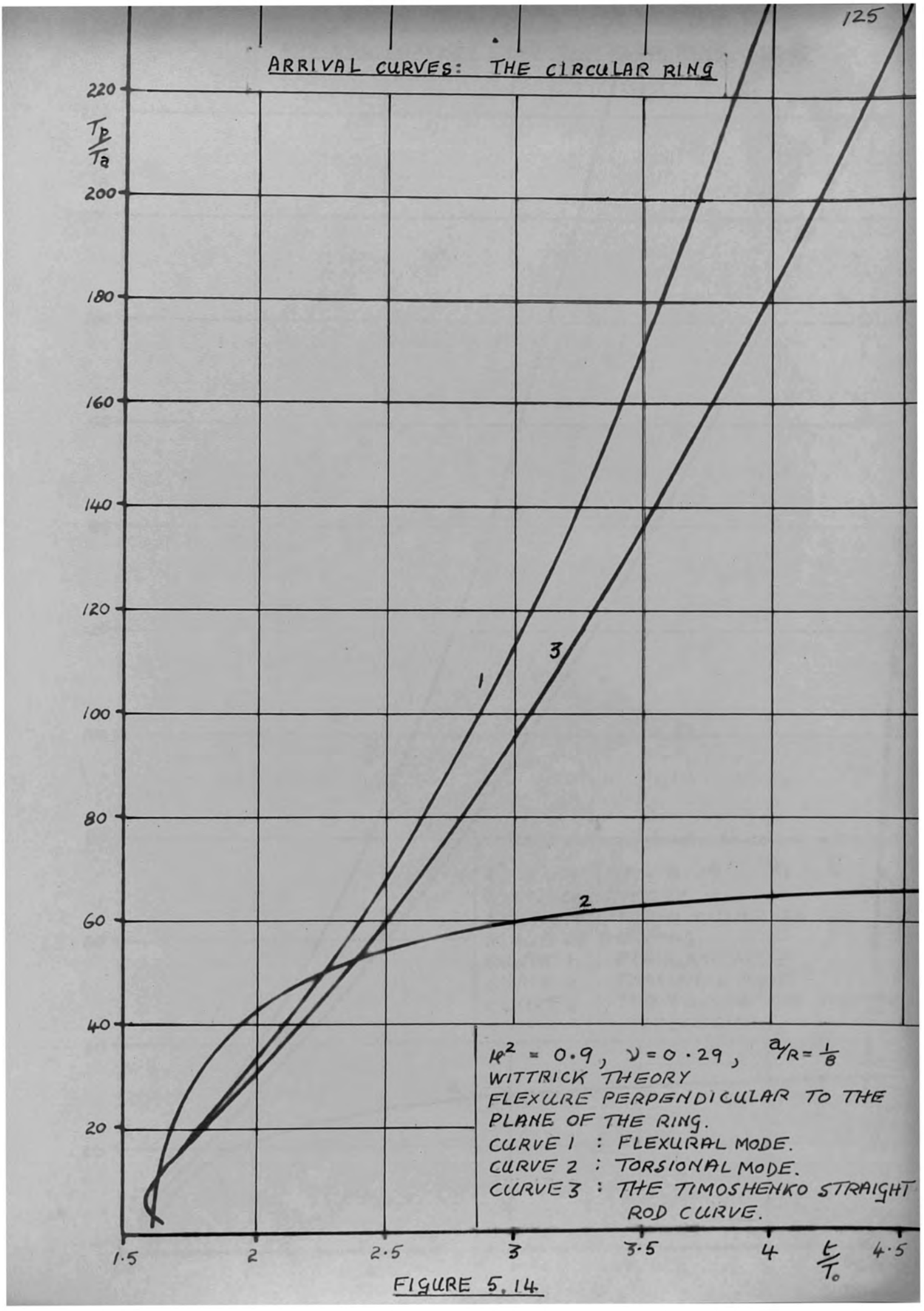
ARRIVAL CURVES: THE CIRCULAR RING
$\frac{T_p}{T_a}$
220
200
180
160
140
120
100
80
60
40
20
1
2
3
$\kappa^2 = 0.9$, $\nu = 0.29$, $a/R = \frac{1}{8}$
WITTRICK THEORY
FLEXURE PERPENDICULAR TO THE PLANE OF THE RING.
CURVE 1 : FLEXURAL MODE.
CURVE 2 : TORSIONAL MODE.
CURVE 3 : THE TIMOSHENKO STRAIGHT ROD CURVE.
1·5
2
2·5
3
3·5
4
4·5
$\frac{L}{T_o}$

FIGURE 5.14

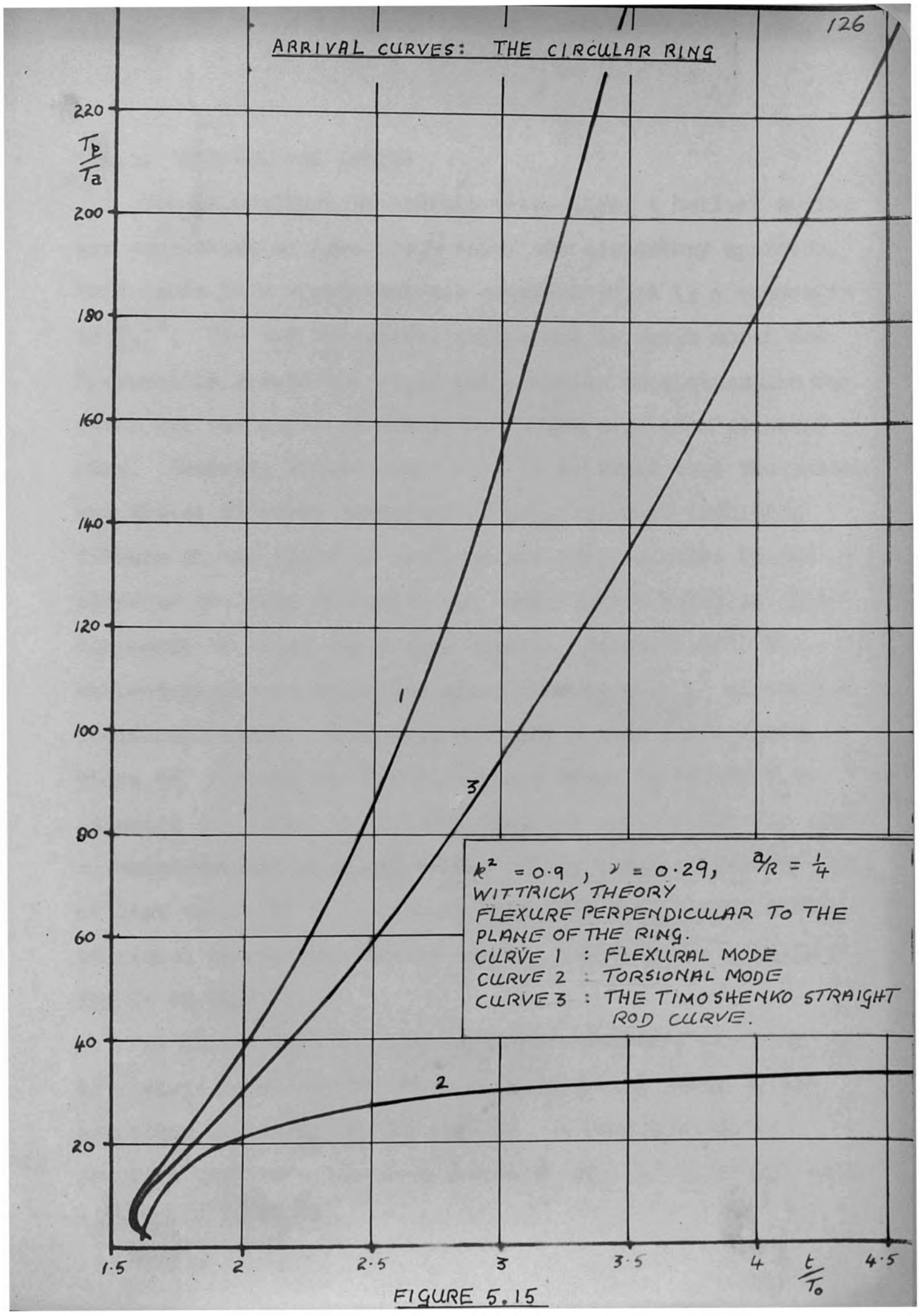
ARRIVAL CURVES: THE CIRCULAR RING
220
200
180
160
140
120
100
80
60
40
20
$\frac{T_p}{T_a}$
1
2
3
$k^2 = 0.9$, $\nu = 0.29$, $a/R = \frac{1}{4}$
WITTRICK THEORY
FLEXURE PERPENDICULAR TO THE PLANE OF THE RING.
CURVE 1 : FLEXURAL MODE
CURVE 2 : TORSIONAL MODE
CURVE 3 : THE TIMOSHENKO STRAIGHT ROD CURVE.
1·5
2
2·5
3
3·5
4
4·5
$\frac{t}{T_0}$

FIGURE 5.15

5.3.c. THE HELICAL SPRING

The propagation of elastic waves along a helical spring was considered by Love [1934] using the elementary approach. This leads to a characteristic equation which is a quadratic in $\left(\frac{C}{Co}\right)^2$. The two velocities correspond to waves which are flexural in nature and it is not possible to distinguish between the two modes as simply as in the case of a circular ring. However, in the limit $\alpha \to 0$ it is found that the faster and slower flexural waves can be identified as involving flexure in the plane of the ring and perpendicular to the plane of the ring respectively. When Love's equations are corrected to allow for rotary inertia [Britton 1957] the characteristic equation becomes a quartic in $\left(\frac{C}{Co}\right)^2$ giving two additional modes. The phase velocity curves for a spring where $a/R = 0.106$ and P = ½ inch are shown in Figure 5.16 assuming $\nu = 0.29$. It is seen that one mode, which has flexural characteristics at low values of a/λ, has a velocity C_T at high values of a/λ. It is also seen that a mode having torsional characteristics at low a/λ has a velocity approaching Co at high a/λ.

As in the case of a straight rods and circular rings it is clearly necessary to add a correction for shear to the equations of motion of the spring. As mentioned in the previous SECTION a Timoshenko-type theory for a helical spring

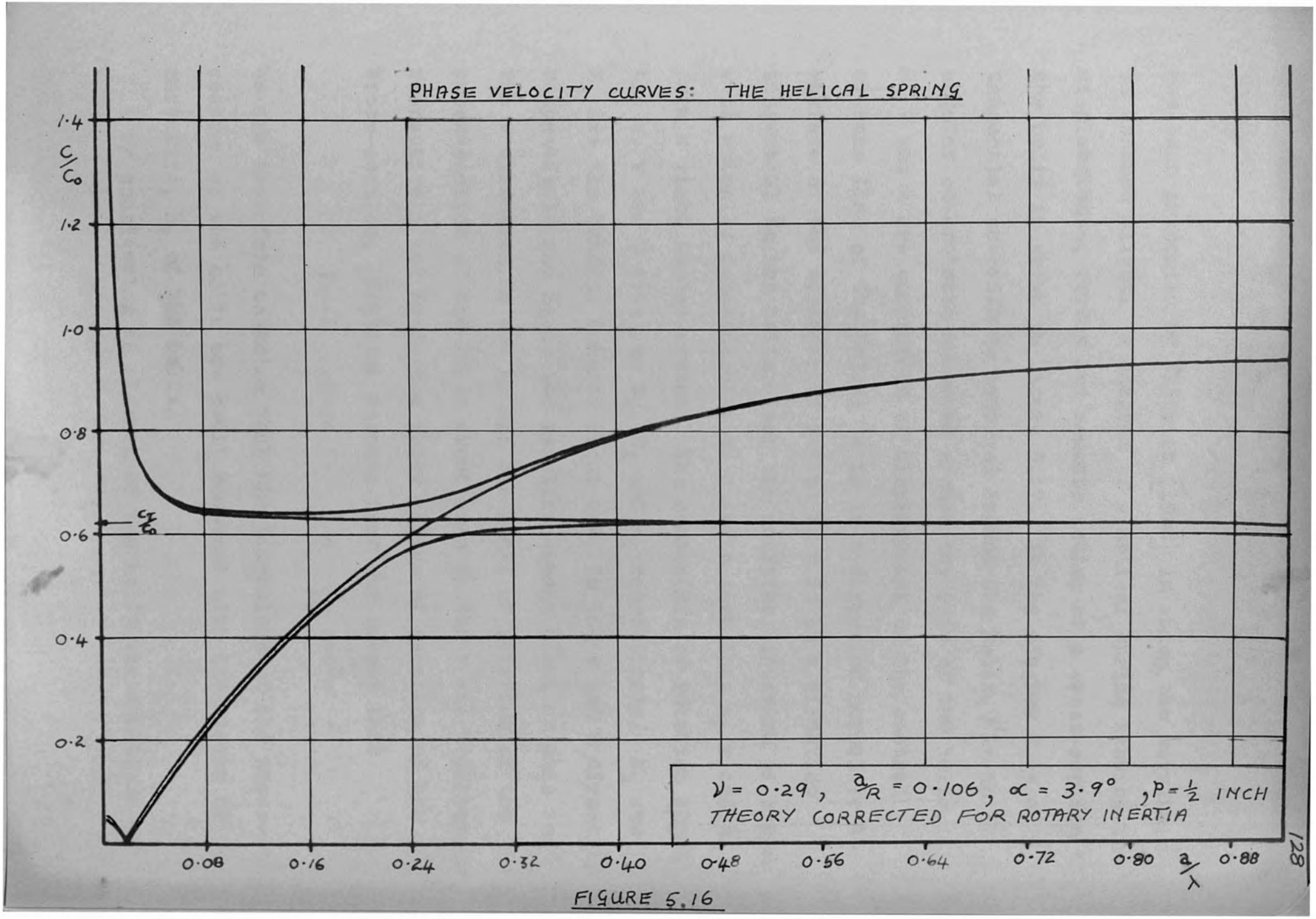
PHASE VELOCITY CURVES: THE HELICAL SPRING
1·4
C/Co
1·2
1·0
0·8
Cf/Co
0·6
0·4
0·2
0·08
0·16
0·24
0·32
0·40
0·48
0·56
0·64
0·72
0·80
a/λ
0·88
ν = 0·29 , a/R = 0·106 , α = 3·9° , P = ½ INCH
THEORY CORRECTED FOR ROTARY INERTIA

FIGURE 5.16

has been presented by Wittrick [1966] in which the curvature is assumed slight. A diagram of a helical spring showing the displacements, forces and moments acting at a cross-section of the helix is shown in Figure 5.17. In the diagram s is a tangential co-ordinate measured around the helix, γ' is an angular co-ordinate measured around the axis of the helix. u, v and w are components of displacement of the central elastic line of the helix; u is in a direction normal to the surface of the cylinder of radius R, w is in a direction tangential to the helix along the positive direction of s and v is mutually perpendicular to u and w such that u, v and w form a right handed system. The components of rotation about the u, v and w axes are θ_2, θ_1 and θ_T respectively. M_1 and M_2 are the bending moments about axes in the v and u direction respectively and M_T is the twisting moment about an axis in the w direction. Kn and Kp are the radii of gyration of the cross-section of the helix about axes in the v and u direction respectively and K_T is the polar radius of gyration of the cross-section. Wittrick assumes from the outset that

$$\gamma^2 \ll 1 \quad \text{where} \quad \gamma = \frac{R}{K_T} \sec^2 \alpha$$

We are therefore assuming that the dimensions of the cross-section of the helix are small compared with the radius of curvature, R, of the helix.

By considering an element of the helix the equations of

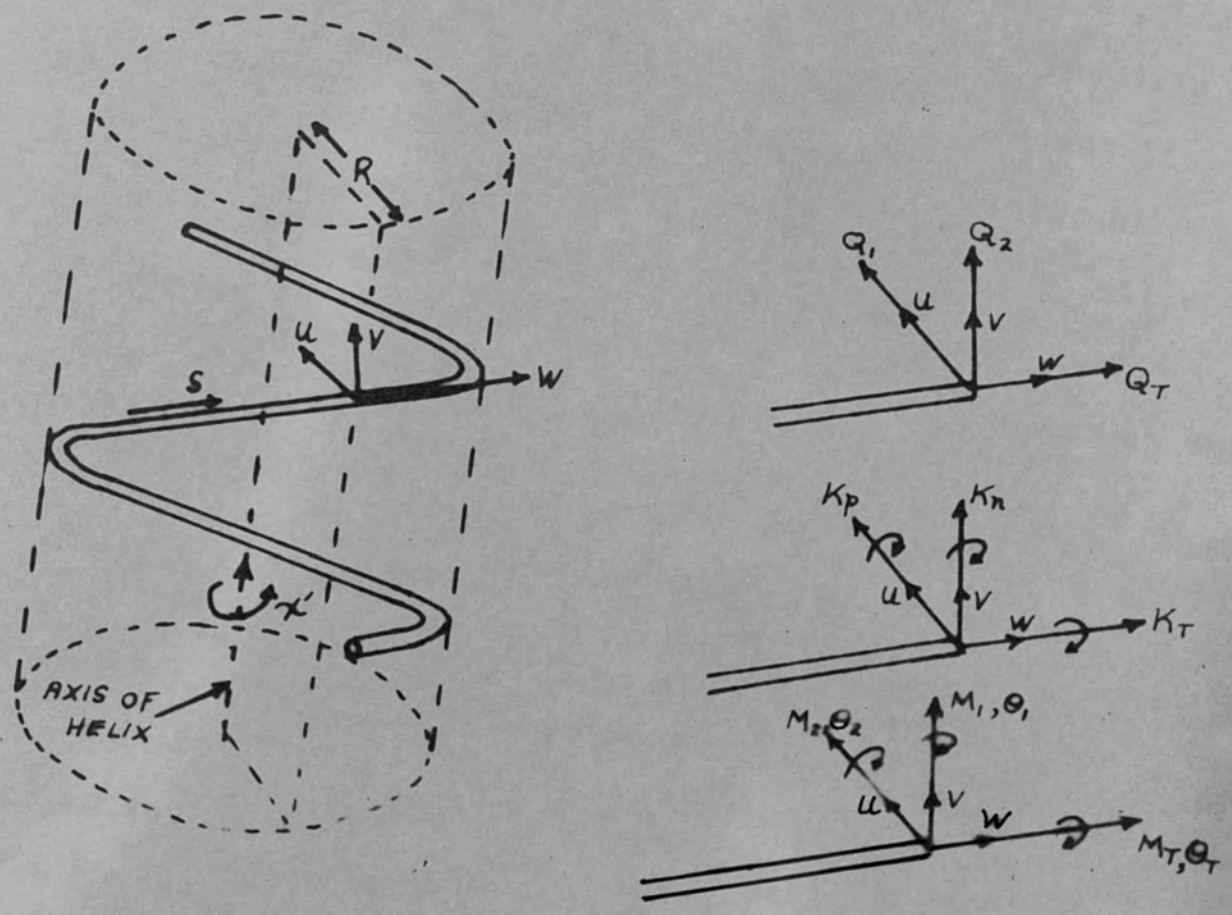

A DIAGRAM OF A HELICAL SPRING SHOWING THE DISPLACEMENTS, FORCES AND MOMENTS ACTING AT A CROSS-SECTION OF THE HELIX.

FIGURE 5.17

elasticity can be written. The three components of the moment acting at a cross-section of the helix (M_1, M_2 and M_T) can be written in terms of rotations at the cross-section and the three components of force acting at a cross-section of the helix (Q_1, Q_2 and Q_T) can be written in terms of the displacements and rotations at the cross-section. Three equations of translational motion and three equations of rotational motion can also be written. Thus twelve equations can be written relating the forces and moments to the displacements and rotations of the element of the helix. It is then assumed that we are investigating the propagation of harmonic trains of waves

$$\text{i.e.} \qquad w = W \exp\left\{ i\frac{2\pi}{\lambda}(s - \Omega C_o t) \right. \qquad 31)$$

where $\Omega = \frac{C}{C_o}$ and W is considered to be a constant deformation amplitude.

Substituting the stresses and deformations, in the form shown in equation 31, into the twelve relating equations we obtain twelve equations involving the stress and deformation amplitudes, W etc. We can then eliminate the stress amplitudes from the twelve equations which results in a set of six linear, homogeneous, simultaneous equations involving deformation amplitudes. These equations are of the form

$$\left[B - \left(\frac{C_o}{C_T}\right)^2 \Omega^2 I_6 \right] Y = 0 \qquad 32)$$

where B is a symmetrical sixth order square matrix, Y is a

column matrix involving deformation constants and I_6 is a sixth-order unit matrix. In order that the equation 32 should have a non-zero solution it is necessary for the determinant

$$\text{Det} \left[B - \left(\frac{C_0}{C_T}\right)^2 \nu^2 I_6 \right] = 0 \qquad 33)$$

The matrix B can be written in the following form for a helical guide of circular cross-section.

$$B = \begin{bmatrix} B_{11} & B_{12} \\ B_{21} & B_{22} \end{bmatrix}$$

where

$$B_{11} = \begin{bmatrix} k^2+\lambda^2 k^2 \tan^2\alpha & \sqrt{2}\lambda\gamma k^2 & 0 \\ \sqrt{2}\lambda\gamma k^2 & 2\left\{\frac{E}{2G} + \lambda^2 \frac{E}{2G} \tan^2\alpha + \lambda^2 + \lambda^2\gamma^2 k^2\right\} & \sqrt{2}\lambda\left\{1+\frac{E}{2G}\right\} \\ 0 & \sqrt{2}\lambda\left\{1+\frac{E}{2G}\right\} & \left\{1+\lambda^2\frac{E}{2G}\right\} \end{bmatrix}$$

$$B_{12} = \begin{bmatrix} 2\lambda k^2 \tan\alpha & \lambda^2 k^2 \tan\alpha & \sqrt{2}\lambda^2\gamma k^2 \tan\alpha \\ \sqrt{2}\lambda^2\gamma k^2 \tan\alpha & 0 & 4\lambda \frac{E}{2G} \tan\alpha \\ 0 & 0 & \sqrt{2}\lambda^2 \frac{E}{2G} \tan\alpha \end{bmatrix}$$

$$B_{22} = \begin{bmatrix} k^2 + \lambda^2 k^2 \tan^2\alpha + 2\lambda^2\frac{E}{2G} & \lambda\left\{\frac{E}{G} + k^2\right\} & \sqrt{2}\lambda\gamma k^2 \\ \lambda\left\{\frac{E}{G} + k^2\right\} & \left\{\frac{E}{G} + \lambda^2 k^2\right\} & \sqrt{2}\lambda^2\gamma k^2 \\ \sqrt{2}\lambda\gamma k^2 & \sqrt{2}\lambda^2\gamma k^2 & 2\left\{\frac{E}{2G} + \lambda^2\frac{E}{2G}\tan^2\alpha + \lambda^2\gamma^2 k^2\right\} \end{bmatrix}$$

B_{21} = B_{12} transposed

It is noted that the matrix B is symmetrical about the leading diagonal which is a requirement for the principle of conservation of energy [Viasov 1951].

Equation 33 can therefore be solved for a given value of λ if we assume $\nu = 0{\cdot}29$, $k^2 = 0{\cdot}9$ and we know the values of a, R and α for the spring considered. The solution involves the expansion of the sixth order determinant into a linear equation of the form

$$a'\left(\frac{C}{Co}\right)^{12} + b'\left(\frac{C}{Co}\right)^{10} + c'\left(\frac{C}{Co}\right)^{8} + d'\left(\frac{C}{Co}\right)^{6} + e'\left(\frac{C}{Co}\right)^{4} + f'\left(\frac{C}{Co}\right)^{2} + g' = 0 \qquad 34B)$$

and then solving this sixth order equation in $(C/Co)^2$ to give six roots representing six modes of vibration in the guide. If we put $\alpha = 0$ into the matrix B and $B_{12} = B_{21} = 0$ and we then have two distinct sets of three linear homogenous equations. In order that these equations have non-zero solution s

$$\text{Det}\left[B_{11} - \left(\frac{Co}{C_T}\right)^2 \Omega^2 I_3\right] = 0 \qquad 35)$$

$$\text{Det}\left[B_{22} - \left(\frac{Co}{C_T}\right)^2 \Omega^2 I_3\right] = 0 \qquad 36)$$

where I_3 is a third order unit matrix and

FOOTNOTE

a', b', c', d', e', f' and g' are all functions of λ as in equation 34 A page 115.

$$B_{11} = \begin{bmatrix} k^2 & \sqrt{2}\lambda\gamma k^2 & 0 \\ \sqrt{2}\lambda\gamma k^2 & 2\left\{\frac{E}{2G} + \lambda^2 + \lambda^2\gamma^2 k^2\right\} & \sqrt{2}\lambda\left\{1 + \frac{E}{2G}\right\} \\ 0 & \sqrt{2}\lambda\left\{1 + \frac{E}{2G}\right\} & 1 + \lambda^2 \frac{E}{2G} \end{bmatrix}$$

$$B_{22} = \begin{bmatrix} k^2 + 2\lambda^2 \frac{E}{2G} & \lambda\left\{\frac{E}{G} + k^2\right\} & \sqrt{2}\lambda\gamma k^2 \\ \lambda\left\{\frac{E}{G} + k^2\right\} & 2\left\{\frac{E}{2G} + \lambda^2 k^2\right\} & \sqrt{2}\lambda^2\gamma k^2 \\ \sqrt{2}\lambda\gamma k^2 & \sqrt{2}\lambda^2\gamma k^2 & 2\left\{\frac{E}{2G} + \lambda^2\gamma^2 k^2\right\} \end{bmatrix}$$

Equation 35 and 36 are obviously cubic equations in $\Omega^2 = \left(\frac{C}{C_0}\right)^2$. When expanded equations 35 and 36 give equations 27 and 26 respectively. It will be remembered that equations 27 and 26 correspond to vibrations perpendicular to, and in, the plane of a circular ring respectively.

The solution of equation 33 to give the phase velocity dispersion curves for the six roots predicted by the Wittrick theory is extremely complex algebraically. Use was made of

the London University Atlas Computer to compute the curves of $\frac{c}{c_o}$ against a/λ shown in Figure 5.18. In this case $a/R = 0.106$ $p = \frac{1}{2}$ inch ($\alpha = 3.9^o$) and it was assumed that $\mu^2 = 0.9$ and $\gamma = 0.29$. The six roots can be associated with a faster and a slower flexural mode, a torsional mode, a longitudinal mode and two bending moment modes as shown in the diagram. It is seen from the diagram that the curves for the two flexural modes are very close, however, the separation is more pronounced than in the case of a circular ring where $\alpha = 0$. The Wittrick theory phase velocity curves for $\alpha = 0$ are shown in Figure 5.19. Comparing Figures 5.18 and 5.19 it is seen that the effect of pitch is to separate the two flexural curves but the separation is small compared to the difference between the circular ring and straight rod curves caused by the finite radius, R, of the ring. In the case of close coiled springs the main effect on the flexural mode dispersion characteristic is due to the mean radius, R, of the spring and in this case both flexural dispersion curves lie close to the corresponding curves for a circular ring of radius R.

The calculation of group velocity by a direct method is an extremely complex algebraic problem and because of this a numerical method of differentiation was used to find $\frac{d\frac{c}{c_o}}{d\,a/\lambda}$ This can be done, to a good accuracy by employing a method described in Numerical Calculus by W.E. Milne [1950] .

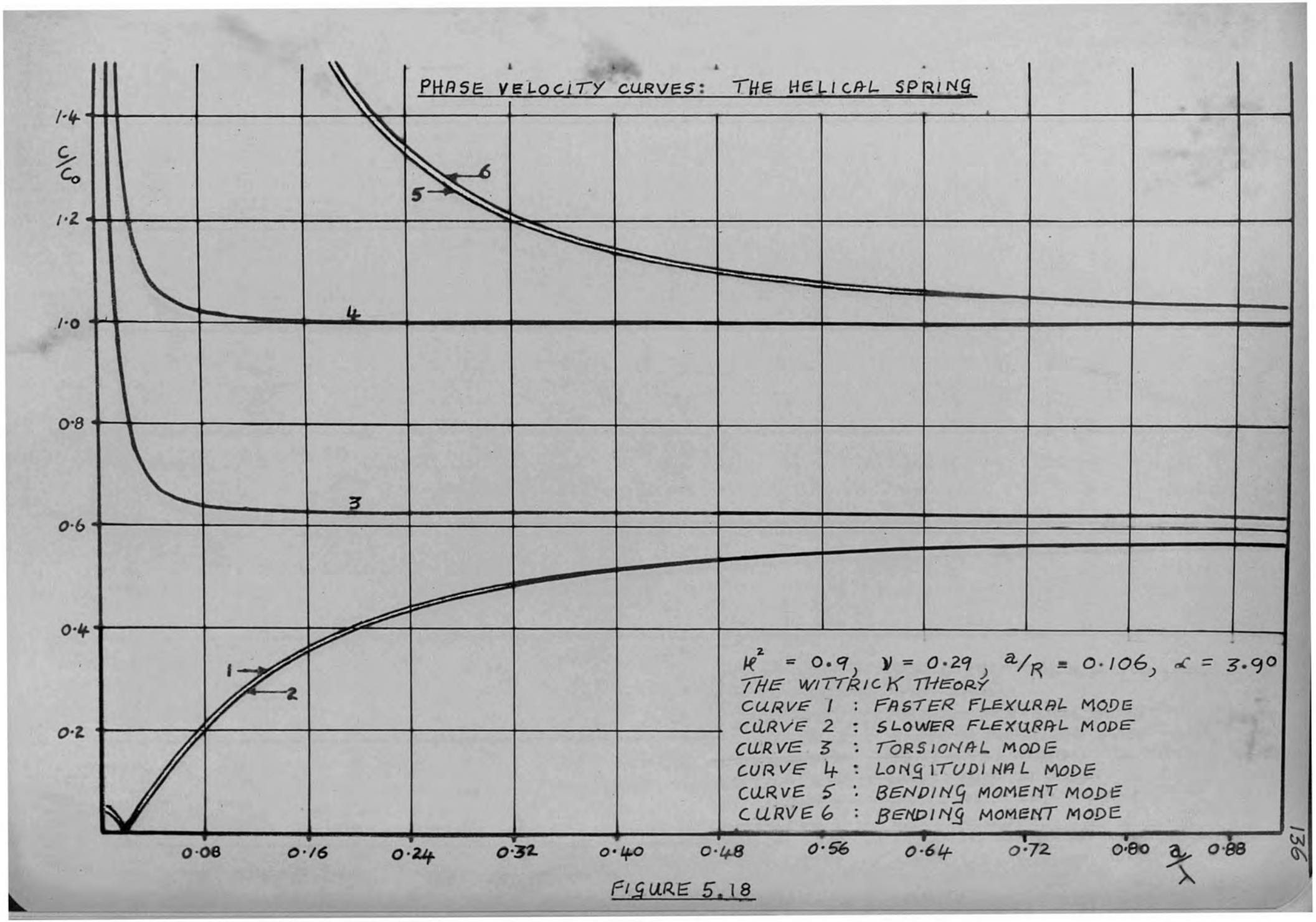
PHASE VELOCITY CURVES: THE HELICAL SPRING
c/c0
1·4
1·2
1·0
0·8
0·6
0·4
0·2
0·08
0·16
0·24
0·32
0·40
0·48
0·56
0·64
0·72
0·80
0·88
a/λ
1
2
3
4
5
6
k² = 0·9, ν = 0·29, a/R = 0·106, α = 3·90
THE WITTRICK THEORY
CURVE 1 : FASTER FLEXURAL MODE
CURVE 2 : SLOWER FLEXURAL MODE
CURVE 3 : TORSIONAL MODE
CURVE 4 : LONGITUDINAL MODE
CURVE 5 : BENDING MOMENT MODE
CURVE 6 : BENDING MOMENT MODE

FIGURE 5.18

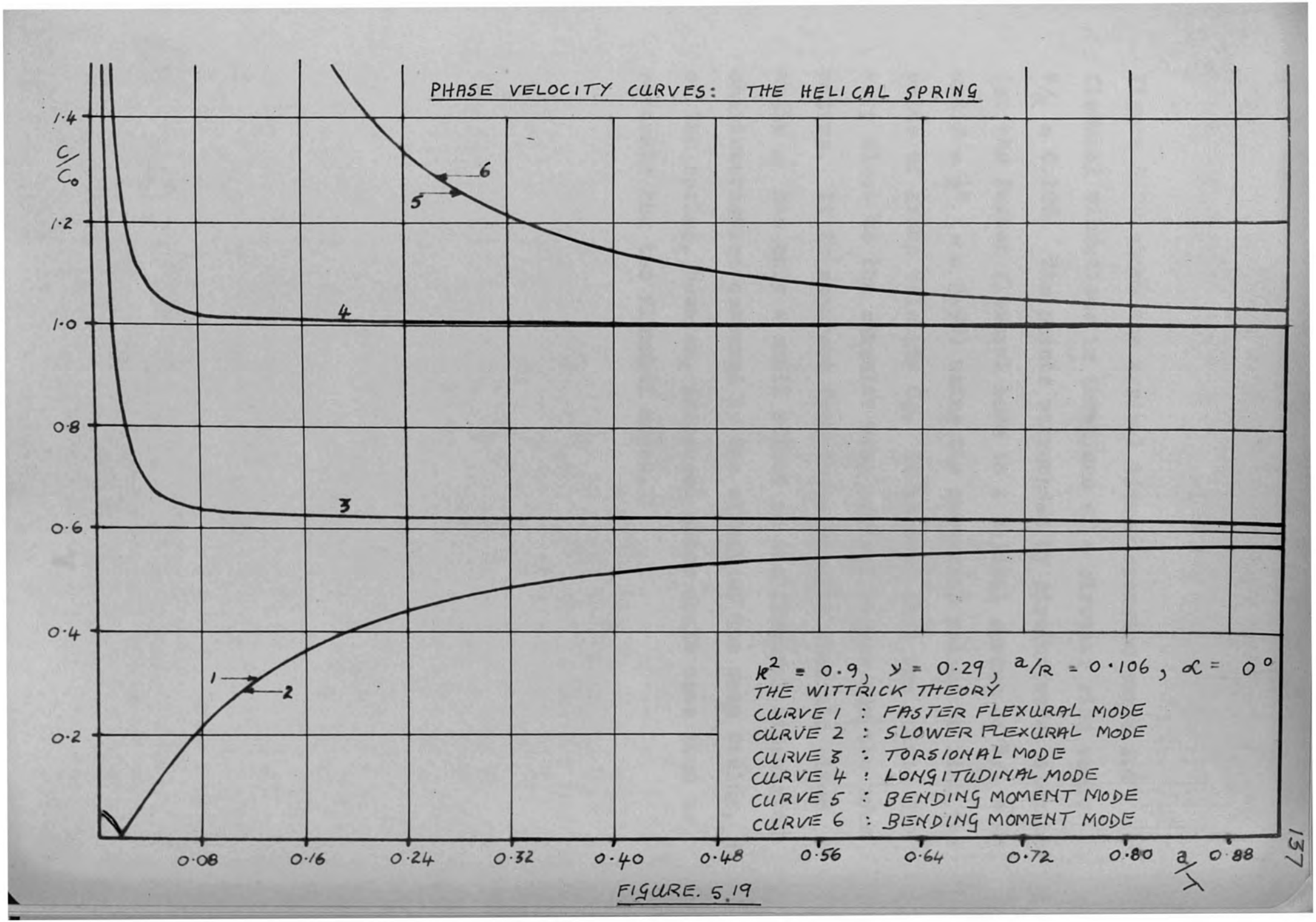
PHASE VELOCITY CURVES: THE HELICAL SPRING
C/C0
1·4
1·2
1·0
0·8
0·6
0·4
0·2
0·08
0·16
0·24
0·32
0·40
0·48
0·56
0·64
0·72
0·80
0·88
a/λ
1
2
3
4
5
6
k² = 0·9, ν = 0·29, a/R = 0·106, α = 0°
THE WITTRICK THEORY
CURVE 1 : FASTER FLEXURAL MODE
CURVE 2 : SLOWER FLEXURAL MODE
CURVE 3 : TORSIONAL MODE
CURVE 4 : LONGITUDINAL MODE
CURVE 5 : BENDING MOMENT MODE
CURVE 6 : BENDING MOMENT MODE

FIGURE. 5.19

Figure 5.20 shows the arrival time dispersion curve for flexural vibrations in the plane of a circular ring where $a/R = 0.106$. The points surrounded by circles were calculated for the faster flexural mode in a helical spring of $a/R = 0.106$ and P = $\frac{1}{2}$" ($\alpha = 3.9^{\circ}$) using the numerical method to find the value of group velocity Cg. It is seen that the points lie very close to the circular ring arrival curves for the same radius. It is apparent from these results that the pitch angle α has only a small effect on the flexural dispersion characteristics compared to the effect of the mean radius, R, of the spring, However, increased pitch angle does tend to separate the two flexural modes.

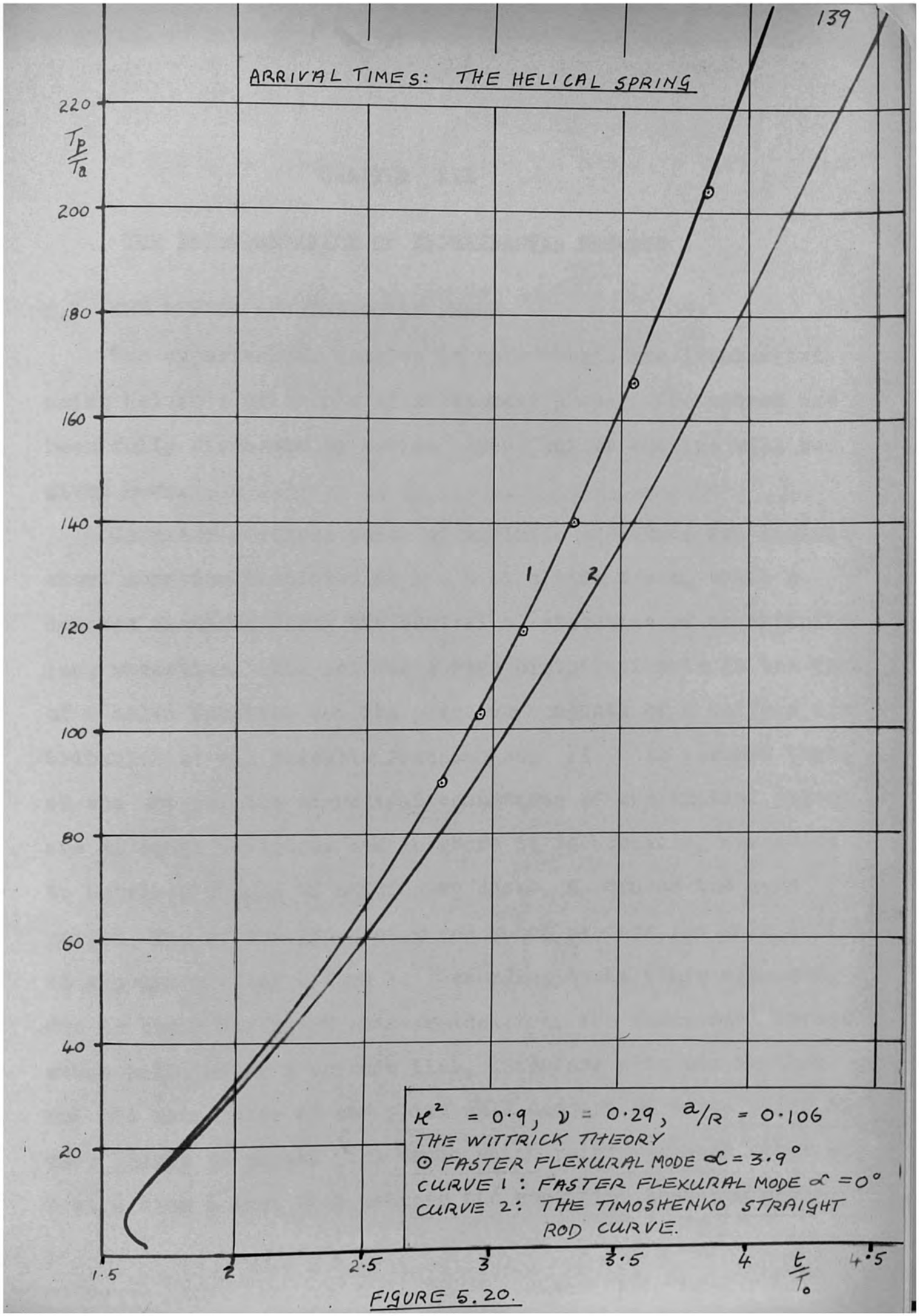
ARRIVAL TIMES: THE HELICAL SPRING
$\frac{T_p}{T_a}$
220
200
180
160
140
120
100
80
60
40
20
1
2
1·5
2
2·5
3
3·5
4
4·5
$\frac{t}{T_o}$
$\kappa^2 = 0.9$, $\nu = 0.29$, $a/R = 0.106$
THE WITTRICK THEORY
⊙ FASTER FLEXURAL MODE $\alpha = 3.9°$
CURVE 1 : FASTER FLEXURAL MODE $\alpha = 0°$
CURVE 2: THE TIMOSHENKO STRAIGHT ROD CURVE.

FIGURE 5.20.

CHAPTER SIX

THE INTERPRETATION OF EXPERIMENTAL RESULTS

6.1 THE METHOD OF STATIONARY PHASE

The experimental results in this thesis are interpreted using Kelvin's principle of stationary phase. The method has been fully discussed by Davies [1948] but an outline will be given here.

Consider a stress pulse of infinite amplitude and infinitely short duration initiated at x = o at a time t = o, where x denotes distance along the central elastic line of an infinitely long waveguide. The initial stress distribution is in the form of a delta function and its spectrum consists of a uniform distribution of all possible frequencies. If it is assumed that, at the origin, the sinusoidal components of the initial pulse are of equal amplitude and in phase it is possible, according to Kelvin's method of stationary phase, to deduce the mean period, Tp, of the group of waves which produce the main effect at a point x after a time t. According to Kelvin's argument, due to their different phase velocities, the sinusoidal stress waves will, after a certain time, interfere with one another and the main pulse at any point will consist of waves which are very nearly in phase. The waves which reinforce each other at x at a time t must then satisfy the condition that the phase,

$\frac{2\pi}{\lambda}(x - ct)$, is stationary and this condition is easily shown to be equivalent to

$$x - Cgt = 0 \qquad 37)$$

where Cg is the group velocity for wavelength λ .

The period, T, of a stress wave of wavelength λ and phase velocity C is given by

$$T = \frac{\lambda}{C} \qquad 38)$$

If we consider this to be the predominant period of a small group of waves which cause the main effect at a distance x along the guide at a time t after the initiation of the pulse then we can say that the arrival time, t, of a group of waves of predominant period $Tp = \frac{\lambda}{C}$, is given by

$$t = \frac{x}{Cg} \qquad 39)$$

where Cg is the group velocity for wavelength λ and phase velocity C.

As mentioned in chapter 5, it is convenient to represent the relationship between the variables Tp, x and t in non-dimensional form by plotting $\frac{Tp}{Ta}$ against $\frac{t}{To}$, where $Ta = \frac{a}{Co}$ and $To = \frac{x}{Co}$; physically Ta and To represent the time taken by infinitely long extensional waves to traverse the radius of cross-section, a, of the guide and the distance x respectively. The values of $\frac{Tp}{Ta}$ and $\frac{t}{To}$ are therefore given by the equations

$$\frac{Tp}{Ta} = \left(\frac{\lambda}{C}\right)\left(\frac{Co}{a}\right) = \left(\frac{\lambda}{a}\right)\left(\frac{Co}{C}\right) \qquad 40)$$

and $$\frac{t}{To} = \left(\frac{x}{Cg}\right)\left(\frac{Co}{x}\right) = \frac{Co}{Cg} \qquad 41)$$

From these equations, and the $\left(\frac{C}{Co}, \frac{a}{\lambda}\right)$ and $\left(\frac{Cg}{Co}, \frac{a}{\lambda}\right)$ curves, the $\left(\frac{Tp}{Ta}, \frac{t}{To}\right)$ curves can be calculated. Experimental values of Tp and t were obtained in the way described in section 3.4.

The method of stationary phase assumes initial pulses of infinitely short duration. However, it is found experimentally, for straight rods, that for large values of x and initial pulses of short duration this method of analysis leads to results which are in good agreement with other methods and with the arrival-time curves of the exact theory.

6.2 THE FLEXURAL MODE RESULTS FOR A STRAIGHT ROD

Figure 6.1 shows a plot of the experimental results obtained using a $\frac{1}{4}$ inch diameter straight rod in the manner described in section 4.1 b. The experimental points are shown together with the Timoshenko dispersion curve for the lowest flexural mode in a straight rod. It is seen that there is close agreement between experiment and theory over a wide range of predominant period. It is also seen that there is very little scatter in the experimental points which indicates that measurements were made on a single mode in this case. From these results it is clear that the method of measuring the

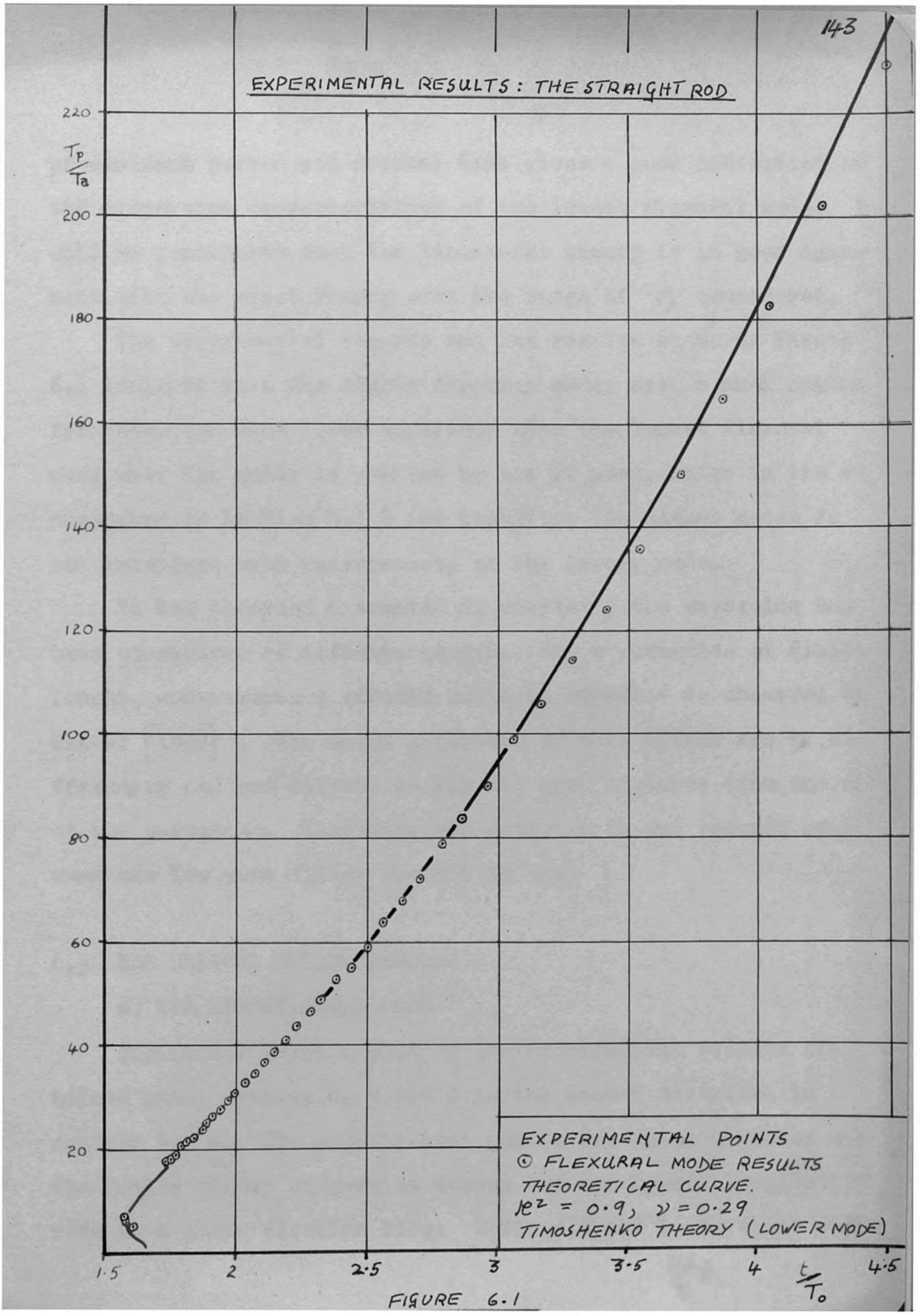
EXPERIMENTAL RESULTS : THE STRAIGHT ROD
220
200
180
160
140
120
100
80
60
40
20
Tp/Ta
1·5
2
2·5
3
3·5
4
4·5
t/To
EXPERIMENTAL POINTS
⊙ FLEXURAL MODE RESULTS
THEORETICAL CURVE.
κ² = 0·9, ν = 0·29
TIMOSHENKO THEORY (LOWER MODE)

FIGURE 6.1

predominant period and arrival time gives a good indication of the dispersion characteristics of the lowest flexural mode. It will be remembered that the Timoshenko theory is in good agreement with the exact theory over the range of a/λ considered.

The experimental records and the results shown in Figure 6.1 indicate that the higher flexural modes have a much higher frequency and much lower amplitude than the lowest flexural mode when the guide is excited by the 20 μsec. pulse in the way described in section 4.1 b and therefore the higher modes do not interfere with measurements on the lowest mode.

In the theories presented in chapter 5 the waveguide has been considered of infinite length. For a waveguide of finite length, end-resonance effects would be expected as observed by Oliver [1957] . The waves generated by this effect are of high frequency and are attenuated rapidly with distance from the end of the waveguide. They were not detected in our records even when the low pass filter was not in use.

6.3 THE HELICAL SPRING RESULTS

a) THE LONGITUDINAL MODE

Figure 6.2 shows a plot of the experimental results obtained using springs A, C and I in the manner described in section 4.2 a. The experimental points are shown together with the Morley theory dispersion curves for the lowest longitudinal mode in a plane circular ring. Springs C and I are close coiled

EXPERIMENTAL RESULTS : THE HELICAL SPRING

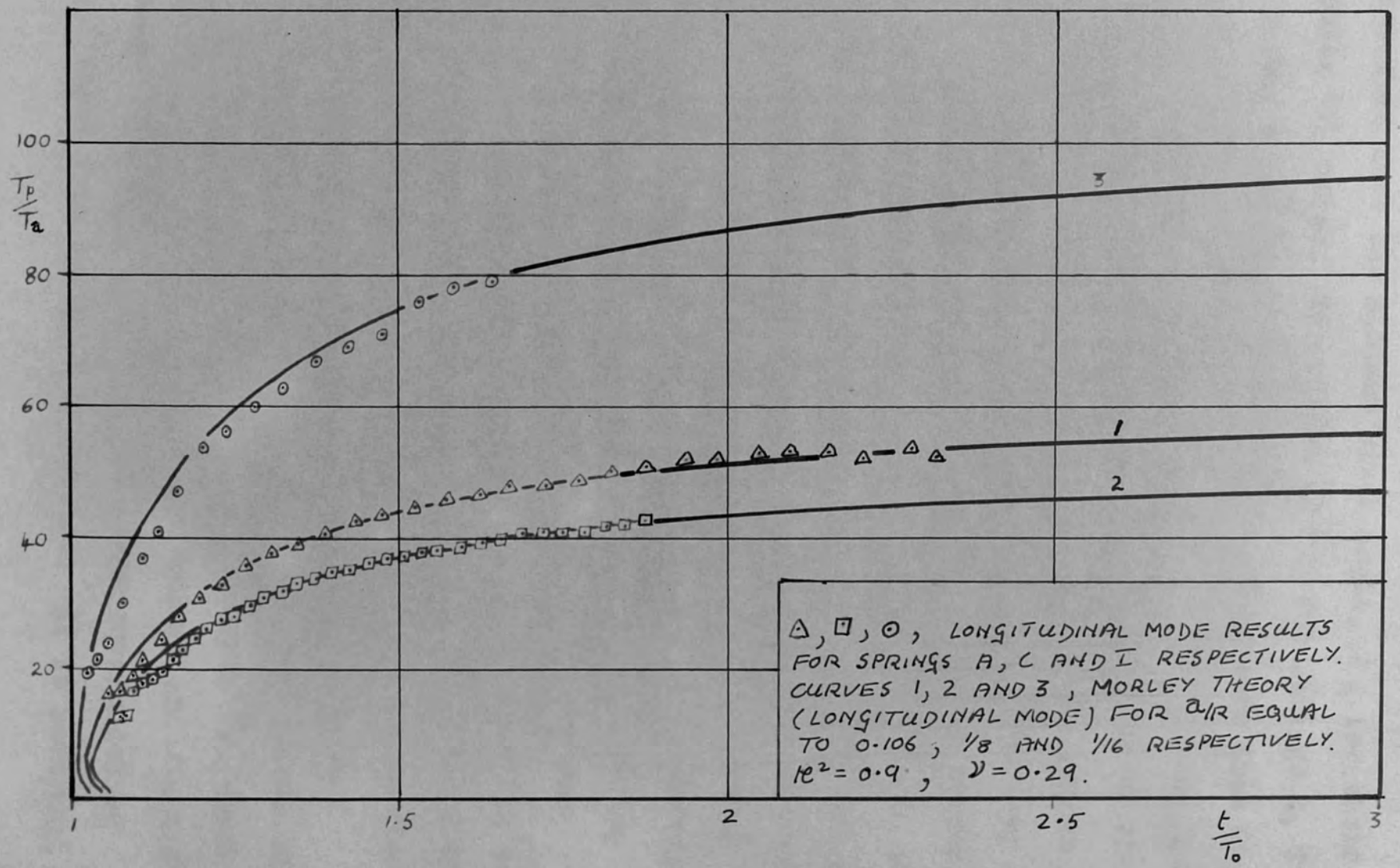

FIGURE 6.2.

and therefore have the minimum pitch angle, α , for their particular a/R value. The values of a/R for springs A, C and I are 0.106, $\frac{1}{8}$ and $1/16$ respectively. It is seen from Figure 6.2 that a change in the mean radius, R, of the spring has a pronounced effect on the dispersion characteristics of the lowest longitudinal mode and that the experimental points lie very close to the corresponding Morley theory curves over the range of predominant period considered. It will be remembered, however, that the Morley theory is only equivalent to an elementary-type theory for this mode and therefore agreement with experimental results is only expected to be good at wavelengths which are large compared with the cross-sectional diameter of the guide. It is seen from Figure 6.2 that the minimum value of $\frac{Tp}{Ta}$ recorded is about 12 which, according to the Morley theory, corresponds to a value of a/λ of about 0.080 and therefore all the experimental points shown in Figure 6.2 correspond to wavelengths longer than 4 cm. We would expect the elementary type theory to give a good indication of the dispersion characteristics in this long wavelength region.

Figure 6.3 shows a comparison of experimental points obtained using springs C and E which have a value of a/R equal to $\frac{1}{8}$ and pitch angles of $\alpha = 2.8^{\circ}$ (close coiled) and $\alpha = 9.0^{\circ}$ respectively. The results from spring C are surrounded by squares and those from spring E by circles. It is seen that

EXPERIMENTAL RESULTS: THE HELICAL SPRING

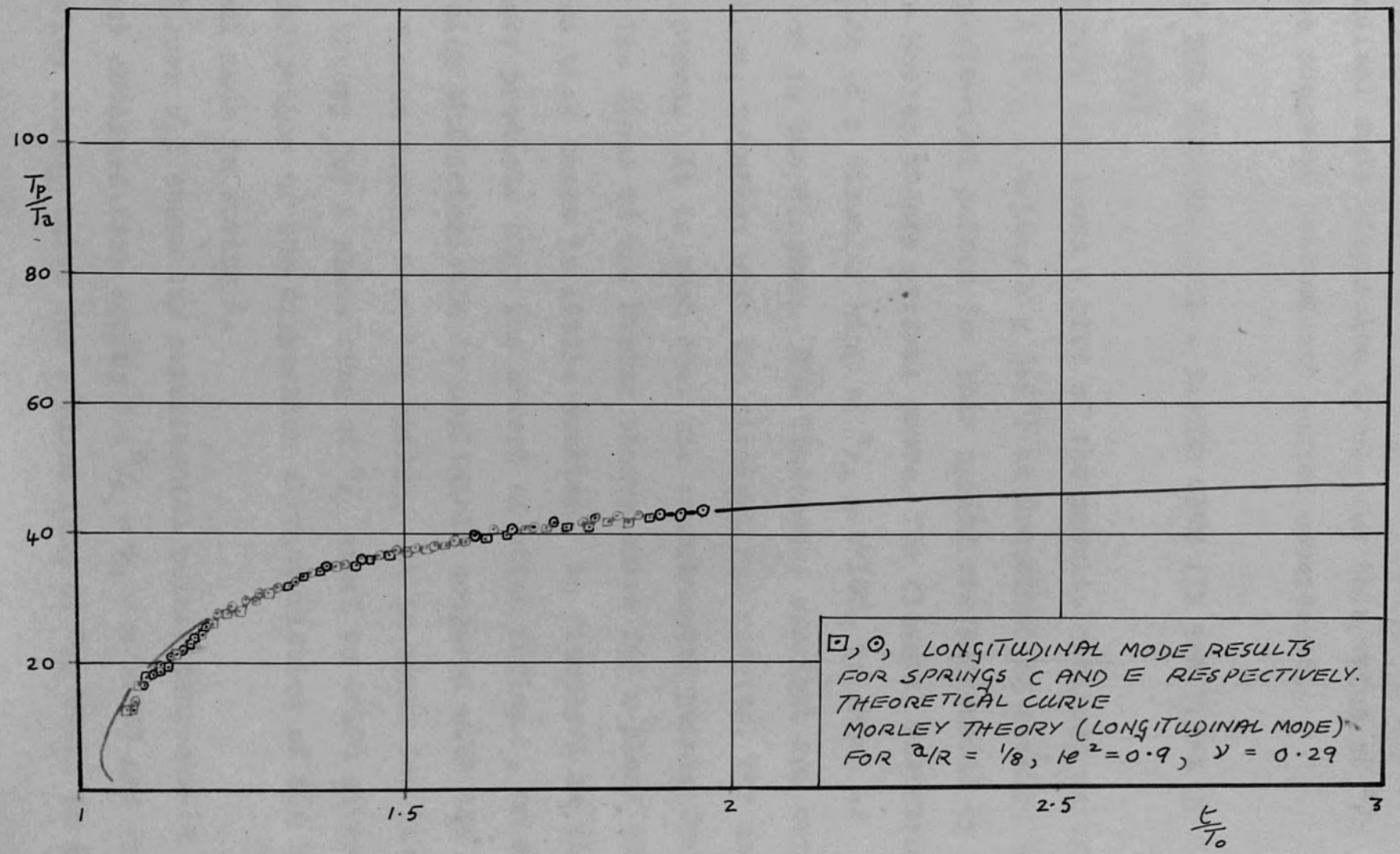

FIGURE. 6.3.

the change in pitch has a negligible effect on the lowest longitudinal mode dispersion curve, for this value of a/R, over the range of predominant period considered.

b) THE FLEXURAL MODE - FASTER WAVE (IN THE PLANE OF THE RING)

Figure 6.4 shows a plot of the results obtained using spring A ($a/R = 0.106$, $\alpha = 3.9^{\circ}$) as described in section 4.2 b. The experimental points for this spring are surrounded by squares and the Morley theory arrival curve, for flexural vibrations in the plane of a circular ring of $a/R = 0.106$, is shown as indicated in the diagram. The Timoshenko straight rod curve is also shown, together with the straight rod results, for comparison purposes. It is seen that the experimental points for the spring lie close to the Morley theory curve for a plane circular ring and that there is little scatter. As discussed in chapter 5, theory predicts that the effect of pitch angle, α, on the dispersion characteristic is negligible compared with the effect of the finite radius R of the spring. It is concluded that the Morley theory for a plane ring of a/R equal to 0.106 gives a good indication of the dispersion characteristics of the faster flexural mode in spring A.

Figure 6.5 shows the experimental points (surrounded by squares) obtained from spring C ($a/R = \frac{1}{8}$, $\alpha = 2.8^{\circ}$) and also the Morley theory curve for a plane ring of a/R equal to $\frac{1}{8}$.

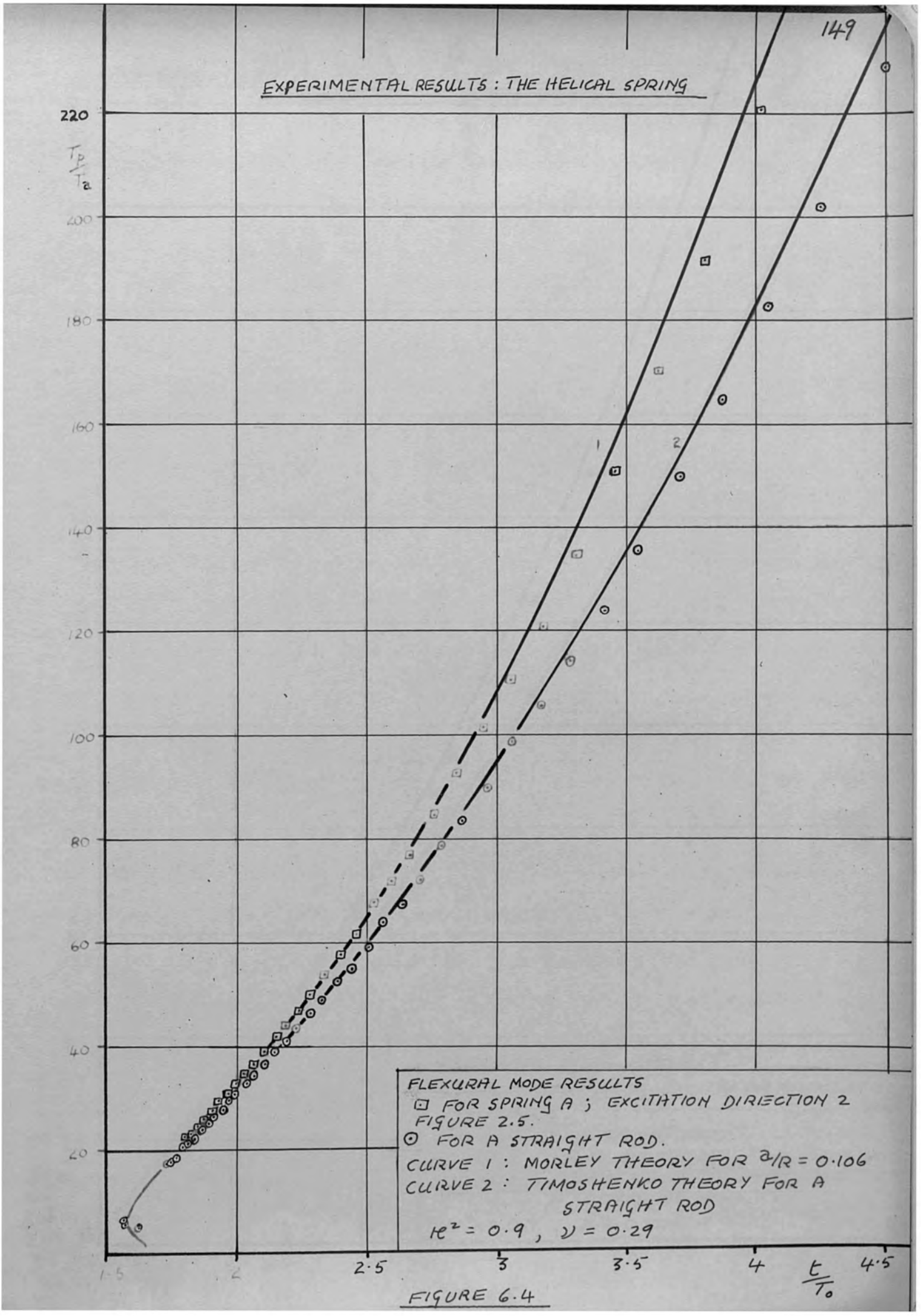
EXPERIMENTAL RESULTS : THE HELICAL SPRING
220
200
180
160
140
120
100
80
60
40
20
T_p/T_a
1
2
FLEXURAL MODE RESULTS
⊡ FOR SPRING A ; EXCITATION DIRECTION 2 FIGURE 2.5.
⊙ FOR A STRAIGHT ROD.
CURVE 1 : MORLEY THEORY FOR $a/R = 0.106$
CURVE 2 : TIMOSHENKO THEORY FOR A STRAIGHT ROD
$\kappa^2 = 0.9$, $\nu = 0.29$
1·5
2
2·5
3
3·5
4
4·5
$\frac{t}{T_0}$

FIGURE 6.4

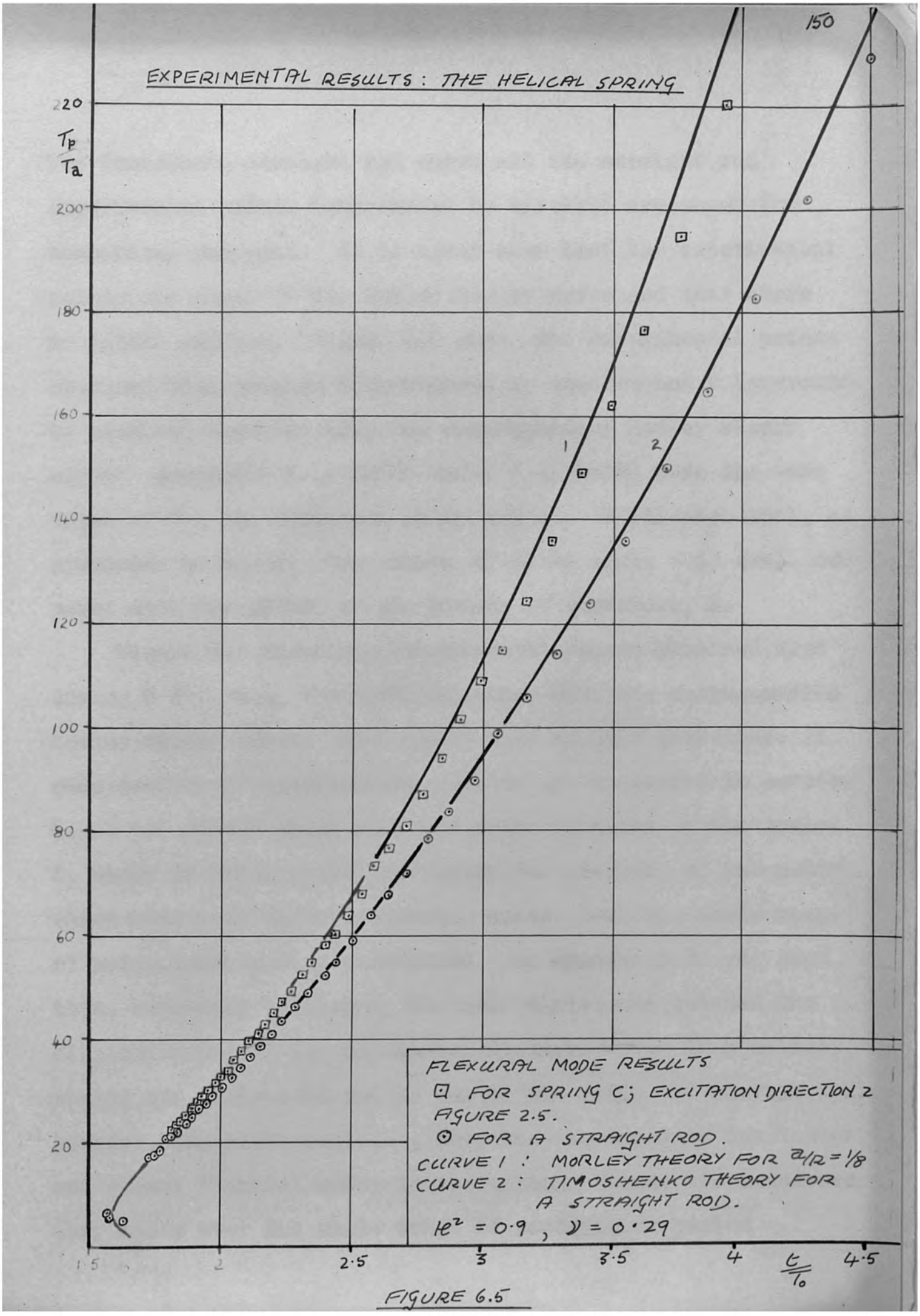
EXPERIMENTAL RESULTS : THE HELICAL SPRING
150
220
T_p
T_a
200
180
160
140
120
100
80
60
40
20
1
2
1·5
2
2·5
3
3·5
4
4·5
$\frac{L}{l_0}$
FLEXURAL MODE RESULTS
⊡ FOR SPRING C; EXCITATION DIRECTION 2 FIGURE 2.5.
⊙ FOR A STRAIGHT ROD.
CURVE 1 : MORLEY THEORY FOR $a/R = 1/8$
CURVE 2 : TIMOSHENKO THEORY FOR A STRAIGHT ROD.
$k^2 = 0.9$, $\nu = 0.29$

FIGURE 6.5

The Timoshenko straight rod curve and the straight rod experimental points (surrounded by circles) are shown for comparison purposes. It is again seen that the experimental points lie close to the Morley theory curve and that there is little scatter. Figure 6.6 shows the experimental points obtained from springs C(surrounded by squares)and D (surrounded by circles) together with the corresponding Morley theory curve; springs C ($\alpha = 2.8^{\circ}$) and D ($\alpha = 4.6^{\circ}$) have the same value of a/R but different pitch angles. It is seen that, as predicted by theory, the effect of pitch angle α is small compared with the effect of the radius of curvature, R.

Figure 6.7 shows the experimental points obtained from spring E ($a/R = \frac{1}{8}$, $\alpha = 9.0^{\circ}$) together with the corresponding Morley theory curve. It is seen that in this case there is some scatter of experimental points. As discussed in section 4.2 b the stress pulse received after 13 turns of the spring E, shown in Figure 4.16, indicates the presence of two modes which have very close dispersion curves over the whole range of predominant period considered. In chapter 5 it was seen that, according to theory, the main difference between the dispersion curves for the lowest flexural modes in a helical spring and a straight rod is due to the radius of curvature R, however, the pitch angle, α, does tend to separate the faster and slower flexural modes in the spring. These two modes are very close over the whole range of predominant period

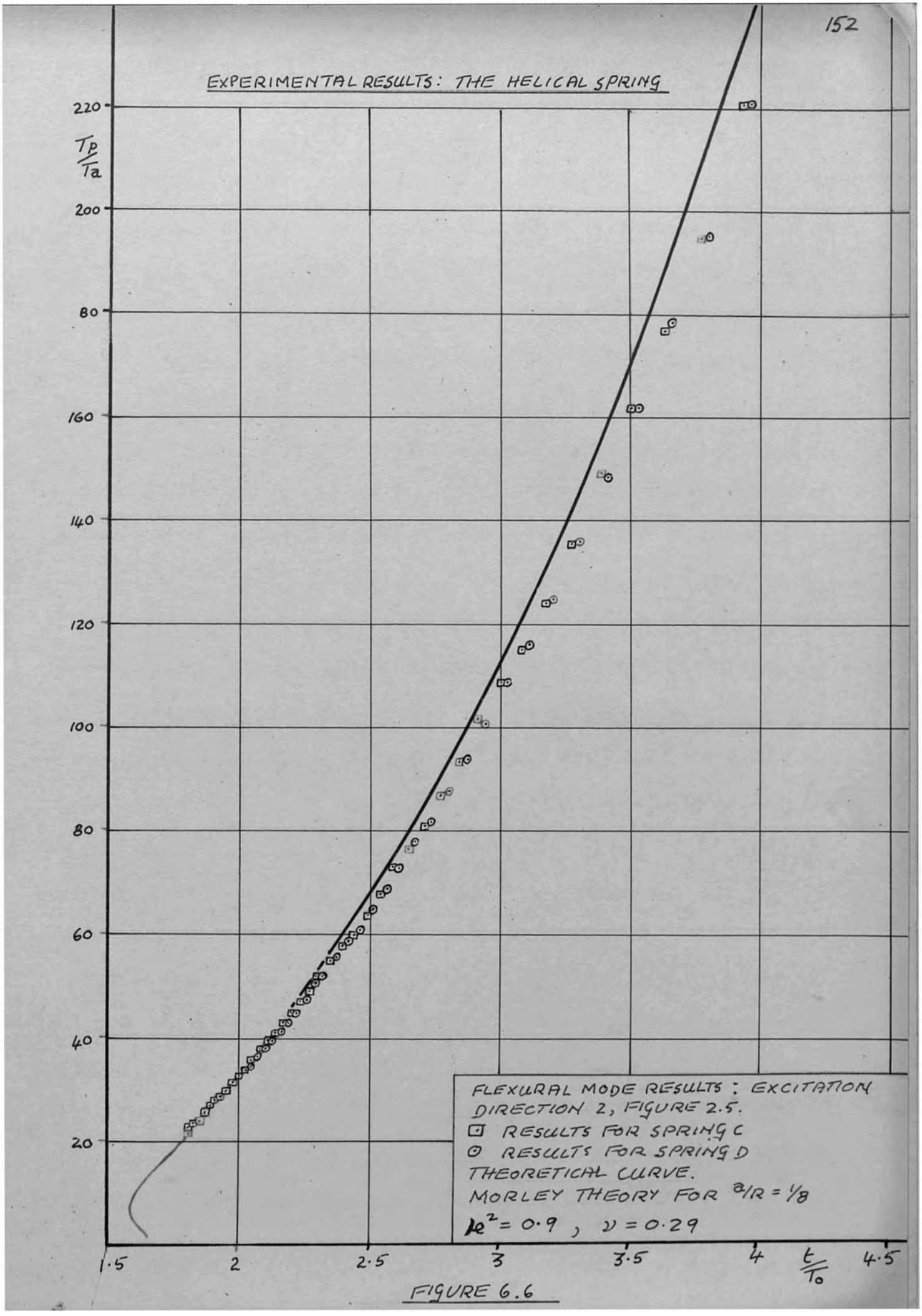
EXPERIMENTAL RESULTS: THE HELICAL SPRING
Tp/Ta
220
200
80
160
140
120
100
80
60
40
20
1·5
2
2·5
3
3·5
4
4·5
t/To
FLEXURAL MODE RESULTS: EXCITATION DIRECTION 2, FIGURE 2.5.
RESULTS FOR SPRING C
RESULTS FOR SPRING D
THEORETICAL CURVE.
MORLEY THEORY FOR a/R = 1/8
λ² = 0·9 , ν = 0·29

FIGURE 6.6

EXPERIMENTAL RESULTS : THE HELICAL SPRING

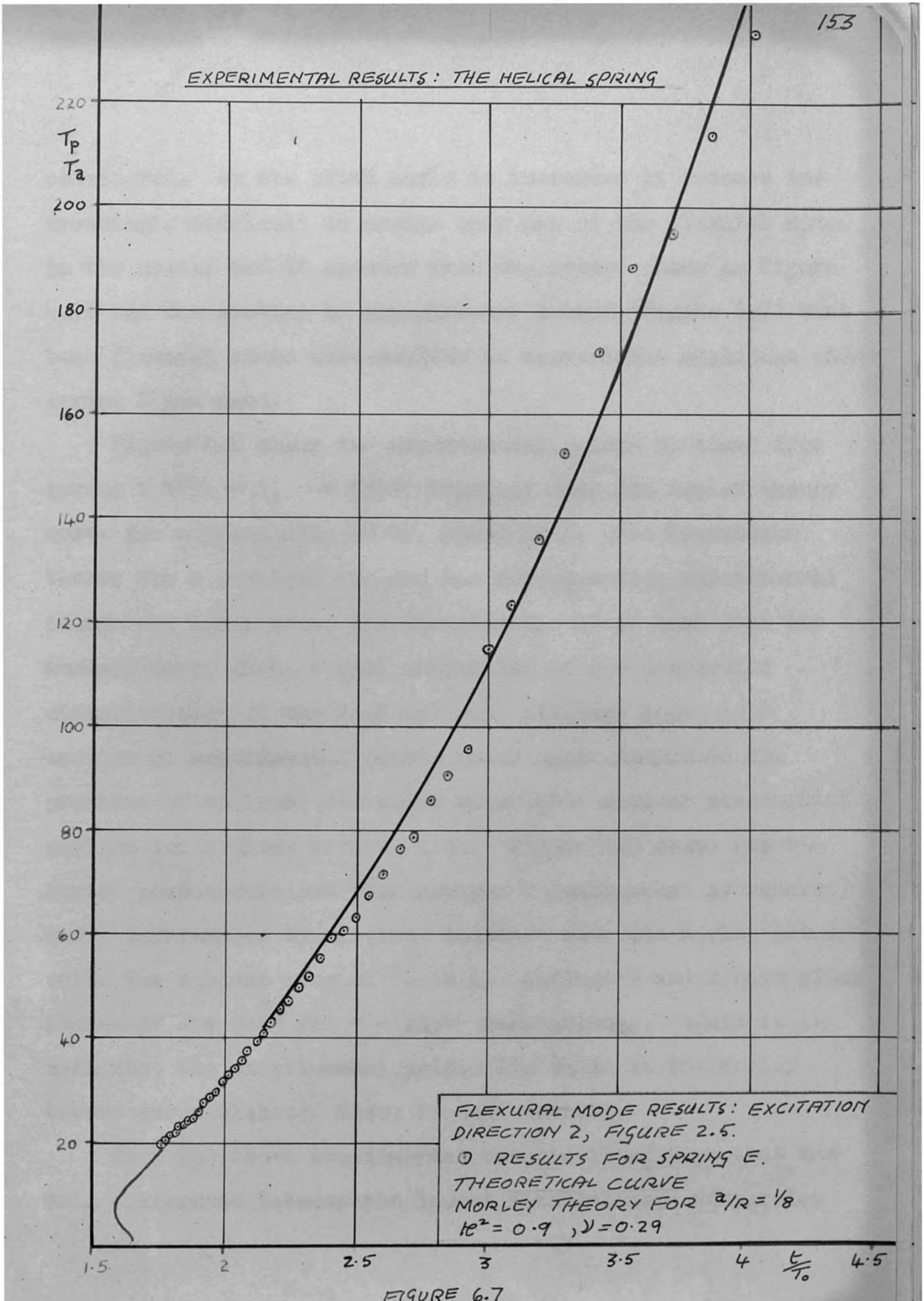

FIGURE 6.7

considered. As the pitch angle is increased it becomes increasingly difficult to excite only one of the flexural modes in the spring and it appears from the record shown in Figure 4.16 and the scatter of experimental points (Figure 6.7) that both flexural modes were excited in appreciable amplitude when spring E was used.

Figure 6.8 shows the experimental points obtained from spring F ($a/R = \frac{1}{4}$, $\alpha = 5.70^{\circ}$) together with the Morley theory curve for a plane ring of a/R equal to $\frac{1}{4}$. The Timoshenko theory for a straight rod and the corresponding experimental points are again shown for comparison. It is seen that the Morley theory gives a good indication of the dispersion characteristic of the flexural mode although there is a scatter of experimental points which again indicates the presence of at least two modes which have similar predominant periods for a given arrival time. Figure 6.9 shows experimental points obtained from springs G (surrounded by squares) and H (surrounded by circles) together with the Morley theory curve for a plane ring of $a/R = \frac{1}{4}$. Springs G and H have pitch angles of $\alpha = 9.00^{\circ}$ and $\alpha = 13.40^{\circ}$ respectively. Again it is seen that the experimental points lie close to the Morley theory curve although there is some scatter.

From the above experimental results it appears that the main difference between the lowest flexural mode dispersion

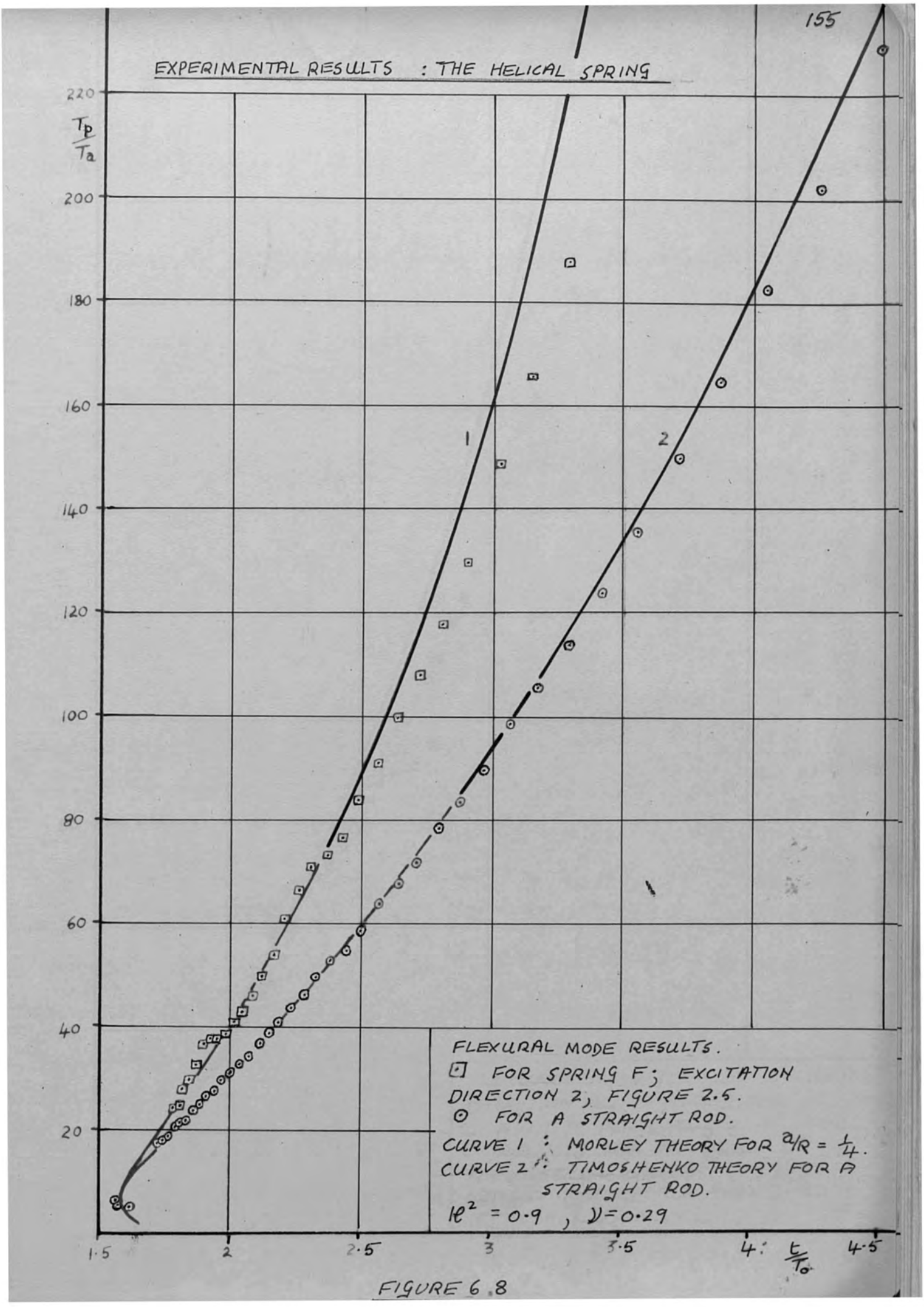
EXPERIMENTAL RESULTS : THE HELICAL SPRING
$\frac{T_p}{T_a}$
220
200
180
160
140
120
100
80
60
40
20
1·5
2
2·5
3
3·5
4
4·5
$\frac{t}{T_o}$
1
2
FLEXURAL MODE RESULTS.
⊡ FOR SPRING F; EXCITATION DIRECTION 2, FIGURE 2.5.
⊙ FOR A STRAIGHT ROD.
CURVE 1 : MORLEY THEORY FOR $a/R = \frac{1}{4}$.
CURVE 2 : TIMOSHENKO THEORY FOR A STRAIGHT ROD.
$k^2 = 0.9$, $\nu = 0.29$

FIGURE 6.8

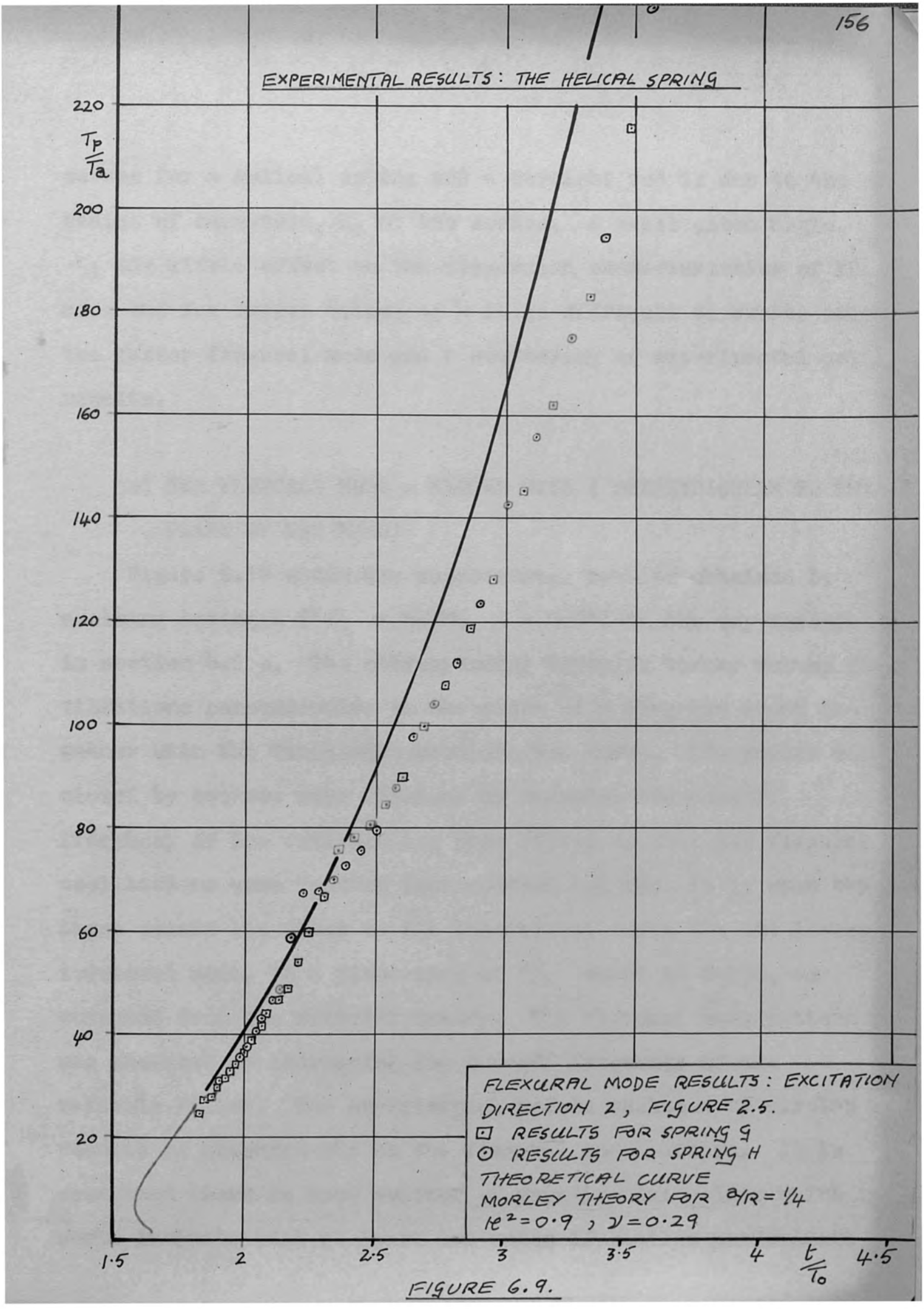
EXPERIMENTAL RESULTS: THE HELICAL SPRING
T_p/T_a
220
200
180
160
140
120
100
80
60
40
20
1·5
2
2·5
3
3·5
4
4·5
t/t_0
FLEXURAL MODE RESULTS: EXCITATION DIRECTION 2, FIGURE 2.5.
⊡ RESULTS FOR SPRING G
⊙ RESULTS FOR SPRING H
THEORETICAL CURVE
MORLEY THEORY FOR $a/R = 1/4$
$k^2 = 0·9$, $\nu = 0·29$

FIGURE 6.9.

curves for a helical spring and a straight rod is due to the radius of curvature, R, of the spring. A small pitch angle, α, has little effect on the dispersion characteristics of this mode but for larger values of α it is difficult to excite only the faster flexural mode and a scattering of experimental points results.

c) THE FLEXURAL MODE - SLOWER WAVE (PERPENDICULAR TO THE PLANE OF THE RING)

Figure 6.10 shows the experimental results obtained by exciting spring A (a/R = 0.106, α = 3.9°) in the way described in section 4.2 c. The corresponding Wittrick theory curves for vibrations perpendicular to the plane of a ring are shown together with the Timoshenko straight rod curve. The points enclosed by squares were obtained by reducing the cut-off frequency of the variable low pass filter so that the flexural oscillations were removed (see section 4.2 c). It is seen that these points lie close to the theoretical curve for the lowest torsional mode, in a plane ring of a/R equal to 0.106, as computed from the Wittrick theory. The flexural mode pattern was observed by increasing the cut-off frequency of the variable filter. The experimental points enclosed by circles are results of measurements on the flexural mode pattern. It is seen that there is some scatter of experimental points which would indicate that at least two modes of similar predominant

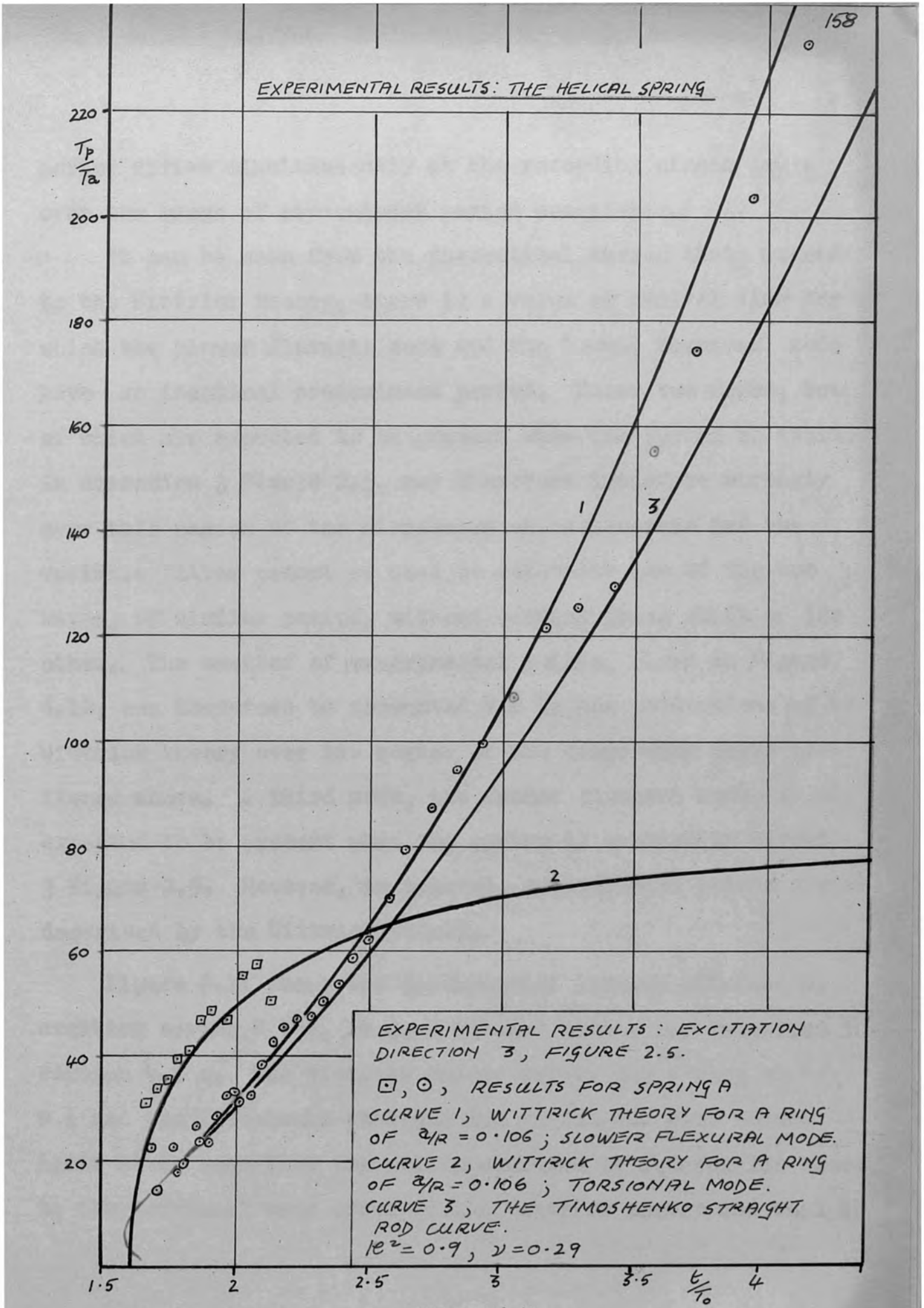
158
EXPERIMENTAL RESULTS: THE HELICAL SPRING
220
T_p/T_a
200
180
160
140
120
100
80
60
40
20
1
3
2
1·5
2
2·5
3
3·5
4
t/t_0
EXPERIMENTAL RESULTS: EXCITATION DIRECTION 3, FIGURE 2.5.
⊡, ⊙, RESULTS FOR SPRING A
CURVE 1, WITTRICK THEORY FOR A RING OF $a/R = 0·106$; SLOWER FLEXURAL MODE.
CURVE 2, WITTRICK THEORY FOR A RING OF $a/R = 0·106$; TORSIONAL MODE.
CURVE 3, THE TIMOSHENKO STRAIGHT ROD CURVE.
$Ie^2 = 0·9$, $\nu = 0·29$

FIGURE 6.10.

period arrive simultaneously at the recording strain gauge over the range of predominant period considered.

It can be seen from the theoretical curves that, according to the Wittrick theory, there is a value of arrival time for which the slower flexural mode and the lowest torsional mode have an identical predominant period. These two modes, both of which are expected to be present when the spring is excited in direction 3 Figure 2.5, may therefore interfere strongly over this region of the dispersion characteristic but the variable filter cannot be used to attenuate one of the two waves, of similar period, without causing phase shift of the other. The scatter of experimental points, shown in Figure 6.10, can therefore be accounted for by the predictions of the Wittrick theory over the region of the dispersion curve mentioned above. A third mode, the faster flexural mode, is also expected to be present when the spring is excited in direction 3 Figure 2.5. However, in general, experimental points are well described by the Wittrick theory.

Figure 6.11 shows the experimental results obtained by exciting spring D ($^a/_R = \frac{1}{8}$, $\alpha = 4.6^\circ$) in the way described in section 4.2 c. The Wittrick theory curves for a ring of $^a/_R = \frac{1}{8}$ and the Timoshenko straight rod curves are also shown. Again it is seen that the points enclosed by squares lie close to the torsional mode curve of the Wittrick theory and that there

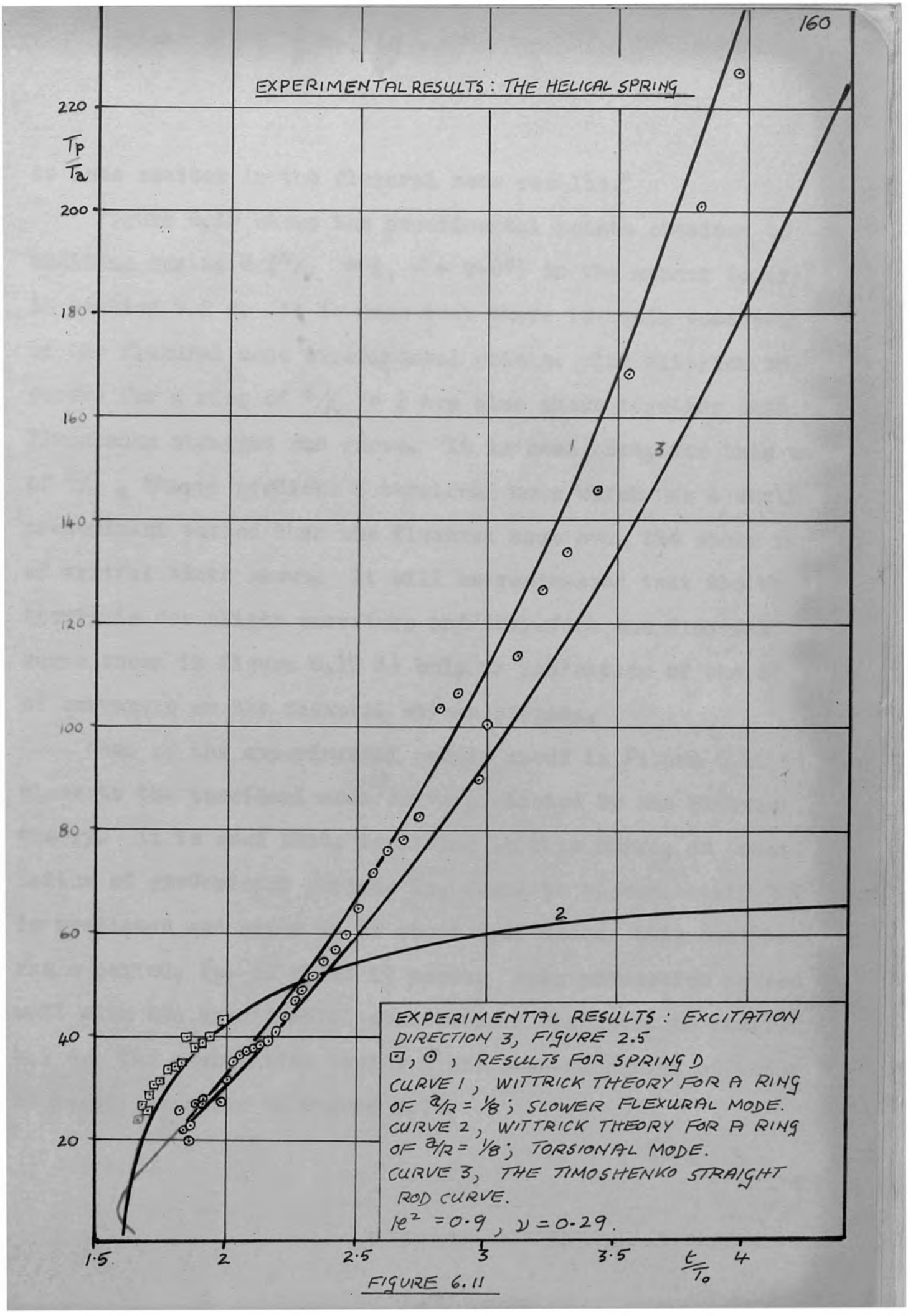
EXPERIMENTAL RESULTS : THE HELICAL SPRING
$\frac{T_p}{T_a}$
220
200
180
160
140
120
100
80
60
40
20
1·5
2
2·5
3
3·5
4
$\frac{t}{T_0}$
1
2
3
EXPERIMENTAL RESULTS : EXCITATION DIRECTION 3, FIGURE 2.5
⊡, ⊙ , RESULTS FOR SPRING D
CURVE 1 , WITTRICK THEORY FOR A RING OF $a/R = 1/8$; SLOWER FLEXURAL MODE.
CURVE 2 , WITTRICK THEORY FOR A RING OF $a/R = 1/8$; TORSIONAL MODE.
CURVE 3, THE TIMOSHENKO STRAIGHT ROD CURVE.
$ke^2 = 0.9$, $\nu = 0.29$.

FIGURE 6.11

is some scatter in the flexural mode results.

Figure 6.12 shows the experimental points obtained by exciting spring G ($^{a}/_{R} = \frac{1}{4}$, $\alpha = 9.0^{\circ}$) in the manner described in section 4.2 c. It is seen that there is again some scatter of the flexural mode experimental points. The Wittrick theory curves for a ring of $^{a}/_{R} = \frac{1}{4}$ are also shown together with the Timoshenko straight rod curve. It is seen that, for this value of $^{a}/_{R}$, theory predicts a torsional mode which has a smaller predominant period than the flexural mode over the whole range of arrival times shown. It will be remembered that the Wittrick theory is for slight curvature and therefore the flexural mode curve shown in Figure 6.12 is only an indication of the effect of curvature on the flexural stress pattern.

Some of the experimental points shown in Figure 6.12 lie close to the torsional mode curve predicted by the Wittrick theory. It is seen that, according to this curve, an oscillation of predominant period, Tp, equal to approximately 30Ta is predicted and since Ta is about 0.62 μsecs. this oscillation has a period, Tp. of about 19 μsecs. This prediction agrees well with the experimental observations discussed in section 4.2 c. The oscillation having a predominant period of about 19 μsecs. is shown in Figure 4.24.

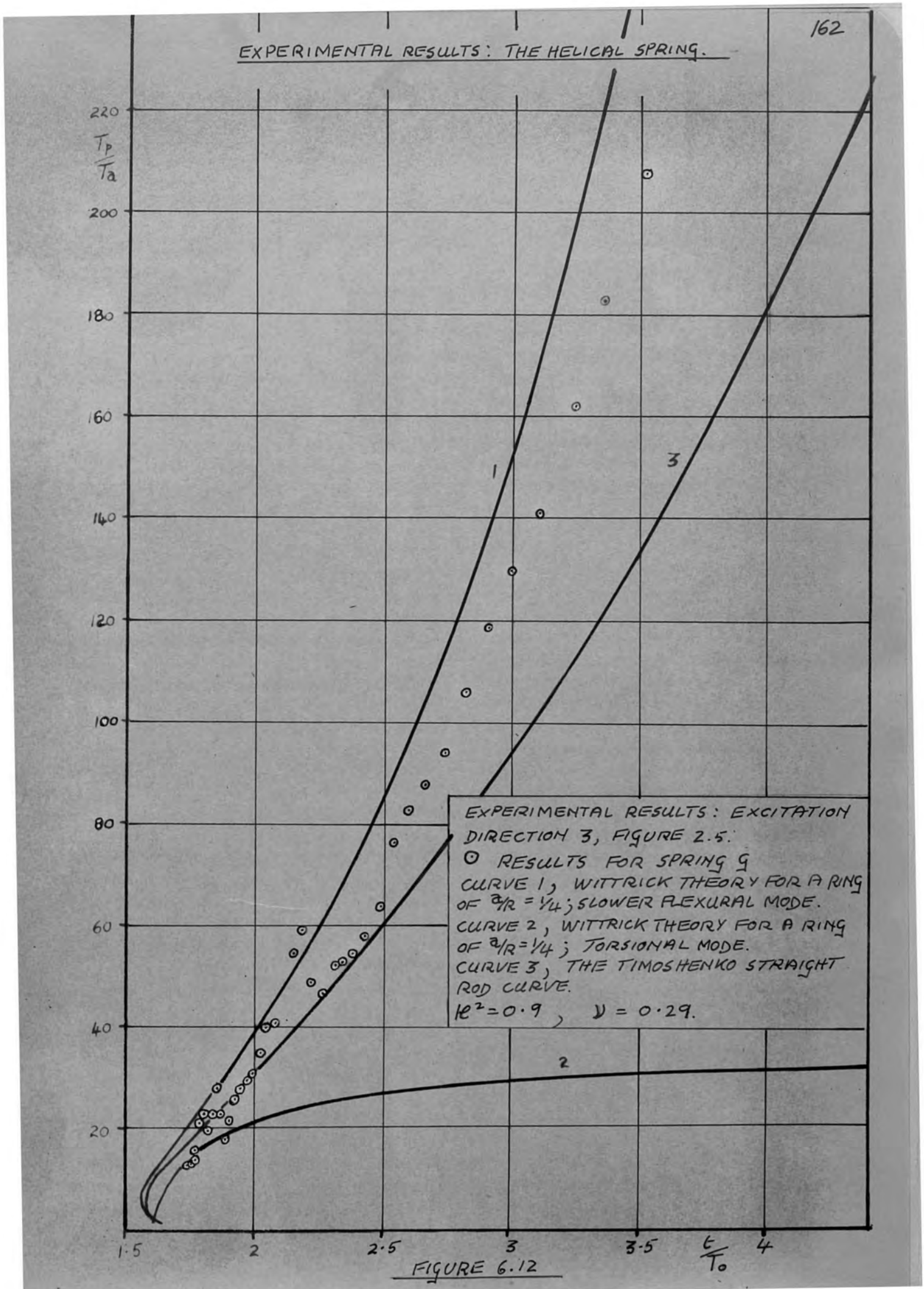
EXPERIMENTAL RESULTS: THE HELICAL SPRING.
220
200
180
160
140
120
100
80
60
40
20
$\frac{T_p}{T_a}$
1
2
3
EXPERIMENTAL RESULTS: EXCITATION DIRECTION 3, FIGURE 2.5.
⊙ RESULTS FOR SPRING G
CURVE 1, WITTRICK THEORY FOR A RING OF $a/R = 1/4$; SLOWER FLEXURAL MODE.
CURVE 2, WITTRICK THEORY FOR A RING OF $a/R = 1/4$; TORSIONAL MODE.
CURVE 3, THE TIMOSHENKO STRAIGHT ROD CURVE.
$k^2 = 0.9$, $\nu = 0.29$.
1·5
2
2·5
3
3·5
4
$\frac{t}{T_0}$

FIGURE 6.12

CHAPTER SEVEN

CONCLUSION

The aim of this work has been to investigate the nature of stress wave propagation in helical springs and to compare the results with the predictions of approximate theories. In this chapter a brief summary of the results of the theoretical and experimental work presented in this thesis is given.

It is well known that the lower flexural mode predicted by the Timoshenko theory for a straight rod gives results which are in good agreement with the lowest flexural mode given by the exact theory. The higher mode predicted by the Timoshenko theory does not, however, give results which are in agreement with a higher mode of the exact theory. A Timoshenko-type theory for flexural vibrations of a helical spring is therefore expected to be a good approximation to an exact theory for the lowest flexural mode only. No exact theory solution for vibrations of a helical spring has been put forward and therefore a direct comparison is not possible in this case. The only Timoshenko-type theory, known to the author, for a helical spring is that due to Wittrick [1966] . In this theory it is assumed that curvature of the waveguide is slight (see chapter 5). This theory was solved for the case of a spring for which $a/R = 0.106$

and $\alpha = 3.9°$, and also for a plane ring for which $a/R = 0.106$ and $\alpha = 0$, to give phase velocity curves for the six modes predicted. The theory predicts two lower flexural modes, a longitudinal mode, a torsional mode and two higher flexural or bending moment modes. All the modes predicted by the Wittrick theory are dispersive. For the plane ring the two lower flexural modes and the two higher flexural modes are very close, the latter being similar to the higher flexural mode of the Timoshenko theory for a straight rod. The effect of increased pitch angle, α, is to separate the two lower flexural modes but this separation was found to be very small compared with the difference between the straight rod and helical spring curves resulting from the finite spring radius, R. The higher flexural modes are also separated by the increased pitch angle. The effect of pitch angle on the longitudinal and torsional mode phase velocity curves was found to be very small.

For the case of $\alpha = 0$ the Wittrick theory characteristic equation can be split into two separate equations each of which predicts three modes of vibration. The two equations can be associated with vibrations in and perpendicular to the plane of the ring. The equation for vibrations in the plane of a ring predicts a lower flexural (faster wave) mode, a longitudinal mode and a higher flexural or bending moment mode which is similar to the higher flexural mode predicted by the Timoshenko theory for a straight rod. All three modes

predicted are dispersive. The equation for vibrations perpendicular to the plane of a ring predicts a lower flexural (slower wave) mode, a torsional mode and a higher flexural mode. Again all three modes are dispersive.

The equation for vibrations perpendicular to the plane of a ring was solved for various values of a/R as shown in chapter 5. The effect of finite radius of curvature on the lowest torsional and flexural mode dispersion characteristics is shown to be pronounced.

In the Wittrick theory it is assumed that the curvature of the guide is slight but a theory due to Morley [1961], for vibrations in the plane of a circular ring, places no restriction on curvature. As expected, it was found that Wittrick's theory for the case of $\alpha = 0$ gives results which are in agreement with the equations obtained by Morley when curvature is assumed slight. The Morley theory characteristic equation was solved for various values of a/R as shown in chapter 5. The effect of finite radius of curvature on the lowest longitudinal and flexural mode dispersion curves is shown to be pronounced.

The experimental results obtained in this thesis were interpreted according to Kelvin's method of stationary phase. The recording techniques were first checked for accuracy by obtaining experimental results for the lowest flexural mode in a straight rod. It was found that the results agreed well with the Timoshenko, and therefore exact, theory. Experimental

results were then taken for various modes of propagation in a helical spring.

Considering first the results for extensional waves in a helical spring, it was found that the agreement between experiment and the Morley theory for a plane ring is good. Earlier experiments [Britton 1957] have shown qualitatively the nature of the longitudinal mode dispersion and Filipczynski [1962], using a resonance technique, has obtained results which are in good agreement with an elementary theory. The expression for phase velocity obtained by Filipczynski is identical to that obtained by Morley for longitudinal waves in a ring of slight curvature. Morley has pointed out that the restrictions made on the deformation of the cross-section of the guide lead to an elementary-type theory for the longitudinal mode but all the experimental results obtained for this mode correspond to values of $a/\lambda < 0.080$ and therefere the elementary type theory is expected to give a good indication of the dispersion characteristics for the relatively long wavelengths considered.

It was found that an increase of pitch angle, α, from 2.8° to 9.00° has little effect on the experimental results obtained for the longitudinal mode in a spring of a/R equal to $\frac{1}{8}$. The effect of decreasing the mean radius, R, of the spring, however, has a pronounced effect on the dispersion characteristics.

Experimental results obtained for the faster flexural wave in springs of $a/R = 0.106$ and $a/R = \frac{1}{8}$ were also found to be in good agreement with Morley's theory for vibrations in the plane of a ring. These results were obtained by exciting the spring in direction 2 Figure 2.5. For small pitch angle, α, the experimental points lie close to the Morley theory curves for the particular value of a/R considered and a small change of α was found to have little effect on the dispersion characteristics of this mode. For springs with larger values of α the experimental points became scattered but they still lie close to the Morley theory curve. The scatter of the experimental points for large values of α is thought to be due to the interference between two modes which have very similar dispersion characteristics. It was mentioned above that the Wittrick theory for a helical spring predicts two lower flexural modes, one involving vibrations predominantly in the plane of the ring (faster wave) and the other predominantly perpendicular to the plane of the ring (slower wave). For the case of small pitch angle these two modes have practically identical dispersion characteristics (see Figure 5.19) and therefore if both modes are excited by the generating system they would interfere constructively over the whole of the dispersion pattern. The effect of increase of pitch angle is to separate the two flexural modes and therefore the resultant

stress pulse, detected at a point x along the guide, may show regions of destructive interference. The first region of destructive interference would, according to this argument, shift closer to the beginning of the dispersed flexural pulse as the pitch angle α is increased. According to the Wittrick theory the separation between these two flexural modes is very small compared with the difference between the corresponding flexural curves for the case of $\alpha = 0$ and the lowest flexural mode predicted by the Timoshenko theory for a straight rod and therefore although the experimental points become scattered for large pitch angles they should remain close to the Morley theory dispersion curves. We therefore conclude that the approximate theories give a good indication of the lowest flexural mode dispersion in a helical spring.

If we consider the experimental points obtained for the faster flexural modes in springs C, D and E, which have a value of $a/R = \frac{1}{8}$ and pitch angles of 2.8°, 4.6° and 9.0° respectively, we observe from Figure 6.6 that there is no scatter of experimental points for the cases of $\alpha = 2.8°$ and $\alpha = 4.6°$. This would indicate that the slower flexural mode is not present in these springs when they are excited in direction 2 Figure 2.5 but a closer examination of the records of the dispersed pulse in springs C and D (Figures 4.14 and 4.15) shows that in the case of spring D the amplitude of the pulse decreases from its maximum value more rapidly than in the case of spring C.

This would suggest that both flexural modes are present even when springs of small pitch angle are used but that the first region of destructive interference between the two modes is outside the range of arrival time considered.

The experimental points for the faster flexural wave in springs of pronounced curvature ($a/R = \frac{1}{4}$) were also found to be in good agreement with the Morley theory although there is some scatter of experimental points which is again attributed to interference between the two lowest flexural modes.

In the case of the slower flexural waves the records, obtained by exciting the spring in direction 3 Figure 2.5, show a more complicated pulse profile than predicted by the two lower flexural modes. The initial portion of the dispersed stress pulse obtained by exciting springs of $a/R = 0.106$ and $a/R = \frac{1}{8}$ in this direction indicates the presence of a third low frequency mode. This mode was studied by filtering out the relatively high frequency components of the lowest flexural modes present in the initial section of the dispersed pulse. It was found that the results are in agreement with the predominantly torsional mode curve of the Wittrick theory. It will be remembered that the lowest torsional mode is non-dispersive in a straight rod. The experimental points obtained for the latter part of the dispersed pulse lie close to the corresponding Wittrick theory arrival curves for the

lower flexural wave in a plane ring but there is some scatter. This would indicate that at least two modes of similar period arrive simultaneously at the receiving strain gauge over a large section of the dispersed pulse. A scatter of experimental points has also been found in bullet-impact experiments on helical springs [Britton 1957] .

The effect of increased curvature of the spring on the torsional and flexural mode dispersion characteristics was found to be pronounced. In the case of a spring for which $a/R = \frac{1}{2}$ a long dispersed torsional mode pulse of almost constant period was observed.

It is concluded that the experimental results discussed in this thesis can be interpreted with respect to four of the six modes predicted by the Timoshenko-type helical spring theory: the two higher flexural, or bending moment modes, were not studied. In addition dispersion curves for the fastest flexural mode in a plane ring can be calculated from the Morley theory. This theory is useful for interpreting results for springs of pronounced curvature and slight pitch whereas the Wittrick theory is limited to slight curvatures (i.e. a/R $\frac{1}{8}$).

The higher order modes of propagation were not studied in this work. When the 20 μsec. mechanical pulse from the nickel wire was used to excite the waveguides, described in chapter 2,

the relatively high frequency, higher order, modes were not detected in appreciable amplitude and therefore they did not interfere with measurements on the lower modes. However, when the 12 or 8 μsec. mechanical pulses were used to excite the waveguides the higher frequency modes appeared in appreciable amplitude. It should therefore be possible to study the higher mode dispersion phenomena: this would be a useful extension of the work described in this thesis.

REFERENCES

ABRAMSON, H.N. 1957 J. Acoust.Soc.Amer. 29, 42. Flexural waves in elastic beams of circular cross-section.

ABRAMSON, H.N., PLASS, H.J., AND RIPPERGER, E.A. 1958 Advances in applied mechanics. 5. Stress wave propagation in rods and beams. Academic Press Inc.

BAKSHI, J.S. AND CALLAHAN, W.R. 1966 J.Acoust.Soc. Amer. 40, 372. Flexural vibrations of a circular ring when transverse shear and rotary inertia are considered.

BANCROFT, D. 1941. Phys.Rev. 59, 588. The velocity of longitudinal waves in cylindrical bars.

BOIT, M.A. 1957. Phys.Rev. 105, 1129. General theorems on the equivalence of group velocity and energy transport.

BRITTON, W.G.B. 1957 Ph.D. Thesis, University of Wales. Transient stresses in helical springs.

CHREE, C. 1889. Trans.Cam.Phil.Soc. 14, 250. The equations of an isotropic elastic solid in polar and cylindrical co-ordinates, their solution and application.

DAVIES, R.M. 1948. Trans.Roy.Soc.(Lond.) A240, 375 A critical study of the Hopkinson pressure bar.

DAVIES, R.M. 1956. Surveys in Mechanics (Batchelor and Davies). University Press, Cambridge.

FILIPCZYNSKI, L. 1962 Proc.vibr.prob.Warsaw 3, 241. Propagation of ultrasonic waves in spirals.

FOLK, R., FOX, G., SHOOK, C.A. AND CURTIS, C.W. J.Acoust. Soc.Amer. 30, 552. Elastic strain produced by sudden application of pressure to one end of a cylindrical bar. Part 1 Theory, Part 2 Experimental observations.

HERRMANN, G. 1954. J.Appld.Mech. 21, 221. Forced motions of elastic rods.

HUDSON, G.E. 1943 Phys.Rev. 63, 46. Dispersion of elastic waves in solid circular cylinders.

KOLSKY, H. 1953. Stress waves in solids 41. Oxford University Press.

KOLSKY, H. 1954. Phil.Mag. 45, 712. The propagation of longitudinal elastic waves along cylindrical bars.

LAMB, H. 1931. The dynamical theory of sound. Chapter 4, 135. Arnold publications, second edition.

LOVE, A.E.H. 1900. Camb.Phil.Trans. 18, 364. The propagation of waves of elastic displacement along a helical wire.

LOVE, A.E.H. 1934. Mathematical theory of elasticity. 287. Cambridge University Press.

MAY, J.E. 1960. I.R.E. trans on Ultrasonic Eng. UE-7, 44. Wire type dispersive ultrasonic delay lines.

MAY, J.E. 1964. Physical Acoustics (Mason) 1 Part A, 417. Academic Press Inc.

MEITZLER, A.H. 1961. J.Acoust.Soc.Amer. 33, 435. Mode coupling occuring in the propagation of elastic pulses in wires.

MICHELL, J.H. 1889. Messenger of Mathematics. 19, 68. The small deformation of curves and surfaces with application to the vibrations of a helix and a circular ring.

MILNE, W.E. 1950. Numerical calculus. 99 PRINCETON

MINDLIN, R.D. AND HERRMANN, G. 1951. Proc.1st. U.S. Nat.Cong.Appld.Mech., Chicago. 187. A one dimensional theory of compressional waves in an elastic rod.

MORLEY, L.S.D. 1961. Quart.J.Mech. and appld.Math. 14, 155. Elastic waves in a naturally curved rod.

OLIVER, J. 1957. J.Acoust.Soc.Amer. 29, 189. Elastic wave dispersion in cylindrical rods by a wide-band, short-duration, pulse technique.

PHILIPSON, L.L. 1956. J.Appld.Mech. 23, 364. On the role of extension in the flexural vibrations of rings.

POCHHAMMER, L. 1876. J. Reine angew.Math. (crelle) 81, 324. Ueber die fortpflanzungsgeschwindigkeiten Kleiner schwingungen in einem unbegrenzten isotropen kreizylinder.

RAYLEIGH, LORD. 1894. The theory of sound. 1, 255 2nd Edn. Macmillan

REDWOOD, M. 1963. Appld.Materials Research 2, 76. A study of waveforms in the generation and detection of short ultrasonic pulses.

SHAW, E.A.G. 1956. J.Acoust.Soc.Amer. 28, 38 On the resonant vibrations of thick barium titanate disks.

TIMOSHENKO, S.P. 1921. Phil.Mag. 41, 744. On the correction for shear of the differential equation for transverse vibrations of prismatic bars.

TIMOSHENKO, S.P. 1922 Phil.Mag. 43, 125. On the transverse vibrations of bars of uniform cross-section.

TIMOSHENKO, S.P. 1941. Strength of Materials, Part II, 2nd edn. chap. ii (New York, 1941).

TOLSTOY, I AND USDIN, E. 1957 J.Acoust.Soc.Amer. 29, 37. Wave propagation in elastic plates: low and high mode dispersion.

TU, L.Y., BRENNAN, J.N. AND SAUER, J.A. 1955. J.Acoust. Soc.Amer. 27, 550. Dispersion and ultrasonic pulse velocity in cylindrical rods.

VLASOV, V.Z. 1951 N.A.C.A. Tech.Memo. 1241 (Translation). Basic differential equations in the general theory of elastic shells.

WAINWRIGHT, W.L. 1964 J.Acoust.Soc.Amer. 35, 511.
On torsional oscillations in a finite cylinder.

WITTRICK, W.H. 1966 Int.J.Mech.Sci. 8, 25. On
elastic wave propagation in helical springs.